The Effect of Saline Solution Conditioning on South African Fly Ash Resistivity

D Lalla

orcid.org/ 0000-0002-9071-647X

Dissertation accepted in fulfilment of the requirements for the degree *Master of Engineering in Chemical Engineering* at the North-West University

Supervisor:	Prof Burgert Hattingh
Co-supervisor:	Prof Hein Neomagus
Co-supervisor:	Dr Gregory Okolo
Industrial mentor:	Pieter Swart

Graduation: April 2024

DEDICATION

I would like to acknowledge and express my gratitude to the following persons who have supported me and made it possible for me to complete this study.

- Prof Burgert Hattingh from North-West University, for his continued support, guidance and encouragement.

- Dr Gregory Okolo from North-West University, for his assistance, supervision and patience with the laboratory work.

- Mr Pieter Swart from Howden Engineering, for his guidance as my industrial mentor.

- Ms Shinelka Singh and Dr Chris van Alphen from Eskom RT&D for assisting with QEMSCAN analysis of samples.

- Mr Romanus Uwaoma from North-West University for assisting with thermogravimetric analysis of samples.

- Ms Marunel de Beer from North-West University for assisting with the proximate analysis on the samples.

- The late Mr Johan van Noordwyk who initiated the concept of saline solution injection for particulate matter control at Eskom.

- My husband and sons, for their ongoing support and encouragement during difficult times.

ABSTRACT

Fly ash resistivity is an important characteristic that not only affects the electrical charge rate of fly ash particles but also the ultimate performance of electrostatic precipitators used for fly ash separation and collection. South African fly ash is highly resistive, thus limiting the collection efficiency of electrostatic precipitators at several coal-fired power generation plants in South Africa. Several flue gas conditioning studies (e.g., duct injection of sulphur trioxide, SO_3) have shown to be effective in reducing fly ash resistivity to subsequently improve electrostatic precipitator performance. An earlier industrial pilot testing campaign involving the injection of a reject saline solution, containing primarily sodium sulphates and chlorides, into the boiler of one of Eskom's coal-fired power station units gave a subsequent reduction in particulate matter emissions. This therefore highlights the possibility of using a waste stream, in this case a reject saline solution from an industrial reverse osmosis plant, as a suitable and cost-effective alternative to other flue gas conditioning agents such as SO_3.

An assay of the reject saline solution from the reverse osmosis plant showed the presence of other ionic species (e.g., Ca, K, Fe, etc.), which, although present in low concentrations, could also contribute to an observed reduction in particulate matter emissions. The observed improvement in particulate matter emissions on industrial scale therefore necessitated further investigation, to elucidate the effect of saline solution conditioning on fly ash resistivity.

Fly ash samples from two Eskom coal-fired power generation stations (PS-1 and PS-2) were sampled and conditioned (treated) with reverse osmosis plant saline solution in different weight ratios by total wet mass of saline solution (5, 8, 10, 20, 30 and 35 wt.% for PS-1; 20, 30 and 35 wt.% for PS-2). The selection of these mixing ratios was based on typical flue gas volumetric flow rates (500–680 Nm^3/s) under varying load factors (generated load as a percentage of the maximum output possible from the power generating unit), as well as saline solution injection rates used earlier during an industrial pilot testing campaign (5 and 25 m^3/hr). After drying at ambient conditions, samples were crushed to obtain homogenous fine powders. Physiochemical characterisation of the unconditioned and conditioned fly ash samples was carried out with various techniques (proximate analysis, thermogravimetric analysis, particle size distribution analysis, X-ray fluorescence and quantitative evaluation of materials by scanning electron microscopy). Ash resistivity was measured in an experimental resistivity rig. The latter was

performed under dry and humid (7 wt.% moisture) conditions for both ascending and descending temperature increments, in the range 90–330 °C.

The observed measurements were found to be within the acceptable error ratio as stipulated by the IEEE Standard 548 of 1984. Under dry conditions, the resistivity measurements for the ascending and descending runs followed the same trends for ash samples of both the power stations (PS-1 and PS-2). The resistivity measurements for temperatures less than 240 °C (range representative of surface resistivity) exceeded the optimum operating range for electrostatic precipitators (1×10^{11} Ω.cm in the temperature range 115–150 °C). Whereas the average resistivity of the dry ash samples, over the entire measurement range, decreased monotonously with increasing temperature, the average resistivity of the 7 wt.% ambient moisture ash samples (unconditioned and conditioned) exhibited an eccentric curve with a local maximum in the range 130–180 °C for both the ascending and descending temperature measurements.

For temperatures less than 210 °C, initial ascending resistivity measurements for the conditioned ash samples (under dry conditions) were found to be substantially lower than the descending runs, while subsequent repeats of the ascending runs showed a similar trend to the results obtained for the descending runs. The observed disparity for the initial ascending runs could be attributed to volatile and soluble chemical species (e.g., carbonaceous impurities not detected with the saline solution assay) adsorbed onto the ash particles and then removed when heating the ash samples. Furthermore, with moisture injection, it was determined that the fly ash resistivity for both PS-1 and PS-2 decreased with an increase in saline solution loading (a subsequent increase in sodium sulphate/chloride species concentration). Ash samples conditioned with a higher ratio of saline solution (greater than 20 wt.%) gave resistivity results within the desired ash resistivity range for optimum electrostatic precipitator performance.

An assessment of the Bickelhaupt model was performed to determine the ability of the model to predict the resistivity of the ash when conditioned with the varying concentrations of saline solution samples.

The original Bickelhaupt model (1979) offered a good prediction for samples with the higher conditioning agent concentrations by mass when compared with the lower concentration conditioned samples. The Bickelhaupt model for sodium-depleted ashes showed an improvement for the volume resistivity of both power station conditioned ash samples. A modification to the

original Bickelhaupt model provided a suitable prediction for the lower and higher concentration ash samples for PS-1 however the same formula was not as suitable for PS-2 ash samples although it did offer a better prediction than the original Bickelhaupt formula.

Key terms

Electrostatic precipitator, Flue gas conditioning, Brine, Saline Solution, Fly ash resistivity, Bickelhaupt Model.

TABLE OF CONTENTS

LIST OF TABLES

LIST OF FIGURES

LIST OF ABBREVIATIONS

Abbreviation	Definition
IEEE	Institute of Electrical and Electronics Engineers
LOI	loss of ignition
PM_{10}	particulate matter with diameter less than 10 µm
$PM_{2.5}$	particulate matter with diameter less than 2.5 µm
PS-1	Power station 1
PS-2	Power station 2
QEMSCAN	quantitative evaluation of minerals by scanning electron microscopy
SABS	South African Bureau of Standards
SANS	South African National Standard
SO_3	sulphur trioxide
STP	standard temperature and pressure
vol.%	percentage by volume
WHO	World Health Organization
wt.%	percentage by weight

LIST OF SYMBOLS

Symbol	Unit of Measure	Description
MW	MW	megawatt
$\dot{c}_g$	kJ/kg	specific heat capacity of flue gas
$\dot{m}_S$	g	mass in grams of saline solution
$\dot{m}_g$	g	mass in grams of flue gas
$\dot{m}_{\boldsymbol{Ash}}$	g	mass in grams of fly ash
$\dot{m}_{\boldsymbol{D,Ash}}$	kg/s	mass flow rate of flue gas
ΔT_S	°C	temperature change of saline solution
ΔT_g	°C	temperature change of flue gas
$P_{(flue\ gas)}$	kPa	pressure of the flue gas (absolute)
Q_S	kJ/kg	heat gained by saline solution
Q_g	kJ/kg	heat lost by flue gas
$V_{(water)}$	m^3	volume of water
$\dot{V}$	m^3/hr	volumetric flow rate
c_S	kJ/kg	specific heat capacity of saline solution
$\dot{m}$	kg/s	mass flow rate
$n_{(Water)}$	-	number of moles of water
χ_S	-	saline solution to ash ratio
R	$J/K^{-1}\ mol^{-1}$	universal gas constant
R	Ω	resistance
T	°C	temperature

ρ	kg/m^3	density
ρ	Ω.cm	resistivity
V	volt	DC power supply
I	ampere	current
A	cm^2	area
L	cm	thickness of the ash layer
d	mm	depth of ash in the bottom electrode
X_n	-	the normalised value for specific ash component n
X_d	%	the determined percentage of the specific ash component
$\sum X_D$	-	sum of all the determined values
X_{mpn}	%	molecular percentage for the specific ash component n
$\sum X_{MA}$	moles	sum of the molecular amount for all the components
X_{acn}	%	the atomic concentration for the specific ash component n
X_{cmn}	mg	the determined cation mass amount for the specific ash component
$\sum X_{CM}$	mg	sum of the cation mass amount for all the components
X	-	atomic mole fraction of sodium
Y	%	atomic concentration of iron
Z	-	atomic mole fraction the sum of magnesium and calcium ions
E	kV	electrical field strength

CHAPTER 1 INTRODUCTION

1.1 Background

The World Health Organization (WHO) has recognised air pollution to be the greatest environmental threat to human health [1]. There is evidence to indicate a correlation between particulate matter with diameter less than 2.5 µm ($PM_{2.5}$) exposure and diseases such as acute lower respiratory infections, chronic obstructive pulmonary disease, ischaemic heart disease, lung cancer and stroke, with recent evidence suggesting links to type II diabetes and impacts on neonatal mortality. With the recent global challenges that came with the coronavirus disease pandemic (it being a respiratory disease), the WHO recognised the contribution that addressing air pollution had as part of the global healthy recovery from the coronavirus disease [1].

A 2022 investigation, published by the journal *Lancet Planetary Health*, found that $PM_{2.5}$ is the leading environmental contributor to the global health burden [2]. The main sources of particulate emissions include the burning of fossil fuel in industry, and use in electricity generation, vehicle and aircraft emissions, and domestic fuel burning [3]. The countries with the highest $PM_{2.5}$ levels include China, India and the United States, while South Africa is listed 24th by the WHO of countries that exceed the WHO Air Quality Guidelines for $PM_{2.5}$ concentrations [4].

The Atmospheric Pollution Prevention Act (Act No. 45 of 1965) was implemented in South Africa, from April 1965, to control and manage the country's air quality. The purpose of the Act was to address the pollution emitted at the point of production rather than considering the various air catchment regions [5]. However, this Act was considered ineffective in managing the development of high air pollution regions in the country. As a result, the National Environment Management: Air Quality Act 39 of 2004 was promulgated on 19 February 2005—it aligned with international best practices regarding the management of air quality. The main difference in the two Acts was the Air Quality Act focuses on controlling the receiving air quality by setting limits to protect human health.

The contribution of the various sources of particulate matter in South Africa depends on the area in which it is measured. The impact of domestic fuel burning is significant in densely populated low-income settlements, some regions are impacted greatly by windblown dust and non-combustion sources, while high concentrations of particulate matter is a concern in areas where most of the coal-fired power stations are located [6, 7]. South Africa is one of 20 countries in the

world where coal is the dominant fuel source for power generation, thus contributing significantly to the $PM_{2.5}$ health impacts in the country [7].

Coal is the predominant fuel source for power generation in South Africa—it comprises approximately 83 % of the total fuel source [8, 9, 10, 11]. The coal combustion process results in airborne waste in the flue gas stream. The latter contains, among other components, particulate matter, sulphur dioxide (SO_2), carbon dioxide and nitrogen oxide [8].

Eskom Holdings Limited is a state-owned power utility in South Africa. The utility has a total installed capacity of 46 466 MW capable of being generated from 30 power stations. The power generating fuel sources (2022 data) are indicated in Table 1-1.

Table 1-1: Power Generating fuel sources (2022 data) installed in Eskom [10]

Type of fuel source	Nominal capacity (MW)
Coal fired	38 773
Nuclear	1 860
Hydro/Pumped storage	3 324
Gas	2 409
Wind	100

Eskom's coal-fired power stations have been installed with particulate matter abatement technologies available at the time of construction. These include electrostatic precipitators, fabric filter plants or additional flue gas conditioning in the form of SO_3 [9].

The Department of Environment, Forestry and Fisheries has licensed each power station to comply with particulate matter emission limits, suitable for the catchment in which they operate, at the time of their construction. The power stations and the particulate matter abatement technology currently employed are indicated in Table 1-2. Currently, the power stations are exceeding their licenced relative particulate matter emission targets, while amendments to these limits have made the targets even stricter [10]. Exceedances are frequently encountered where electrostatic precipitators are used for particulate matter capture, which implies that the performance (particulate matter collection efficiency) of the electrostatic precipitators needs to be improved to ensure compliance [11].

Table 1-2: Particular matter abatement technologies (2022 data) installed at Eskom coal-fired power stations [11]

Power station	Electrostatic precipitator	Fabric filter plant	Flue gas conditioning (SO_3)
Arnot		✓	
Camden		✓	
Duvha	✓	✓	✓
Grootvlei		✓	
Hendrina		✓	
Kendal	✓		✓
Komati	✓		✓
Kriel	✓		✓
Kusile		✓	
Lethabo	✓		✓
Majuba		✓	
Matimba	✓		✓
Matla	✓		✓
Medupi		✓	
Tutuka	✓		

Fly ash resistivity influences the rate at which fly ash particles are electrically charged within an electrostatic precipitator, which in turn affects the collection efficiency. South African fly ash is highly resistive, thus limiting the electrostatic precipitator performance [12]. Fortunately, fly ash resistivity can be manipulated by flue gas conditioning through the injection of conditioning agents such as steam, sulphur trioxide (SO_3), ammonia or other sodium-based solutions [13, 14, 15, 16, 17, 18].

The technologies used for the removal of particulates from a flue gas stream at Eskom's coal-fired power stations are electrostatic precipitators or fabric filter bags [11]. Fabric filters can achieve high collection efficiencies and are independent of ash resistivity [19]. The fabric filter

bags work on the principal of filtration—they exclude particulates greater than the pore size of the filter bags, while electrostatic precipitators utilise the electrical forces to collect the suspended dust particles from the flue gas stream [13].

Flue gas, with high particulate matter, enters the electrostatic precipitator, encounters a strong electric field and exits with a reduction in particulate matter. The flue gas / air molecules in the flue gas are ionised by the corona discharge and create negative ions. These negative ions migrate towards the positively charged collecting plates. While migrating, the ions come in contact with, and adhere to, suspended ash particles in the gas stream and are attracted by the collection plates. The negatively charged ash particles adhere to the collection plates and subsequently pass their charge to earth. For the negative charge to be passed to earth, the collected particles should exhibit at least a small degree of conductivity otherwise there is a decline in electrostatic precipitator performance. The ash particles are dislodged via a process known as ‘rapping’ and travel down, vertically, towards the hoppers for disposal [20].

A potential solution to solving the problem of high particulate matter emission is to convert the electrostatic precipitators to fabric filter plants—however, the duration of such projects is lengthy and comes at a very high cost. The cost of converting six electrostatic precipitator units on one power station to fabric filter plants has been estimated to be greater than R 10 billion [11]. Such strategies will also require significant downtime of the generating units for implementation. An alternative, cost-effective solution to reduce the particulate emissions will be beneficial to the power supplier, the electricity consumers as well as the environment. The collection efficiency of an electrostatic precipitator is affected by the electric field strength, the fly ash resistivity, the adhesive and cohesive properties of the fly ash, plate spacing, electrode design and an average particle size distribution, amongst other parameters [20]. Various options may be considered to improve the collection efficiency of an electrostatic precipitator depending on the cause of performance limitation. These include adjusting the power supply, flue gas conditioning, modifying the electrostatic precipitator or installing polishing devices [19, 20].

Resistivity is a measure of the resistance that a material exhibits towards the flow of electrons. The resistivity of fly ash is influenced by either surface or volume conduction. Surface conduction occurs over the surface of the particles at relatively low temperatures. Volume conduction is defined as the area where ionic conduction occurs through the bulk volume of the ash particles and is dominant at higher temperatures [14].

Fly ash resistivity is regarded as the primary parameter that dictates electrostatic precipitator performance. An optimum resistivity range has been reported, between 1 x 10^8 and 1 x 10^{11} Ω.cm, facilitating high particulate matter collection efficiencies [20, 21, 22]. Ash particles with high resistivity have trouble in attaining a charge but they also do not easily lose their negative charge once reaching the collection plates, thereby impacting the collection efficiency of the electrostatic precipitator [22]. The high resistivity ash also disturbs the electrical condition across the electrostatic precipitator, leading to sparking and a condition known as 'back–corona', which is the inability of the particle to leak its accumulated charge to the ground [22]. When the fly ash resistivity is too low, the ash is more readily charged but also does not retain the charge long enough for it to be collected at the collecting electrodes. This eventually leads to decreased electrostatic precipitator performance. The fly ash resistivity of the ash produced at South African power stations typically ranges from 1 x 10^{12} to 2,4 x 10^{13} Ω.cm [12], which contributes to poor electrostatic precipitator performance [22]. The electrostatic precipitator collection efficiency achieved to date for fly ash resistivity within the optimum range is greater than 95 %, while the collection efficiency decreases to about 80 % at a resistivity of approximately 1 x 10^{12} Ω.cm; it is down to 40 % at 1 x 10^{13} Ω.cm [23]. The high resistivity of South African fly ash has been attributed to the result of combusting low-grade coal that has a low sulphur content, as well as sodium and lithium (alkali metals) [12]. Conditioning agents have been found to enhance the properties of the fly ash, thereby affecting its performance in an electrostatic precipitator [22].

Conditioning agents that adsorb onto the ash particles affect the surface resistivity of the ash particles, and those agents that are absorbed impact the volume resistivity [24].

Different conditioning agents such as SO_3, ammonia, water vapour, amines and alkali compounds affect the electrostatic precipitator collection efficiency through different conditioning mechanisms [12, 20, 25, 26]. They may adsorb onto the surface of the fly ash and reduce the surface resistivity or change the adhesion and cohesion properties of the ash, increase the particle concentrations for space charge enhancement, increase the electrical breakdown strength of the flue gas, increase the mean ash particle size or change the acid dew point in the flue gas [25]. These mechanisms all result in reducing the fly ash resistivity. The extent of the reduction in the fly ash resistivity is dependent on several variables for a specific installation, e.g., the ash composition (coal quality), the flue gas temperature and the size of the electrostatic precipitator. It has been found that the conditioning mechanism for moisture conditioning is a reduction in the fly ash resistivity as a result of the formation of a very thin water layer on the surface of the fly ash particles, creating a medium for the transfer of the ions, while ammonia improves the adhesion

and cohesion of the ash particles, and SO_3 and alkali compounds (sodium sulphate or sodium carbonate) improve the ionic charge of the ash particles, thereby reducing the fly ash resistivity [25].

Fly ash resistivity has also been found to be inversely proportional to the amount of sodium in the ash of coal of the northern hemisphere [14]. It was found that when a sodium containing compound is injected into the ash, the resistivity is reduced in the same way as when the sodium content in the ash itself is increased, to achieve the desired reduction in fly ash resistivity [14]. The thermochemical properties of the sodium substance added (sodium carbonate, sodium sulphate or sodium hydroxide) must be such that it decomposes, vaporises or melts at boiler temperatures [14].

Sodium ions are present in some of the waste streams utilised for ashing purposes at Eskom's power stations [27, 28, 29]. Eskom has implemented a 'zero liquid effluent discharge' philosophy, which means that all waste streams generated on site are recovered and reused as far as reasonably practical [30]. The water management philosophy adopted by the power stations is to utilise the final waste streams to meet the requirements for ashing (ash conditioning, transfer of ash in slurry form to the ash dams, or for dust suppression at the ash dumps) [31]. The World Bank recognises that, as the global demand for water increases, there is an increasing need to use abstracted water multiple times [32]. As a means of reducing the raw water intake from the catchment, some power stations recover the excess mine water from their tied collieries [31]. The water is treated, by a desalination process (including reverse osmosis), to enable it to be of a suitable quality for use within the power station processes. However, desalination results in the salts being rejected into a concentrated brine/saline solution stream (herein referred to as saline solution), with high concentrations of sodium and sulphate [27].

1.2 Problem Statement

The utilisation of saline solutions, such as those originating from the power station water treatment plants, has been proposed to be a simpler and more cost-effective alternative to SO_3 injection for particulate matter emission reduction [28]. The saline solutions contain high concentrations of chemicals utilised in typical conditioning agents (e.g., sodium and sulphate). A pilot test carried out in July 2010 addressing the injection of an Eskom produced saline solution into the boiler at one of Eskom power utilities gave promising results in terms of a reduction in the particulate emissions for that unit [28]. Figure 1-1 provides a graphical indication of the particulate emission concentrations measured on the test unit, at varying generating loads, with and without the

addition of saline solution [29]. Within the higher end load range, the pilot test indicated that an almost 20 % reduction in particulate emissions can be achieved by injecting the saline solution into the boiler.

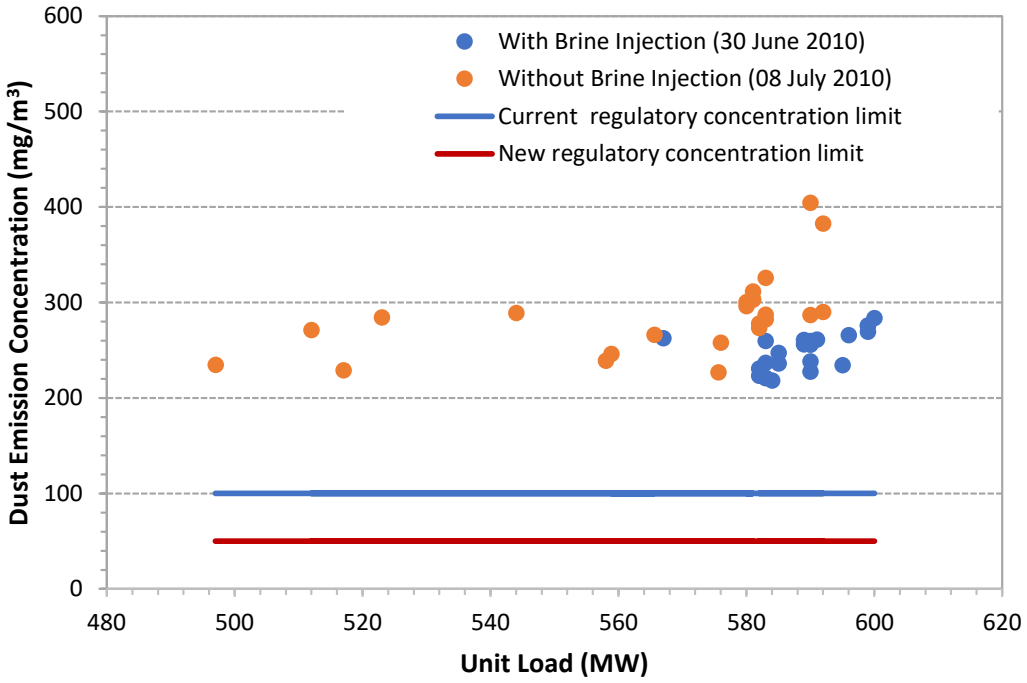

Figure 1-1: Impact of saline solution injection on dust emission concentrations [Adapted from 29]

The pilot test was unable to achieve the regulatory limits for particulate matter emission concentrations. However, should saline solution conditioning prove effective in improving the electrostatic precipitator performance, the implementation thereof might serve as an interim or even medium- to long-term solution to reduce particulate emissions from power stations while the fabric filter plant projects are still underway. The nominal prefeasibility cost for the fabric filter plant retrofit projects for the fleet is estimated to be in excess of R 10 billion [9]. The use of synthetically prepared conditioning agents such as sodium sulphate, SO_3 or ammonia will add to the operating cost of the power plant at an additional cost of approximately R 42 to R 56 per kilowatt [41, 81]. Whereas, utilising a freely available saline waste stream that can be repurposed to achieve the result of improving fly ash resistivity will be a cost-effective solution. Information on the influence of such solutions on South African fly ash resistivity is currently lacking—hence it certainly warrants investigation.

South African power stations need to reduce their particulate emissions in the flue gas stream in order to comply with revised legislation [11]. Whilst various mechanisms to enhance the electrostatic precipitator performance have been considered/evaluated at the different sites, utilising the saline effluent to achieve a reduction in the particulate emissions may prove to be a favourable cost-effective solution.

1.3 Aim and Objectives

The overall aim of this study is to determine the effect/s of the Eskom process-derived reverse osmosis plant reject (saline solution) on the resistivity of fly ash produced from South African power stations. This is to determine whether the active constituents dissolved in the saline solution (e.g., sodium, sulphate) behave similarly to the traditional conditioning agents, and whether there is any contribution to performance improvement in the electrostatic precipitators.

The following were the objectives of the study.

- Correlate the effect of the Eskom saline solution concentration and fly ash chemical composition with the fly ash resistivity and evaluate if the fly ash resistivity for optimum electrostatic precipitator performance can be achieved.
- Evaluate the suitability of the Bickelhaupt model for predicting fly ash resistivity with the saline solution conditioning by utilising the experimental data in the published model.
- Comparing the adequacy of prediction through the use of the existing Bickelhaupt model derivations for South African coal-derived fly ashes
- With the aid of non-linear regression, evaluate and propose improvements to the Bickelhaupt model parameters where required.

1.4 Scope

The scope of the study incorporated the following:

1.4.1 Evaluation and characterization of a saline solutions generated at an Eskom power station.

The intention is to understand the chemical properties of the saline solution being tested. The main chemical constituents will be compared with those presented in available literature, should the active constituent responsible have an influence on the fly ash resistivity.

1.4.2 Characterisation of fly ash samples

The fly ash being tested was characterised in terms of its chemical and physical properties, to determine their influence on the fly ash resistivity measurements. Analytical techniques to be used included X-ray fluorescence, particle size distribution, thermogravimetric analysis, quantitative evaluation of minerals by scanning electron microscopy and proximate analysis.

1.4.3 Measurement of fly ash resistivity

Resistivity measurements were recorded for ash samples that have been conditioned with the saline solution from a power station. The degree of conditioning in terms of the moisture addition were varied in an effort to understand the correlation between the amount (by weight percentage) of saline solution added and fly ash resistivity and identify the optimum percentage of injection for the fly ash resistivity improvement and subsequent electrostatic precipitator performance.

1.4.4 Correlation of the effect of saline solution concentration and composition with fly ash resistivity

The results were evaluated in order to determine the impact of the saline solution as a conditioning agent on the ash resistivity against the raw unconditioned ash.

1.5 Layout of the document

The first chapter presents a background to the wider field, then this particular study. It includes the problem statement—serving as motivation for this study—, followed by the aim and specific objectives. Chapter 2 presents the literature review—it highlights previous research pertaining to the application of various conditioning agents to different fly ash qualities (based on the source of the coal) and the reduction in fly ash resistivity achieved. It includes mention of predictive models developed for fly ash resistivity, considering the conditioning agents, and shortcomings when evaluating South African ashes. Chapter 3 describes details of the sample preparation and the tests conducted to determine the chemical and physical properties of the various ash samples. A resistivity oven was utilised to perform the fly ash resistivity tests. The experimental setup of the resistivity rig as well as the methodology adopted for this study is explained in Chapter 4. Results of the resistivity measurements, findings in terms of correlations, as well as the suitability of the Bickelhaupt model are presented in Chapter 5. In the final chapter, Chapter 6, I present the conclusions to this study and make recommendations for further research.

CHAPTER 2 LITERATURE REVIEW

A summarised account of applicable literature is presented in this chapter. The focus is on electrostatic precipitators and the factors that influence their performance. The topic of fly ash resistivity is addressed (for a better understanding) and consideration given to factors that could improve the resistivity (including flue gas conditioning). The chapter also addresses methods to determine fly ash resistivity as well as the challenges experienced in obtaining data and drawing meaningful comparisons between the resistivity of international fly ashes and those produced from South African coal. Methods used for flue gas conditioning were reviewed for various conditioning agents and how they influence the resistivity. Finally, the research conducted on developing predictive mathematical models for determining fly ash resistivity and the applicability of the models for South African fly ashes was assessed.

2.1 Fly Ash Formation

Ash is a by-product of the coal combustion process. The resultant ash is in the form of fly ash or coarse ash. Fly ash is a very fine powdery material formed as a result of the burning the pulverised coal in the boiler and is carried out with the flue gas stream from the boiler. Coarse or bottom ash refers to the ash particles that are too large to be transported with the flue gas and exits the boiler through the bottom of the furnace [33, 34, 35]. The fly ash comprises about 80 % of the total ash produced while the coarse ash makes up the remaining 20 % [34].

The chemical composition of the fly and bottom ash is similar when produced from the same coal, with the exception that the bottom ash has a larger concentration of unburnt carbon [34]. Bottom ash particles fuse during cooling in the bottom ash collection system resulting in the particles being much coarser and larger than the fly ash particles [35]. Fly ash particles range in size from 0.5 µm to 300 µm and are more spherical in shape [36].

The main mineral constituents of South African coal are quartz (SiO_2) and kaolinite ($Al_2O_3.2SiO_2.2H_2O$). Other mineral constituents include dolomite (Ca, $Mg(CO_3)_2$), calcite ($CaCO_3$), gypsum ($CaSO_4.2H_2O$), pyrite (FeS_2) and siderite ($FeCO_3$) [8]. These constituents undergo various physical and chemical changes during the combustion process of the pulverised coal, which, in turn, has an influence on the chemical composition of the fly ash produced.

2.2 Particulate Matter Emissions

The South African Air Quality Act defines air pollution and any change in the composition of the air caused by smoke, soot, dust (including fly ash), cinders, solid particles of any kind, gases, fumes, aerosols and odorous substances [37]. Particulate matter refers to the solid matter contained in the gas stream, in the solid state, as well as the insoluble and soluble solid matter entrained droplets in the gas stream [38]. Globally, particles are reported in terms of two size ranges. Particles with diameters ≤ 10 µm are classified as PM_{10}, while particles with diameters ≤ 2.5 µm are classified as $PM_{2.5}$. The $PM_{2.5}$ is a subset of the PM_{10} data [38].

The particulates sized ≤ 2.5 µm can remain airborne for long periods and can travel long distances from the source, while the range of settlement for the larger particles is closer to the source [38]. Primary particles refer to particles that are released directly into the atmosphere, such as dust or elemental carbon from the combustion source, while secondary particles are the term used to describe particles that have formed as a result of chemical reactions [38]. These particles can form away from the sources that release the precursor gases with examples such as sulphates which form from sulfur dioxide emissions from power plants and industrial facilities or nitrates that are formed from nitrogen oxides released from power plants and other combustion sources [38]. Due to the size of particulate matter, it can enter the respiratory system of those exposed to it through inhalation. The $PM_{2.5}$ particles pose a higher risk factor than larger particles [39].

Studies have shown that these oxides and heavy metals in the fly ash can cause respiratory diseases, cancer, heart failure and immunological reactions in humans [1, 40]. Fly ash that is transferred with the flue gas exiting the smoke stack, eventually settle on water or ground surfaces leading to contamination of the environment.

2.3 Electrostatic Precipitators

Emission abatement technologies are installed at Eskom coal-fired power generating units, one of them being electrostatic precipitators [11, 20, 41]. An electrostatic precipitator uses electrical forces to transfer the particles out of the flowing gas stream (flue gas) which exits the boiler, onto collector plates [42].

There are various types of electrostatic precipitators, namely the plate-wire precipitator, the flat-plate precipitator, the tubular precipitator, the wet precipitator and the two-stage precipitator [42]. The plate-wire precipitator is the most common type; it is used in coal-fired boilers, as well as

elsewhere (cement kilns, solid waste incinerators and paper mill recovery boilers) [42]. In the plate-wire electrostatic precipitator, high-voltage electrodes in the form of long wires are hung between parallel metal plates. The flue gas stream flows between the plates and particles come into contact with the electrodes [42]. The area between the plates is referred to as an electrical field [20]. A voltage is applied to the electrodes, which causes the air to break down electrically, generating ions. This is known as 'corona' (Section 1.1). The electrons attach themselves onto the suspended dust particles in the flue gas stream [20]. The charged particles migrate towards and adhere to the positively charged collecting plates due to the electrostatic attraction. To remove the particles from the plates, a 'rapping' mechanism is used to dislodge the particles from the plates into collection hoppers [42]. During the dislodging process, some of the collected dust particles re-enter the flue gas stream (typically 12 %). This is termed 're-entrainment' [42].

2.4 Fly Ash Resistivity

Fly ash resistivity is the primary parameter in the operation of electrostatic precipitator performance [20, 26, 43]. The electrical resistivity of the fly ash is a result of the conductivity of the ionic species contained within the ash particles (oxides, silicates and other inorganic compounds) [26]. Besides the fly ash chemistry, the temperature of and the moisture within the gas stream influence the resultant conductivity in the electrostatic precipitators [26]. The fly ash resistivity is the inverse of the measurement of the ability of the particulate matter to accept and retain the charge gained as it passes through the electrostatic precipitator [44].

In electrical systems, Ohm's law is used to determine resistance by the following equation:

$$R = \frac{V}{I} \qquad 2\text{-}1$$

where R is the sample resistance, V is the applied voltage and I is the measured current. The resistivity was calculated using Ohms law, multiplied by a factor (A/d) which relates to the type and dimensions of the electrode used. The resultant equation to determine the resistivity of the sample is as per equation 2-2.

$$\rho = R \ \frac{A}{d} \qquad 2\text{-}2$$

Where ρ is the resistivity, d is the depth of the ash and A is the surface area of the electrode in contact with the ash.

Electrostatic precipitators provide optimum ash removal within a fly ash resistivity range. Too high resistivity will result in back-corona within the electrostatic precipitator (resulting in the collected dust particles being dislodged from the plates and becoming re-entrained into the flue gas stream), while too low resistivity results in the fly ash not being able to retain the charge long enough for it to be removed by the electrostatic precipitator. The desired resistivity range for efficient electrostatic precipitator operation is 1×10^8 to 1×10^{11} Ω-cm [20, 45]. If the fly ash resistivity is too high (1×10^{12} to 1×10^{14} Ω-cm), the particles are held too tightly onto the collecting plates and the charge is not conducted to the ground. If the fly ash resistivity is too low (1×10^4 to 1×10^7 Ω-cm), the dust easily conducts its charge to the ground, however, there is insufficient residual charge to remain on the plates [45].

The fly ash resistivity is influenced by the sulphur content of the coal, the flue gas temperature, the moisture content of the flue gas, the composition of the fly ash, as well as the particle size of the dust particles [12, 19, 46].

2.4.1 Effect of sulphur content

The process of coal combustion results in the conversion of the sulphur to SO_2, with a fraction being converted to SO_3. The reaction with water vapour in the flue gas stream results in sulphuric acid vapour (H_2SO_4), which absorbs onto the ash particles, thereby increasing the surface electrical conductivity and reducing the fly ash resistivity [13, 24, 47]. Coals with low sulphur content results in low fly ash resistivity. A coal sample is regarded as having a low sulphur content if the content is less than 1 wt.%, a medium sulphur coal contains 1–2.5 wt.% sulphur and a coal with high sulphur content contains greater than 2.5 wt.% sulphur [46]. The South African fly ash samples from most of the Eskom power plants have been determined to have low sulphur content (0.5–0.7 %) [12, 47]. Ash from the combustion of South African coal has been classified as being highly resistive [47].

2.4.2 Effect of temperature

Irrespective of the fly ash composition, the flue gas temperature has an effect on fly ash resistivity. For ascending resistivity measurements (temperature raised from approximately 80 °C to 350 °C), the resistivity measurements show an increasing trend up to about 120 °C [12, 15, 20, 47, 48]. This is attributed to the moisture that is adsorbed onto the fly ash particles at room temperature, which is driven off as the temperature is increased, resulting in an increase in the fly ash resistivity [26, 46]. The resistivity influenced under these conditions is referred to as surface

resistivity [26, 46]. The surface resistivity is attributed to the moisture or adsorption of chemical species on the fly ash particles, forming a conductive film [46].

Following peak resistivity measurement at approximately 120 °C, there is a steady decrease as the temperature is increased [12, 15, 20, 47, 48, 49]. Once the moisture is lost from the ash particles, the ionic conductivity increases as a result of the cations within the ash particles, resulting in a decrease in the fly ash resistivity [15, 26, 46]. The resistivity influenced by the chemical composition of the fly ash particles and the ability to conduct the applied current through the bulk volume of the fly ash is referred to as volume resistivity [15, 26, 46].

2.4.3 Effect of moisture

Moisture affects the surface resistivity by adsorbing onto the fly ash particles and forming a thin conductive layer through which the transfer of electrons takes place along the surface of the fly ash particles [15, 46]. The moisture is driven off the ash particles at temperature of approximately 120 °C. Fly ash resistivity is influenced by the amount of moisture in the flue gas stream—there is a decrease in resistivity as the amount of moisture increases [15].

2.4.4 Effect of composition of the fly ash

The mineral constituents of the coal used in the combustion process influences the fly ash composition. The main constituents of all coal ash are oxides of silica, aluminium, iron, calcium, magnesium, sodium, potassium and titanium [46]. High concentrations of silica, alumina and iron in the fly ash makes the surface of the fly ash glassy, which then affects its adsorption capability and its response to the use of conditioning agents [46, 48]. Sodium and potassium in fly ash serve as ionic contributors, as well as the principal charge carriers for volume resistivity, while the calcium absorbs the SO_3 [15, 45, 48]. The iron oxide exhibits the property of increasing the solubility and mobility of the alkali ions [48].

2.4.5 Effect of particle size

Fine fly ash particles have a larger surface area than course particles, hence the available contact area for electron transfer is increased. This, in turn, results in a decrease in fly ash resistivity (temperatures less than 120 °C) [15, 45]. Coarse particles are indicated to improve volume resistivity (temperatures greater than 150 °C) because of the larger diameter and reduced porosity resulting in larger volumes for electron transfer. This results in a reduction in volume resistivity [15].

2.5 Improving Fly Ash Resistivity

Although the above-mentioned influences and characteristics of the coal that is burnt are taken into consideration during the initial design of the electrostatic precipitators, fly ash resistivity efficiency may require improvement / enhancing during the operating life of the power plant. The need for optimisation may be as a result of deviations in the coal quality, combustion process or air quality legislation [16, 40, 45].

2.5.1 Electrostatic precipitator performance improvement through design and operational changes

The physical properties that influence the collection efficiency of fly ash particles within the electrostatic precipitator include the flue gas temperature, the velocity of the gas, the surface area of the collection plates and the electrical charge applied [20, 46, 50]. A reduction in the flue gas temperature from 120–130 °C to 90–95 °C results in increased particulate matter removal, attributed to the fly ash particles aggregating and adhering to the coarse particles and creating a larger surface area for the SO_3 to condense, with or without SO_3 injection [51]. Reducing the velocity of the flue gas increases the residence time of the fly ash particles within the electrostatic precipitator, allowing more time for the charged particles to migrate to the collecting electrodes [44]. Increasing the surface area of the collecting plates has the same influence as reducing the flue gas velocity in that the time available for collection of the charged ash particles is increased.

2.5.2 Electrostatic precipitator performance improvement through fly ash physiochemical adjustments

2.5.2.1 Moisture conditioning

The moisture in the flue gas improves the surface resistivity of the fly ash by being adsorbed onto the ash particles, forming a thin conductive film [13, 46]. The injection of water or steam is also observed to reduce the flue gas temperature [13]. Resistivity measurements taken without the introduction of moisture show a linear relationship between the log of the resistivity measurements and temperature [12, 47]. When moisture was introduced, a reduction in the resistivity measurements was observed for temperatures below about 150 °C for the ascending temperature measurements [12, 15, 20, 24, 46]. As the moisture percentage increased (by volume in relation to gas flow rate), the resistivity measurements decreased for the surface resistivity range [15]. At

temperatures greater than 200 °C, the effect of moisture is reduced and the resistivity measurements coincide with those of the dry resistivity measurements [15].

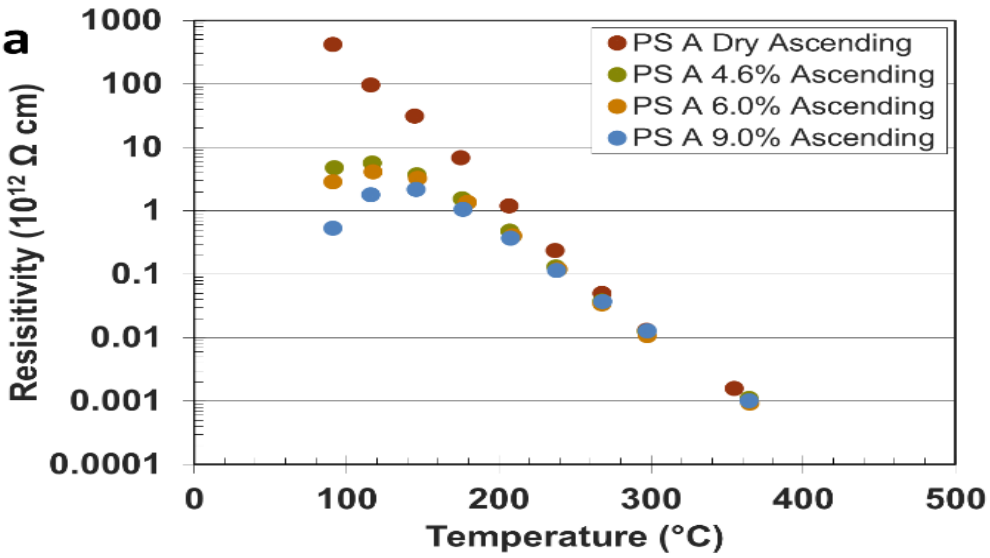

Figure 2-1: Graph showing influence of moisture on fly ash resistivity (taken from [15])

The application of flue gas conditioning agents (chemical additives) to adjust the chemical composition of the fly ash particles has been investigated, together with the mechanism responsible for the improvement in fly ash resistivity, by various researchers [13, 14, 25, 45, 46, 53]. Different chemicals added to the flue gas improve the electrostatic precipitator collection efficiency by either adsorbing onto the ash surface, thereby reducing the surface resistivity, or changing the adhesion and cohesion properties of the ash, increasing the mean particle size, changing the acid dew point in the flue gas, increasing the particles concentrations of the fines to enhance the space charge or increasing the electrical breakdown strength of the flue gas [25].

2.5.2.2. Sulphur trioxide conditioning

Sulphur trioxide is the most common chemical used as a conditioning agent for the reduction of high resistivity fly ash particles [12, 22]. The first commercial application of SO_3 as a conditioning agent was implemented in 1960 in Scotland [52] and is still used today. SO_3 conditioning is suitable for coals/fly ash containing low concentrations of naturally occurring sulphur, as it increases the fly ash resistivity from the low resistivity values [54]. The effect of SO_3 conditioning is more pronounced at higher temperatures, when compared to moisture conditioning, due to the

lower vapour pressure of the resulting H_2SO_4 that is formed [47]. The fly ash resistivity measurements improve with increasing concentrations of SO_3 added (by mass percentage), however the temperature at which the reduction occurs differs [47]. For temperatures greater than 200 °C, concentrations of SO_3 in excess of 20 ppm result in fly ash resistivity measurements within the optimum electrostatic precipitator operating range, whereas at 170 °C, the injection of a 10 ppm SO_3 concentration sample give resistivity measurements within the optimum electrostatic precipitator range.

2.5.2.3 Sodium conditioning

Sodium has been identified to be a charge carrier for ionic conduction for both surface and volume resistivity [12]. Sodium carbonate (Na_2CO_3), sodium sulphate (Na_2SO_4), sodium hydroxide (NaOH) or sodium nitrate ($NaNO_3$) are the conditioning agents used to modify the sodium content of the ash, and lead to a reduction in the fly ash resistivity [13, 55]. Sodium chloride (NaCl) is not a suitable conditioning agent or source of sodium because of the corrosive nature of the chloride on the metallurgy within the electrostatic precipitator system [14]. It was found that the addition of the sodium source with the coal feed prior to the combustion process has the same effect on the fly ash composition as combusting coal with a high sodium content [14]. Sodium concentrations (expressed as Na_2O) of about 1 wt.% in the ash were found to be sufficient to reduce the fly ash resistivity to within the required electrostatic precipitator operating range [17].

2.5.2.4 Ammonia conditioning

Not all fly ashes respond to conditioning agents that adsorb onto the ash particulates to reduce the fly ash resistivity because of the high content of silica, alumina and iron [13]. These components reduce the capability of the ash particles to adsorb the conditioning chemicals because they form a glassy layer around the ash [13]. Ammonia conditioning has been found to result in larger fly ash particles by the creation of a sticky layer on the ash at higher temperatures (greater than 150 °C), causing the ash particles to adhere to each other [13] or to the collector plates [56]. The larger particles result in an improvement in collection efficiency because re-entrainment is limited after rapping, as a result of the dense particles [13, 48]. Ammonia has also been utilised in applications where the fly ash resistivity is too low. The ammonia reacts with the excess SO_3 in the fly ash, thereby increasing the fly ash resistivity [56].

2.1.1.5 Other conditioning additives

Various additives have been tested as conditioning agents for improved fly ash resistivity, cohesion of the ash particles or electrostatic precipitator collection efficiency. In the early 1940s, triethylamine was evaluated, without success; however, studies conducted around 1980 indicated significant improvement in fly ash resistivity with high resistivity ash [25]. Triethylamine decomposes at approximately 90 °C to form ammonia, hydrogen cyanide and nitrogen—it was subsequently found to be effective in fly ash resistivity [25].

Naturally occurring products and compounds that are utilised in the food and cosmetic industries in the United States, such as surfactants, adhesives, polymer resins, foams and emulsions, were evaluated for their contribution to fly ash resistivity any improvement in the cohesion of ash particles [18]. These products were considered because of low toxicity and hence should not impact fly ash utilisation [56].

Additives that are hydrates or hydrate-forming compounds were considered and evaluated as a means of influencing the moisture effect in the fly ash [56]. Salts of sodium, potassium, aluminium, calcium, magnesium, zinc and iron contain hydrates [57]. Some chemicals adsorb water onto the surface or include the water molecules in their structures, such water bonds with the ions, here the terminology ‘hydrates’ and ‘water of crystallisation’ applies [57]. The moisture within the hydrate or the water of crystallisation remains within the chemical compound beyond the boiling point of water, and the moisture is only released at the melting point of the organic compound to which it is bound. The result is that the effect of moisture conditioning is gained at higher temperatures [56].

2.5.3 Saline solutions with fly ash

Earlier research was conducted at North-West University utilising a synthetic saline solution (i.e., laboratory chemicals, including sodium chloride and sodium sulphate were added in concentrations to simulate the major constituents of a saline solution generated at a South African power station) to determine the influence on fly ash resistivity for ash samples conditioned with the saline solution [53]. The latter solution comprised predominantly sodium, which resulted in an increase in the sodium concentration of the ash samples that were prepared [53]. The raw ash was immersed in the prepared saline solution for a period of 30 min to allow adsorption of the components of the solution onto the ash particles and prevent the chemical components leaching from the ash into the solution, because extended contact time results in leaching as determined

by studies explained below [53, 58]. The X-ray fluorescence analysis of the dried, conditioned samples showed an increase in the sodium content of the conditioned ash samples compared with the unconditioned samples [53]. The wt. % of sodium achieved in PS-1 and PS-2 conditioned ash samples were 1.2 and 0.97 respectively [53].The results revealed an inverse relationship between the moisture percentage (by volume with the gas flow) and the fly ash resistivity measurements, i.e., the fly ash resistivity was lower with high moisture content [53]. However, the resistivity results obtained were not within the optimum range for efficient electrostatic precipitator performance [53].

Studies were also conducted by researchers at the University of the Western Cape—they investigated the interaction of saline solution with ash on a dry ash disposal facility [58]. The saline solution was utilised for dust suppression on the ash disposal facility and sprayed onto the ash particles to prevent airborne dust emanating from the dump. Tests were conducted on the fly ash samples that were immersed in the saline solution under atmospheric conditions for varying lengths of time (between 1 week to 1 year) [58]. The objective of the research was to determine the exchange of chemical compounds between the ash and saline solution over time [58]. The saline solution was analysed after soaking to determine the chemical constituents that leached from the ash into solution. The ash was strained and dried in an oven at 50 °C before performing X-ray diffraction analysis to determine the change in elemental composition [58]. Results showed that there was an exchange of ions both from the saline solution to the ash particles as well as from the ash to the saline solution. Some of the ions found to leach from the ash into the saline solution were aluminium, silica, calcium and iron [58]. X-ray diffraction analysis of the dried ash after the soaking time indicated that high concentrations of sodium and sulphur ions had adsorbed onto the ash particles, and the concentration of sodium ions on the ash increased with the soaking time in the saline solution [58]. Analysis of the decanted saline solution post-soaking times showed that the sodium, chloride and sulphur from the saline solution decreased proportionally with the increased soaking times [58]. The research concluded that sodium, chloride and sulphate adsorbed onto the ash particles over various periods of contact times [58].

The concentration of salts in the reverse osmosis reject stream (saline solution) is dependent on the quality of the desalination plant feed water [64]. The typical total dissolved solids concentration of the reject stream from treating brackish water with a total dissolved solids concentration of 5 000–15 000 mg/l is approximately 10 000–75 000 mg/l, while that of the saline stream from a reverse osmosis plant treating sea water is approximately 60 000–80 000 mg/l [65]. The feed water to the reverse osmosis plant at Eskom is brackish water and the total dissolved solids of

the reject stream is within the range of other plants treating similar water [27]. Although the salts found in the reject stream depend on the composition of the feed water, many reject streams are reported to contain salts of sodium, typically NaCl, sodium bicarbonate ($NaHCO_3$) and Na_2CO_3, which may be recovered for beneficial use [65].

2.6 Determining Fly Ash Resistivity

Fly ash resistivity can be determined either by utilising an empirical laboratory method, requiring a resistivity oven and ash samples, or theoretically, using predictive models (derived from experimental work) using ash composition analysis.

2.6.1 Laboratory measurement

The method adopted for the laboratory measurement of fly ash resistivity is as per the requirements of the IEEE Standard 548 of 1984 [59]. The laboratory resistivity measurement is based on the ratio of the applied electric field across the layer of a fly ash sample to the induced current density. The resistivity is dependent on the temperature, composition of the gaseous environment (moisture or H_2SO_4 vapour), the applied electric field strength and the porosity of the ash layer. The procedure requires the assessment of repeatability and cross-laboratory confirmation as a means of validation of the results obtained [59]. During the test, a resistivity cell current across the ash sample in the bowl is measured and a total of 12 readings is recorded. The bowl is the term used to refer to the round, 5 mm deep, stainless steel dish that contains the ash sample on which the electrode rings are placed (Figure 4-3). An average of 12 readings is taken of the current across the ash sample. Challenges experienced with the laboratory method include maintaining the environmental conditions consistently for the entire duration of the test, specifically the moisture concentration.

The resistivity can then be calculated using the following formula,

$$\rho = \frac{A}{L}\ \frac{V}{I} \qquad \text{2-3}$$

where A is the cross-section area of the conductor, L is the conductor length, V the electrical potential applied and I the measured current flow (Figure 4-2, 4-3, 4-4).

2.6.2 Predictive models

In the 1970s, Roy E. Bickelhaupt at the Southern Research Institute (Alabama, USA), researched and developed an empirical model, involving parameter fitting to predict fly ash resistivity from

coal ash samples. The need for the research was based on acquiring the information to enable the optimum design of electrostatic precipitators. The objective of the research included determination of the ability to predict the fly ash resistivity for alternative fuel sources once the electrostatic precipitator was constructed [60]. The model, developed in 1979, was, however, based on tests conducted on fly ash samples from North America [60]. The mineralogy of the North American ash deviated from that of the South African ash samples analysed in this study. The sodium content of the coal ashes utilised in the development of the Bickelhaupt model were found to be higher than PS-1 and PS-2 coal ash samples, together with the iron, manganese, calcium and potassium [12, 60]. Aluminium and silicon were also seen to be the main elements that influenced the Bickelhaupt model developed [12, 60]. Results of that research revealed that the fly ash resistivity was inversely proportional to the combined molecular concentration of sodium and lithium and that the alkali metal ions serve as the charge carrier responsible for surface conduction [61]. A relationship between the concentrations of lithium, sodium, iron, calcium and magnesium in the fly ash, the moisture levels and SO_3 concentrations, was obtained, and formed the basis for the model that was developed.

The formula for the volume resistivity is the same for both models, as per equation 2-4.

$$\rho_v = \exp[\mathrm{A}_1\, lnX - \mathrm{B}_1\, lnY + \mathrm{C}_1\, lnZ + \mathrm{D}_1) - (\mathrm{F}_1)E + \frac{\mathrm{G}_1}{T}] \qquad 2\text{-}4$$

where A_1 = -1.8916, B_1 = 0.9696, C_1 = 1.237, D_1 = 3.62876, F_1 = 0.069078, G_1 = 9980.58 are the constants applied and the variables X is the atomic molar fraction of sodium in the ash sample, Y is the atomic concentration of iron, Z is the atomic molar fraction of the sum of magnesium and calcium ions, E is the electrical field strength applied to the ash sample and T is the temperature in °Kelvin.

The formula for surface resistivity for the original model and in the later model when the sum of the atomic concentrations of magnesium and calcium ions is less than or equal to 10, is given by equation 2-5.

$$\rho_s = \exp[\mathrm{A}_2 - \mathrm{B}_2\, lnX - \mathrm{C}_2(H_2O) - \mathrm{D}_2E - \mathrm{F}_2(H_2O)(\exp\left(\frac{\mathrm{G}_2}{T}\right)] \qquad 2\text{-}5$$

where A_2 = 27.59774, B_2 = 2.233348, C_2 = 0.00176, D_2 = 0.069078, F_2 = 0.00073895, G_2 = 2303.3 are the constants applied and the variables X is the atomic molar fraction of sodium in the ash

sample, H_2O is the volume percent of moisture added, E is the electrical field strength applied to the ash sample and T is the temperature in °Kelvin.

The model was later revised (1980–1985), as a result of the observation of increased sensitivity to moisture for ash samples having high calcium and magnesium concentrations [61] with the formula for the surface resistivity modified as indicated in equation 2-6.

$$\rho_s = \exp\left[A_3\, lnX - B_3(H_2O - 9) + C_3 Z - D_3(E - 2) + F_3(H_2O)\exp\left(\frac{G_3}{T}\right)\right] \qquad 2\text{-}6$$

where A_3 = 10.7737, B_3 = 0.128, C_3 = 0.056, D_3 = 0.03, F_3 = 0.000320924, G_3 = 2303.3 are the constants applied and the variable X is the atomic molar fraction of sodium in the ash sample, H_2O is the volume percent of moisture added, Z is the atomic molar fraction of the sum of magnesium and calcium ions, E is the electrical field strength applied to the ash sample and T is the temperature in °Kelvin.

The combined contribution of the volume and surface resistivity ,ρ_{vs}, is determined using equation 2-7.

$$\rho_{vs} = \frac{\rho_v \rho_s}{\rho_v + \rho_s} \qquad 2\text{-}7$$

where ρ_v is the volume resistivity determined by equation 2-4 and ρ_s is the surface resistivity determined by equation 2-5 or 2-6.

Further research was conducted between 1980 and 1984, specifically on an effect known as sodium depletion, which affects the volume resistivity of the fly ash particles [62]. Results of this research confirmed that, for power plants where the electrostatic precipitator is installed upstream of the air heater, the temperature in the electrostatic precipitator is higher than when installed downstream of the air heater, and the operating conditions are such that the resistivity is independent of the effect of water vapour or H_2SO_4 vapour [63]. Sodium depletion is explained as the phenomenon that occurs as a result of the thin ash layer that forms and adheres onto the electrostatic precipitator collection plates because of the inherent resistivity [62]. The alkali metals within this ash layer (e.g., sodium) serve as the charge carrier through the ash layer, improving the volume resistivity of the ash particles. Over time, the migration of sodium ions to the collection plate results in the fly ash layer that is formed on the collection plate becoming depleted of the

sodium ions, thereby causing an increase in the fly ash resistivity [61]. Although this phenomenon is known for hot-side electrostatic precipitators (electrostatic precipitator installed upstream of the air heater), there is some evidence that cold-side electrostatic precipitators (electrostatic precipitator installed downstream of the air heater) may also experience sodium-depletion, especially where there is little or no SO_3 present in the flue gas. The predictive model was updated in 1984 as per equation 2-8

$$\rho_{dep} = \exp\left[-7.3759 + 1.0412 ln\rho_v + \frac{4788.1}{T}\right] \quad 2\text{-}8$$

where ρ_{dep} is the modified value for the volume resistivity, ρ_v is the volume resistivity determined by equation 2-4 and T is the temperature in °Kelvin.

The combined contribution of the modified volume and surface resistivity ,ρ_{vsd}, is determined using equation 2-9.

$$\rho_{vsd} = \frac{\rho_{dep}\rho_s}{\rho_{dep} + \rho_s} \quad 2\text{-}9$$

where ρ_{dep} is the modified volume resistivity determined by equation 2-8 and ρ_s is the surface resistivity determined by equation 2-5 or 2-6.

The initial Bickelhaupt model was tested on 35 different coal ash samples from America and Canada, and two samples from Australia—it was found to be favourable in being able to predict the resistivity of the ash samples [61]. Analyses indicated that for high-sulphur coals the deviation between the predicted and measured resistivity values was approximately 1.1 order of magnitude and for low-sulphur coals approximately 0.7 order of magnitude [61]. Caution should be exercised, however, when utilising the Bickelhaupt model for ash samples where the mineral composition differs from the ash utilised in the development of the model.

The original version of the model was tested on coal ashes from Indian power plants. Here, the Bickelhaupt model was found to be unsuitable in terms of predicting the resistivity of the coal ash generated from these power plants in that the parameters were unable to achieve the required fit to the measured data [48]. This was attributed to the differences in the concentrations of sulphur (as SO_3), lithium (as LiO_2) and sodium (as NaO_2), as well as the alumina (as Al_2O_3) and silica (as

SiO_2), between the coal ashes from North America (upon which the Bickelhaupt model was based) and the Indian coal ash [48]. The model was later modified to achieve an improved correlation between the measured and predicted resistivity measurement of the Indian ashes [48].

The Bickelhaupt model was also found to be unsuitable to predict fly ash resistivity for South African ashes, after being evaluated and modified by previous studies on the similar ash samples with moisture conditioning, SO_3 conditioning or synthetic saline solutions [12, 15, 47, 53]. The basic structure of the model appeared to be valid in the shape and form of the data under varying temperatures, however the parameters did not offer a suitable fit to the measurements obtained. The reasons hypothesised for the variations include the following: South African fly ashes contain very low quantities of lithium compared with American ashes, the forms in which the calcium and magnesium is found in South African ashes differs from those in the North American ashes [12], and the South African ashes have a low sodium content [15, 47].

CHAPTER 3 FLY ASH SAMPLE PREPARATION AND CHARACTERISATION

In this chapter, the rationale for the ash samples selected and the chemical constituents of the saline effluent solution (Section 3.1) are discussed. In Section 3.2, an explanation of the method used to determine the mixing ratio of the conditioning agent with the ash, and calculations is provided. Section 3.3 describes calculations used to confirm the resultant moisture addition required during experiments. Chemical analysis of the raw and conditioned ash samples, particle size distribution and quantitative evaluation of minerals by scanning electron microscopy of the ash samples are discussed in Sections 3.4, 3.5 and 3.8. Thermogravimetric and proximate analysis results are presented in Sections 3.6 and 3.7.

3.1 Sample Selection and Preparation

3.1.1 Fly Ash Samples

The impact of conditioning the fly ash with the waste saline solution is of interest at PS-1 where the saline solution is produced. Fly ash samples from a second power station (PS-2) were selected as a benchmark in order to determine the effect of the fly ash composition on the test results and minimize any systematic bias towards a preferred ash sample. PS-2 was selected because it also operates a desalination plant where a waste saline solution is generated with the potential for future use as a flue gas conditioning agent. The source of coal for PS-1 is from an underground Highveld coalfield in Mpumalanga, while the coal for PS-2 is sourced from an opencast Sasol coalfield in the Free State [15]. Fly ash samples (approximately 3 kg each) were obtained from the ash hoppers from both power stations, whilst the power stations were online, in the absence of any flue gas conditioning [12]. As per IEEE requirements, the ash was sieved through 180 µm screens to remove any foreign objects and larger fly ash particles, then stored in sample bags [15]. Hereafter, the ash samples were thoroughly mixed for homogeneity. The ash samples were stored in air-tight bags in the laboratory cupboard at ambient temperature.

Previous research work on fly ash resistivity [12, 15, 47, 53] was conducted earlier, utilising samples from the PS-1 and PS-2, which now allows for a certain degree of comparison among the results and the impact of various conditioning agents and methodologies researched. Results from previous studies indicated that PS-2 fly ash has low ash resistivity and low particulate emissions levels, while PS-1 has medium to high resistivity and high particulate emission levels

[11, 12, 15]. However, the ash from both power stations was subjected to different flue gas conditioning agents: moisture, SO_3 and synthetic saline solutions.

3.1.2 Saline solution sample

PS-1 and PS-2 operate a desalination plant for the reduction of saline effluent on site. The process of the system installed at PS-1 is described. The feed water to the plant comprises cooling water blowdown and rundown mine water from the associated colliery. A typical water treatment process for the desalination of this feed water is indicated in the block diagram depicted in Figure 3-1. The desalination process is designed to treat a feed of 1041 m^3/hr with 87 vol.% of clean water (permeate) recovery. The treatment process involves lime softening for hardness reduction, followed by membrane-based microfiltration and reverse osmosis desalination processes. The permeate (total clean water volume produced of approximately 916 m^3/hr) is recovered back into the power station processes. The reverse osmosis reject stream (total saline solution volume produced of approximately 125 m^3/hr) is processed further in a secondary desalination system before final disposal in an evaporation pond.

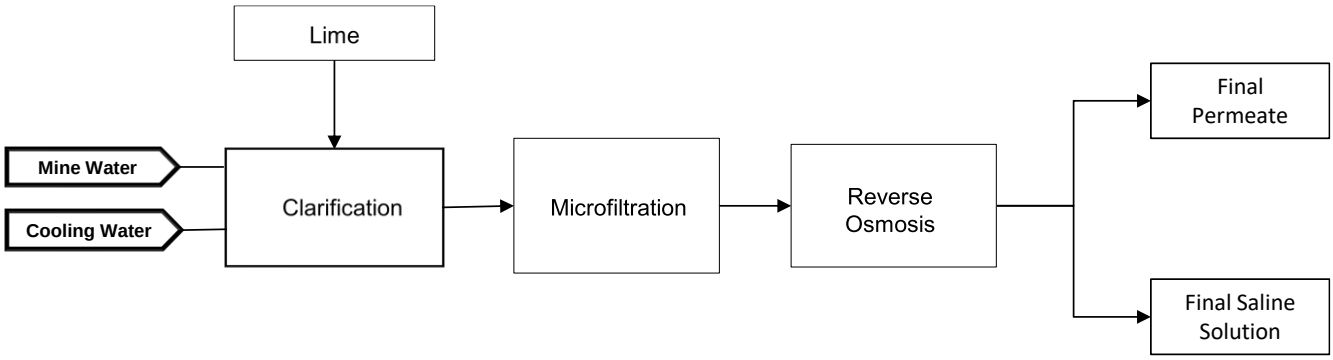

Figure 3-1: Block diagram of waste water treatment plant at PS-1 producing the reject saline waste stream

The reject saline solution stream from the primary desalination system is the saline solution that will be considered for re-purposing as a potential flue gas conditioning agent. A volume of the reject stream (1 litre) was sampled on the 04/09/2020, under stable, steady-state plant operation conditions from the final storage tank outlet where the reject saline solution stream has stabilised in terms of quality . The sample was kept cool (in ice) until it was analysed to prevent microbiological growth. Various analytical measurements were conducted on the sample obtained in order to characterise its physiochemical properties. Results of the chemical analysis of the

solution are tabulated in Table 3-1. The analysis was conducted by the laboratory personnel at Eskom's Research Testing and Development (RT&D) laboratory.

Table 3-1: Chemical analysis of saline stream produced at PS-1

Chemical parameter	Unit of measure	Value
pH		9.1
Conductivity	µS/cm	43 990
Total dissolved solids	mg/l	34 994
Total suspended solids	mg/l	365
Sulphate	mg/l as SO_4^{2-}	26 540
Sodium	mg/l as Na^+	11 370
Chloride	mg/l as Cl^-	4 986
Calcium	mg/l as Ca^{2+}	781
Magnesium	mg/l as Mg^{2+}	956
Potassium	mg/l as K^+	434
Ammonia	mg/l as N	1.8

From Table 3-1 it is evident that the predominant components of the reject stream are sulphate (as SO_4^{2-}), followed by sodium (as Na^+) and chloride (as Cl^-). This is an indication that the waste stream produced by the waste water treatment plant is mainly a Na_2SO_4 / NaCl solution. The pH of the sample indicates that it is alkaline and would not create acidic conditions within the flue gas stream.

3.2 Preparation of Conditioned Ash Samples

Use was made of the design information for the boiler and the flue gas at PS-1 to determine the conditions and concentrations for in situ injection and conditioning of the fly ash in the flue gas stream, and subsequently the conditioning ratio of saline solution to fly ash, to apply to the test samples.

Table 3-2 indicates the boiler design parameters and flue gas data for PS-1 at the unit load factors from 100 % to 60 % of the boiler maximum designed load output, i.e., the percentage of the average energy output of the total possible energy production.

Table 3-2: Boiler design parameters and flue gas data for PS-1

Parameters	Units	Values at indicated unit load factors (% maximum continuous rating)				
		100	**90**	**80**	**70**	**60**
Gas mass flow	kg/s	904.9	832.6	747.7	699.0	657.8
Dust flow (90 wt.% fly ash)	kg/s	23.7	21.2	18.6	17.1	14.6
Gas volume flow	Nm^3/s	682.7	628.8	565.1	528.6	498.9
Dust burden	g/Nm^3	34.7	33.7	32.9	32.3	29.2
Flue gas temperature	°C	169.0	161.7	154.4	146.4	129.8

Dust is typically composed of fly ash, soot, unburnt carbon, sand, extraneous minerals, etc. The flue gas mass flow rate varies as the unit load changes, together with a related change in the fly ash mass flow. The saline solution conditioning is injected at a fixed flow rate, hence the saline solution to ash ratio will change under varying load.

A saline solution injection rate of 5 m^3/hr (minimum) and 25 m^3/hr (maximum) was used in the calculations to establish the baseline for the experimental design.

In the heat transfer calculations, it is assumed that saline solution ends up with the same temperature as the flue gas stream. The volumetric flow rate of the saline solution was converted to mass flow rate using equation 3-1. The density of the saline solution was assumed to be similar to that of water at STP. The total dissolved solids of the saline solution stream was measured as 35 g/l (Table 3-1). The total mass of one litre of sample is therefore 1035 g, resulting in a density of 1.04 g/l which is approximately 1.0 g/l.

$$\dot{V}\rho = \dot{m} \qquad 3\text{-}1$$

where $\dot{V}$ is the volumetric flowrate of the saline solution, ρ is the density of the solution and $\dot{m}$ is the resultant mass flowrate.

The saline solution injection rate of 5 m^3/hr was determined to be equal to 1.4 kg/s and the 25 m^3/hr equal to 7 kg/s. These mass flow rates were used to calculate the weight ratio/mass fraction of saline solution to ash at the varying unit load factors in Table 3-2 using equation 3-2.

$$x_S = \frac{\dot{m}_s}{\dot{m}_{D,Ash}}\ 100\ \% \qquad 3\text{-}2$$

where x_S is the saline solution to ash ratio, $\dot{m}_s$ is the mass of the saline solution and $\dot{m}_{D,Ash}$ is the mass flowrate of the flue gas.

In field applications, the saline solution addition is done at ambient temperature (20 °C), hence it will influence the flue gas temperature. The acid dew point temperature of H_2SO_4 in the flue gas is approximately 120 °C, therefore, it is imperative that the injection of the saline solution will not cool the flue gas beyond this temperature [63].

A simplified heat balance was performed to determine the final flue gas temperature at the varying unit load factors. The heat of vaporisation was utilised to determine the moisture addition to the flue gas using equation 3-3 and 3-4.

$$Q_S = Q_g \qquad 3\text{-}3$$

Where Q_S is the heat gained by the saline solution and Q_g is the heat lost by the flue gas.

$$\dot{m}_S c_S \Delta T_S = \dot{m}_g c_g \Delta T_g \qquad 3\text{-}4$$

where $\dot{m}_S$ is the mass of the saline solution, c_S is the specific heat capacity of the saline solution and ΔT_S is the temperature change of the saline solution while $\dot{m}_g$ is the mass of the flue gas, c_g is the specific heat capacity of the flue gas and ΔT_g is the temperature change of the flue gas.

Using the saline solution flow rate of 5 m^3/hr followed by 25 m^3/hr , the final flue gas temperature and weight percentage of saline solution at the varying load factors were determined. The results of the calculations for the saline solution to ash ratio for the 2 flow rates—5 m^3/hr and 25 m^3/hr, at the 5 unit load factors, are tabulated in Table 3-3.

Table 3-3: Expected final gas temperature at saline solution injection rate of 5 m^3/hr and 25 m^3/hr

Parameters	Units	Values at indicated unit load factors (% maximum continuous rating)				
		100	**90**	**80**	**70**	**60**
Calculation results for saline solution injection rate of 5 m^3/hr						
Gas mass flow	kg/s	904.9	832.6	747.7	699.0	657.8
Dust flow (90% fly ash)	kg/s	23.7	21.2	18.6	17.1	14.6
Gas temperature	°C	169.0	161.7	154.4	146.4	129.8
Saline solution to ash ratio at saline solution injection rate of 5 m^3/hr (1.4 kg/s)	wt.%	6	7	8	8	10
Final gas temperature for 5 m^3/hr saline solution injection	°C	168.1	160.8	153.5	145.4	128.9
Calculation results for saline solution injection rate of 25 m^3/hr						
Gas mass flow	kg/s	904.9	832.6	747.6	699.0	657.8
Dust flow (90 wt.% fly ash)	kg/s	23.7	21.2	18.6	17.1	14.6
Gas temperature	°C	169.0	161.7	154.4	146.4	129.8
Saline solution to ash ratio at saline solution injection rate of 25 m^3/hr (7 kg/s)	wt.%	30	33	38	41	48
Final gas temperature for 25 m^3/hr saline solution injection	°C	163.4	155.9	148.3	140.3	124.2

To reflect the saline solution conditioning at an injection rate of 5 m^3/hr, ash samples conditioned to 5 wt.%, 8 wt.% and 10 wt.% saline solution were prepared. It is to be noted that the final flue gas temperature will theoretically drop below the acid dew point temperature at load factors less than 60 %.

To reflect the saline solution conditioning at an injection rate of 25 m^3/hr, ash samples conditioned to 20 wt.%, 30 wt.% and 35 wt.% saline solution were prepared. At ratios of mixing exceeding 40 wt.% moisture to 60 wt.% fly ash, there is a risk of forming a high-density fly ash slurry mixture which is not practical for the application being investigated, as this could result in caking within the flue gas ducting and precipitators [67]. The suggested saline solution mass to achieve the required ash / saline solution ratios were calculated and is shown in Table 3-4.

Table 3-4: Mass of fly ash and saline solution required for the conditioned ash samples

Total sample mass (g)	Saline solution mass (g)	Saline solution (wt.%)
105.3	5.3	5
108.7	8.7	8
111.1	11.1	10
125.0	25.0	20
142.9	42.9	30
153.9	53.9	35

Fly ash from a second power station (PS-2) was also prepared according to the saline solution loading procedure described in the previous paragraphs and summarised in Table 3-4 . Only the higher salt loading was selected (20 wt.%, 30 wt.% and 35 wt.%) to evaluate PS-2 ash samples because of the hypothesis that a more pronounced effect on fly ash resistivity measurements will be observed from the higher saline (or salt) addition.

Untreated and treated fly ash samples (from both PS-1 and PS-2) were air dried for a period of two weeks before being crushed in a pestle and mortar to ensure removal of any clumping. The samples were placed in a fume cupboard in the laboratory to prevent contamination during the air drying process, then stored in air-tight bags until required for the experiments. All the samples were done at the same time under the same ambient conditions. Samples were taken from the main dried ash sample prepared for the various tests to be conducted: X-Ray Fluorescence, QEMSCAN, thermogravimetric analysis, particle size distribution and proximate analysis. The sample bags were shaken thoroughly, manually, before withdrawing the required quantity of sample into sterile vials. The distribution of the 5 % conditioned ash sample for testing is indicated in Figure 3-2. The same methodology was applied to all prepared ash samples.

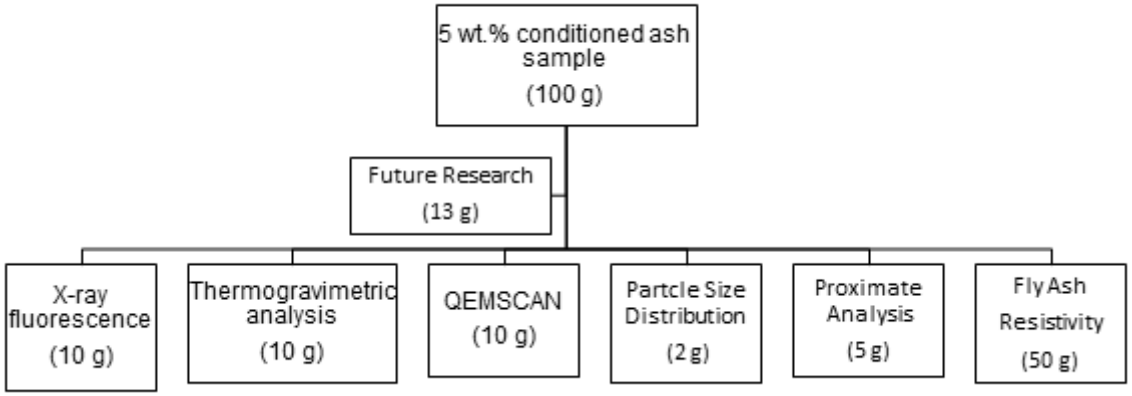

Figure 3-2: Distribution of prepared samples for analyses (all mass based on dry weight)

3.3 Influence of Saline Solution Injection on Flue Gas Moisture

The addition of the saline solution into the flue gas stream will result in additional moisture in the stream, hence it is important to know to what extent the injected saline solution will increase the moisture content. The ideal gas law was used to calculate the volume of water introduced with the saline solution [68].

$$V_{(water)} = \frac{n_{(Water)}\, R\, T}{P_{(system)}} \qquad 3\text{-}5$$

where $V_{(water)}$ is the volume of the water, $n_{(Water)}$ is the number of moles of water, R is the gas constant, T is the temperature of the flue gas stream and $P_{(system)}$ is the pressure of the system in the flue gas duct.

The resultant volumes of moisture added are given in Table 3-5 for the saline solution injection rate of 5 m^3/hr and 25 m^3/hr. The method for calculating the volume is given in Appendix A. The ratio of the moisture from the saline solution to the gas volume was also determined. The average moisture content in the flue gas is approximately 4 vol.% without any conditioning [15]. Therefore, with the inherent moisture of 4 vol.% and the maximum moisture addition from the saline solution being 3 vol.%, a moisture volumetric flow of 7 vol.% to air was utilised for fly ash resistivity measurements of the conditioned ash samples.

Table 3-5: Moisture influence from the saline solution at injection rate of 5 m^3/hr and 25 m^3/hr

Parameter	Units	Values at indicated unit load factor (% maximum continuous rating)				
		100	**90**	**80**	**70**	**60**
Calculation results for saline solution injection rate at 5 m^3/hr						
Saline solution to ash ratio (m/m) at saline solution injection rate of 5 m^3/hr (1.4 kg/s)	wt.%	6	7	8	8	10
Final gas temperature for 5 m^3/hr saline solution injection	°C	168.1	160.8	153.5	145.4	128.9
Volume of water added for 5 m^3/hr saline solution injection	m^3/s	3.4	3.4	3.3	3.2	3.1
Moisture % of saline solution: Gas volume flow	vol.%	0.50	0.53	0.58	0.61	0.62
Calculation results for saline solution injection rate at 25 m^3/hr						
Saline solution to ash ratio (m/m) at saline solution injection rate of 25 m^3/hr (7 kg/s)	wt.%	30	33	38	41	48
Final Gas Temperature for 25 m^3/hr saline solution injection	°C	163.4	155.9	148.3	140.3	124.2
Volume of water added for 25 m^3/hr saline solution injection	m^3/s	16.9	16.6	16.3	16.0	15.4
Moisture % of Saline solution: Gas Volume Flow	vol.%	2.48	2.64	2.89	3.03	3.08

3.4 Fly Ash Physiochemical Characterisation

The raw and conditioned ash samples were analysed using X-ray fluorescence, QEMSCAN and particle size distribution in order to determine the baseline composition (from the raw ash) and the changes that occurred after conditioning with the varying concentrations of the saline solution. The analysis also allowed a comparison between the ash samples from the two power stations. Thermogravimetric and proximate analyses were conducted on the raw and conditioned ash samples to determine the changes in mass during heating as well as the temperatures at which the changes occur

3.4.1 X-ray fluorescence analysis

X-ray fluorescence analysis was conducted at Bureau Veritas Testing and Inspection, in compliance with the ASTM D4326 X-ray fluorescence test method. X-ray fluorescence analysis

was used to provide an estimate of the elemental composition of each fly ash sample (raw and conditioned). Glass discs were prepared for analysis by mixing 6 g of flux—chemical used to dissolve the oxidised sample— (consisting of lithium tetraborate, $Li_2B_4O_7$, and lithium metaborate, $LiBO_2$, in a 2:1 weight ratio) with 0.6 g of ash sample in a 32-mm crucible. The crucibles were placed in an oven pre-set to 1050 °C and exposed to a heating cycle of 24 minutes. Melted samples were transferred to discs, which were then cooled. The cooled discs were analysed in the X-ray apparatus. The results of elemental composition results obtained from X-ray fluorescence analysis of the various samples are reported as elemental oxides (e.g., CaO or MgO) and expressed as weight percentages of the total sample amount. The results were normalised on a loss of ignition (LOI) free basis and subsequently converted to atomic concentrations. The elemental composition of raw and conditioned PS-1 ash samples is summarized in Table 3-6 and that for PS-2 ash samples in Table 3-7.

Table 3-6: X-ray fluorescence analysis of PS-1 ash samples

Elemental parameter	**Raw ash sample**	**5 wt.% sample**	**8 wt.% sample**	**10 wt.% sample**	**20 wt.% sample**	**30 wt.% sample**	**35 wt.% sample**
Al_2O_3	28.51	28.56	28.67	28.55	28.26	28.15	28.03
CaO	5.32	5.16	5.15	5.13	5.30	5.25	5.25
Cr_2O_3	0.04	0.08	0.08	0.09	0.04	0.04	0.04
Fe_2O_3	5.70	5.46	5.45	5.45	5.54	5.50	5.49
K_2O	0.68	0.72	0.71	0.71	0.70	0.69	0.72
MgO	1.40	1.37	1.37	1.37	1.32	1.35	1.37
MnO	0.04	0.04	0.05	0.04	0.04	0.04	0.04
Na_2O	0.14	0.23	0.30	0.34	0.50	0.65	0.79
P_2O_5	0.37	0.37	0.39	0.38	0.38	0.38	0.38
SiO_2	55.54	55.68	55.46	55.53	55.25	55.02	54.82
TiO_2	1.63	1.60	1.60	1.60	1.60	1.60	1.59
V_2O_5	0.02	0.03	0.03	0.03	0.02	0.02	0.02
ZrO_2	0.07	0.07	0.07	0.07	0.05	0.05	0.06
BaO	0.13	0.13	0.13	0.13	0.11	0.11	0.11
SrO	0.12	0.13	0.13	0.13	0.13	0.12	0.13
SO_3	0.30	0.38	0.42	0.46	0.75	1.02	1.16
Total	100.01	100.01	100.01	100.01	99.99	99.99	100

Table 3-7: X-ray fluorescence analysis of PS-2 ash samples

Elements	Raw ash sample	20 wt.% sample	30 wt.% sample	35 wt.% sample
Al_2O_3	30.00	29.69	29.49	29.46
CaO	4.46	4.44	4.41	4.40
Cr_2O_3	0.04	0.04	0.04	0.04
Fe_2O_3	3.60	3.59	3.55	3.54
K_2O	0.71	0.71	0.71	0.72
MgO	0.98	1.00	1.02	1.03
MnO	0.02	0.02	0.02	0.02
Na_2O	0.23	0.66	1.01	1.04
P_2O_5	0.36	0.35	0.35	0.35
SiO_2	57.56	57.01	56.66	56.46
TiO_2	1.56	1.55	1.53	1.53
V_2O_5	0.03	0.03	0.03	0.02
ZrO_2	0.05	0.05	0.05	0.05
BaO	0.09	0.09	0.09	0.09
SrO	0.10	0.10	0.10	0.10
SO_3	0.20	0.66	0.95	1.16
Total	99.99	99.99	100.01	100.01

The most significant change in concentrations with the increasing conditioning ratios were found for sodium and sulphur atoms (as highlighted in the tables above)—changes in sodium were most predominant (Figure 3-3). The other components remained relatively constant with the increasing amount of saline solution addition.

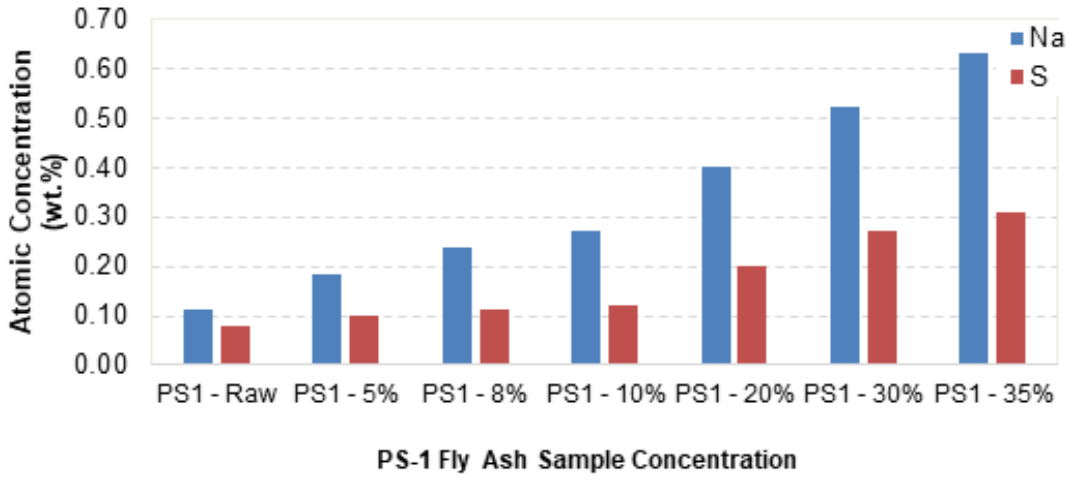

Figure 3-3: Sodium and sulphur atomic concentrations (LOI free basis) of PS-1 ash samples

The same trend was observed with PS-2 ash samples (Figure 3-4); however, here the concentrations of the sodium in the 30 and 35 wt.% samples were much higher compared with in PS-1. The reasons for this are discussed in Section 5.2 and Section 5.6.

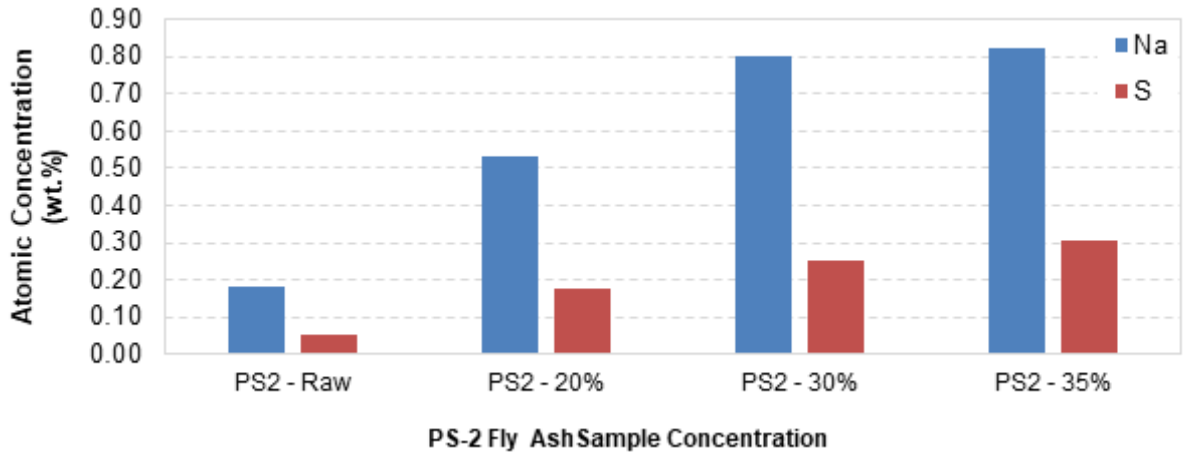

Figure 3-4: Sodium and sulphur atomic concentrations (LOI free basis) of PS-2 ash samples

3.4.2 Particle Size Distribution

The purpose of the evaluation was to determine whether or not the addition of the conditioning agent would increase the particle size of the fly ash particulates, and if this particle size distribution would influence the fly ash resistivity measurements obtained. The particle size distribution of the ash samples was determined using a Malvern Mastersizer 3000 at North-West University. The instrument uses laser diffraction to measure the particle size and the particle size distribution for a specific sample, by measuring the scattered light from a laser beam which passes through a flowing dispersed sample. The data is analysed by the instrument and calculates the size of the particles that created the scattering effect.

A beaker was filled with potable water, prepared by reverse osmosis—it was free of particulates greater than 0.0001 µm (the pore rejection size of the reverse osmosis membranes) [70]. Water was used as the medium for the fly ash samples because there was no risk of the ash particles dissolving in water. Silica was selected as the input requirements of the samples to be analysed by the instrument, the analysis model was selected as non-spherical and the medium was water. The ash sample was placed into the medium while being automatically stirred to keep the particles in suspension. Sufficient sample was added until the obscuration range was 10–20 %. Once this condition was met, the instrument was used to measure the sample. The instrument measures the sample three to six times before determining the average particle size. The results obtained

indicate the average size of the particles for which a defined percentage—10, 50 or 90— falls under: e.g., the volume distribution d(10) 6.43 µm is interpreted as 10 % of the particles in the sample are less than 6.43 µm, d(50) 35.8 µm indicates that 50 % of the particles in the sample are less than 35.8 µm, and d(90) 111.0 µm indicates that 90 % of the particles in the sample are less than 111.0 µm. This distribution of the particle size is indicative of the particle size distribution of the samples. The d(10), d(50) and d(90) results for the ash samples are plotted in Figure 3-5.

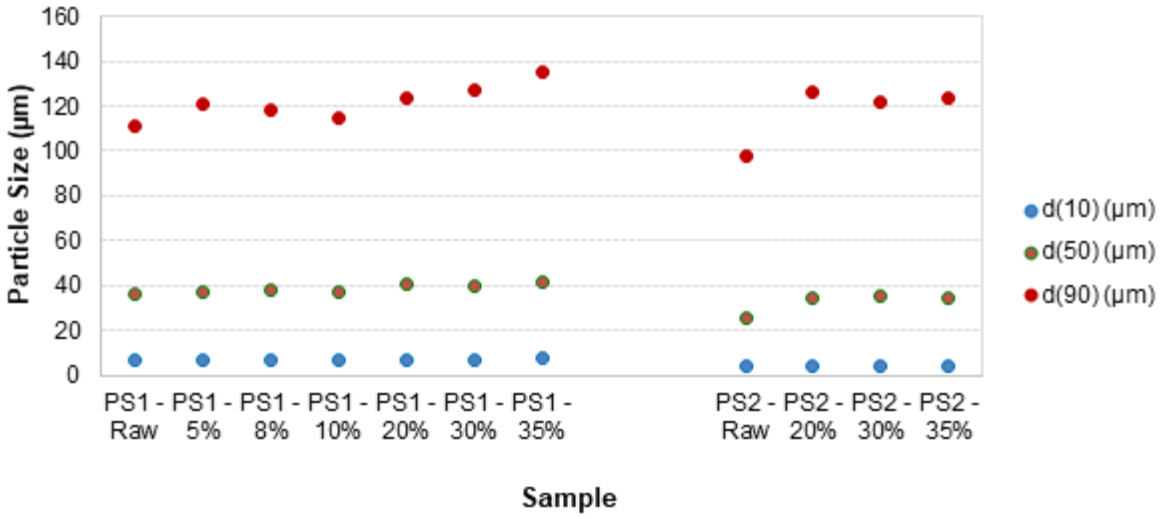

Figure 3-5: Particle size distribution of conditioned ash samples

A comparison of the ashes for both power station shows similar results, with the average particle size for all samples approximately 10 µm. The particle size of fly ash from China has been found to be in the range 0.3–250 µm, with the major fraction in the range 20–25 µm [71]. The fly ash particle size from PS-1 and PS-2 are within the range of the China ashes and the results showed that there was insufficient variation in the ash particle size distribution to determine if it was a factor influencing the resistivity. Fine ash particles improve surface resistivity while coarse ash particles show a reduction in volume resistivity (section 2.4.5).

3.4.3 Thermogravimetric Analysis

Thermogravimetric analysis or thermal gravimetric analysis is a method of thermal analysis in which the mass of a sample is measured over time as the temperature changes. Here, thermogravimetric analysis was conducted to determine any thermal anomalies that may be associated with the conditioning of the ash using the saline solution [72]. The thermogravimetric analysis was conducted using a SDT Q600 small particle thermogravimetric analysis instrument

at North-West University. All samples (each approximately 20 mg) were subjected to thermal analysis. Inert conditions were applied using argon gas at a flow rate of 75 ml/min, while the samples underwent heating from room temperature to 350 °C at a rate of 10 °C/min. The trends observed for the 5 % and 30 % conditioned samples are plotted in Figure 3-6, for the change in mass as a percentage (derivative weight %) with increasing temperature. A similar pattern was observed for all the ash samples considered in this study.

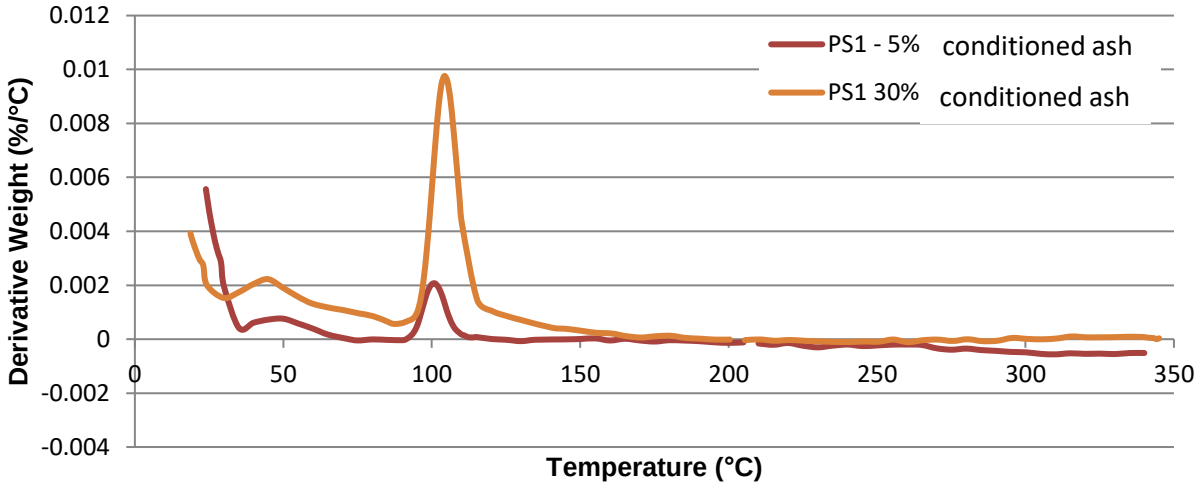

Figure 3-6: PS-1 ash samples: thermogravimetric analysis derivative weight comparison

An initial loss of mass is observed from ambient to up to about 45 °C due to loss of free moisture [73]. The highest rates of mass loss were observed at temperatures of 45 °C and 100 °C. The derivative weights recorded for these peaks for all the ash samples are tabulated in Table 3-8.

Table 3-8: Derivative weight at 45 °C and 100 °C for ash samples during thermogravimetric analysis

Ash samples	Mass loss (%) at 45 °C	Mass loss (%) at 100 °C
PS-1 unconditioned fly ash	0.001	0.001
PS-1 5 wt.% conditioned	0.001	0.002
PS-1 8 wt.% conditioned	0.001	0.002
PS-1 20 wt.% conditioned	0.001	0.006
PS-1 30 wt.% conditioned	0.002	0.010
PS-1 35 wt.% conditioned	0.001	0.011
PS-2 unconditioned fly ash	0.001	0.001
PS-2 20 wt.% conditioned	0.004	0.007
PS-2 30 wt.% conditioned	0.012	0.010
PS-2 35 wt.% conditioned	0.012	0.010

The mass loss at 45 °C is fairly consistent for PS-1 ash samples. This suggests that the initial loss of mass observed from ambient to up to approximately 45 °C is due to moisture loss from the ash samples [73] or hydrates of sodium salts [74]. This may apply to PS-2 samples because of the mass loss observed between the unconditioned and conditioned ash samples. However, the derivative weight measured at approximately 100 °C increased with an increasing volume of saline solution used to condition the ash samples. This then suggests the vaporisation of hydrates such as magnesium chloride ($MgCl_2 \cdot 6H_2O$) at a temperature of approximately 117 °C [75] and the dehydration of calcium chloride ($CaCl_2 \cdot 4H_2O$) at approximately 115 °C [76].

The mass loss for the unconditioned ash sample from PS-1 and PS-2 were similar (highlighted cells in Table 3-8); however, the mass loss of the conditioned ash samples for PS-2 ash samples was higher than that of PS-1 ash samples. This suggests that the ash samples (PS-2) absorbed more moisture from the saline solution, which vaporised at around 45 °C. The derivative weights recorded at 100 °C for PS-2 conditioned samples were the same as observed for PS-1 samples. This again indicates vaporisation of hydrates contained in the conditioned ash samples, for the same mass of saline solution added, at approximately 100 °C, as was observed for the conditioned PS-1 ash samples. Thermal stability was observed for all ash samples at temperatures greater than 150 °C.

3.4.4 Proximate Analysis

Proximate analysis was conducted to determine the percentage of volatile matter loss from the samples during a slow heating process, in the coal analysis laboratory at North-West University. Proximate analysis is performed to determine the ash content, volatile matter and moisture content of the sample [77]. The test is based on the following international methods.

Table 3-9: Standard methods for proximate analysis

Sample preparation	SANS 18283:2007 / ISO 18283:2006
Moisture content (wt.%)	SANS 5925:2007
Ash content (wt.%)	SABS ISO 1171:1997
Volatile matter content (wt.%)	SABS ISO 562:1998

The results of the proximate analysis for PS-1 and PS-2 raw and conditioned ash samples are presented in Table 3-10.

Table 3-10: Proximate analysis results (ash dry base) for PS-1 and PS-2 raw and conditioned ash samples

Saline solution percentage (%)	PS-1 % Moisture	PS-2 % Moisture	PS-1 % Volatile matter	PS-2 % Volatile matter	PS-1 % Ash	PS-2 % Ash
0	0.02	0.04	0.12	0.08	99.82	99.93
5	0.02	-	0.11	-	99.94	-
8	0.02	-	0.10	-	99.80	-
10	0.04	-	0.13	-	99.80	-
20	0.04	0.02	0.17	0.10	99.76	99.90
30	0.03	0.06	0.26	0.13	99.70	99.85
35	0.03	0.05	0.26	0.14	99.70	99.82

Results indicated that PS-2 ash samples contained more moisture that PS-1 samples as unconditioned ash and subsequently a higher percentage of moisture with an increase in percentage of saline solution added. This correlates with the thermogravimetric analysis results (Table 3-8) which indicates the higher mass loss between the conditioned and unconditioned ash samples from PS-2.

The volatile matter in the PS-1 raw ash samples exceed that of the PS-2 ash samples. The increase in the percentage of volatile matter with the higher conditioned ash samples suggests that the volatile salts were from the saline solution added.

3.4.5 Quantitative Evaluation of Minerals by Scanning Electron Microscopy

Quantitative evaluation of minerals by scanning electron microscopy is a technique that is used to determine the composition and quantify the fine mineral particles in ash samples. It provides additional information when compared with the X-ray fluorescence in that it provides information on what compounds the minerals are associated with/bound to [78]. Samples of fly ash are mixed with epoxy resin in 30 mm moulds and allowed to cure. The cured epoxy resin sections are then polished, exposing the particles in cross-section. A scanning electron microscope is positioned at pre-defined points across the particles and the elemental proportions were used to identify the phases at each point [77]. QEMSCAN results for the ash samples are given in Table 3-11 and Table 3-12. The results indicate that the samples are predominately fly ash phases, which are characterised by surface deposits of sodium sulphate and sulphur, with the vol.% increasing with the higher % conditioned ash samples [43].

Table 3-11: QEMSCAN results for PS-1 ash samples (vol.%)

Species	PS1-0	PS1-5	PS1-8	PS1-10	PS1-20	PS1-30	PS1-35
Sodium sulphate	0.0	0.0	0.0	0.2	0.8	2.0	1.7
Fly Ash: Sulphur coated	0.3	0.4	0.5	0.7	1.5	2.0	1.6
Fly Ash: Calcium oxide(Calcite)	1.5	1.5	1.1	1.5	1.4	1.9	2.3

Table 3-12: QEMSCAN results for PS-2 ash samples (in vol.%)

Species	PS2-0	PS2-20	PS2-30	PS2-35
Sodium sulphate	0.0	0.6	2.5	1.7
FA:Sulphur coated	0.4	2.8	2.7	3.7
FA:Calcium oxide(Calcite)	1.3	0.7	0.7	0.7

The following images were obtained for a PS-1 ash sample conditioned to 35 wt.% saline solution compared with a PS-2 ash sample conditioned with the same saline solution. The images reveal that the fly ash phases are characterised by a surface deposit of sodium sulphate (adsorption) as observed by the yellow highlighted particles depicting the sulphur coated fly ash. They also indicate that the fly ash particles with high calcium content serve as the preferable seeds for the sodium ions [43]. This can be seen with the increased blue highlighted areas (calcium components) in Figure 3-7 and the attached red particles depicting the sodium sulphate. The PS-1 ash samples contain a higher vol.% of calcium than the PS-2 ash samples.

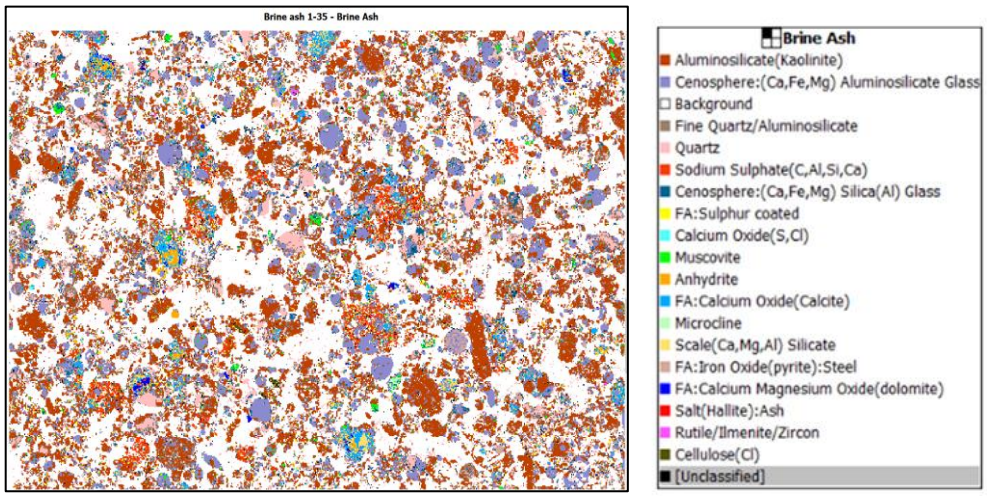

Figure 3-7: QEMSCAN image of 35 wt.% conditioned PS-1 ash sample

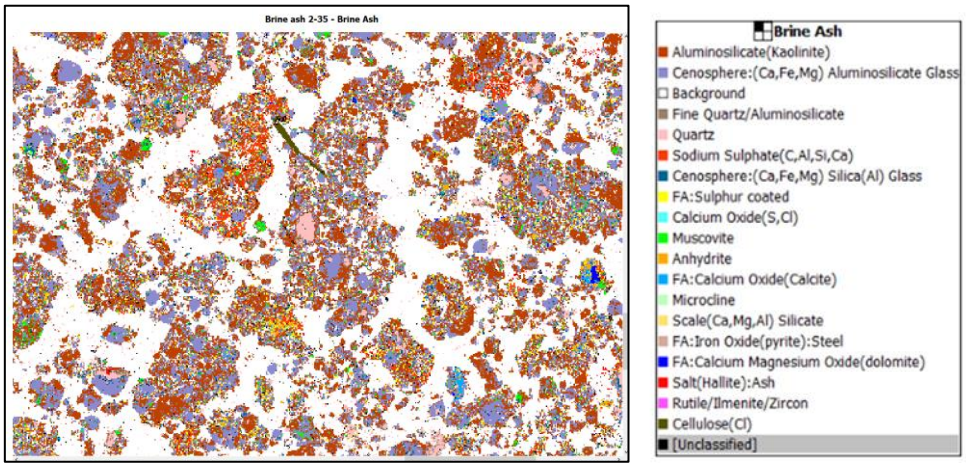

Figure 3-8: QEMSCAN image of 35 wt.% conditioned PS-2 ash sample

CHAPTER 4 EXPERIMENTAL METHODOLOGY

In this chapter, the experimental setup that was utilised to perform the ash resistivity tests is described, together with various experimental procedures followed. The commissioning of the resistivity oven and the calibration of the equipment was performed, before recording the resistivity measurements on the conditioned ash samples. The experimental setup utilised to perform the ash resistivity tests and experimental procedures followed are described in Section 4.1. Section 4.2 addresses the experimental procedures that were followed for the fly ash resistivity measurements taken for the various conditioned ash samples. The commissioning of the experimental equipment (oven) and the calibration tests and results are addressed in Section 4.3.

The experimental equipment utilised was originally constructed by Eskom's Research, Testing and Development department (1994) for Eskom research on fly ash resistivity—later it was donated to North-West University (2014) [15]. Since then, several research projects have been conducted on the equipment [12, 15, 47, 53], with further optimisation and development conducted to allow for testing using moisture injection, SO_3 injection or dry resistivity measurements.

4.1 Experimental Setup

The fly ash resistivity oven was constructed in accordance with the IEEE Standard 548 of 1984 [59]. The setup does not allow for the physical injection or spraying of liquid streams into the ash, but rather allows the fly ash resistivity to be measured in a gaseous environment, specifically water- and H_2SO_4 vapour.

The fly ash resistivity measurement is dependent on the temperature, composition of the gaseous environment, the electric field strength as well as the porosity of the ash layer [26, 48, 59]. A schematic of the experimental setup is shown in Figure 4-1.

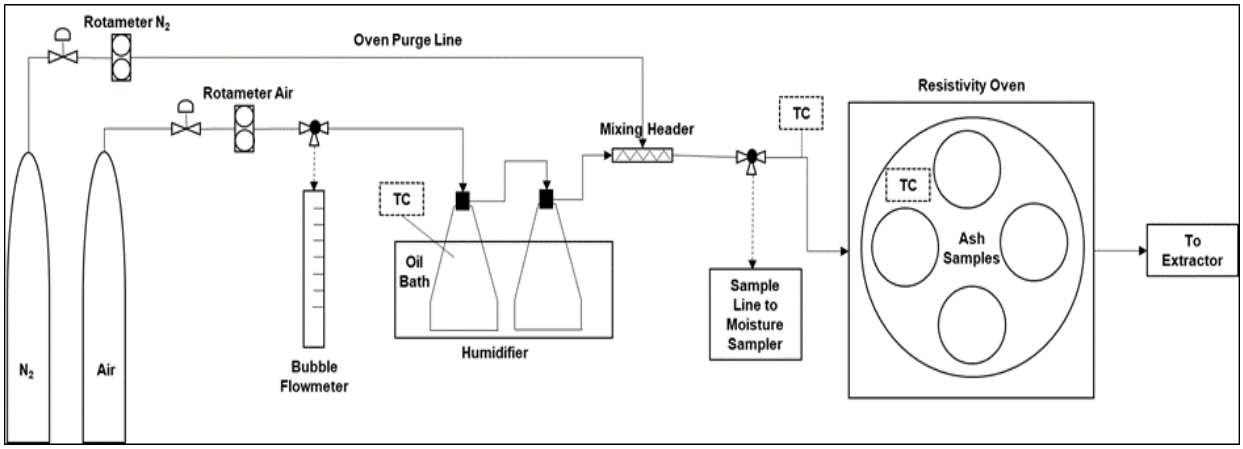

Figure 4-1: Schematic of the resistivity oven test apparatus

The ash samples were placed in the oven and enclosed within a glass dome to control the environment that the ash is exposed to. The chamber can accommodate four ash samples in specific metal bowls. One of the bowls was filled with a raw PS-1 ash sample. The blank sample was fitted with a thermocouple to provide temperature measurement, assumed to be representative of other three samples. The electrodes from each of the ash sample bowls were connected to a Keithley picoammeter. The high voltage applied to the guard ring electrode caused a current through the ash layer, which was measured between the current measuring electrode and the guard ring electrode. The wiring diagram of the ash bowl is shown in Figure 4-2. This enables three different ash samples to be placed into the oven and the fly ash resistivity measurements determined as they are exposed to the same climatic conditions, for example moisture injection and oven temperature. The control panel contains the picoammeter with its own display screen, a separate display screen for the voltage indication, rotameters for the gas flow rates, temperature control for the oil bath as well as the temperature indication of the water in the flasks. The oven temperature control is located on the resistivity oven itself.

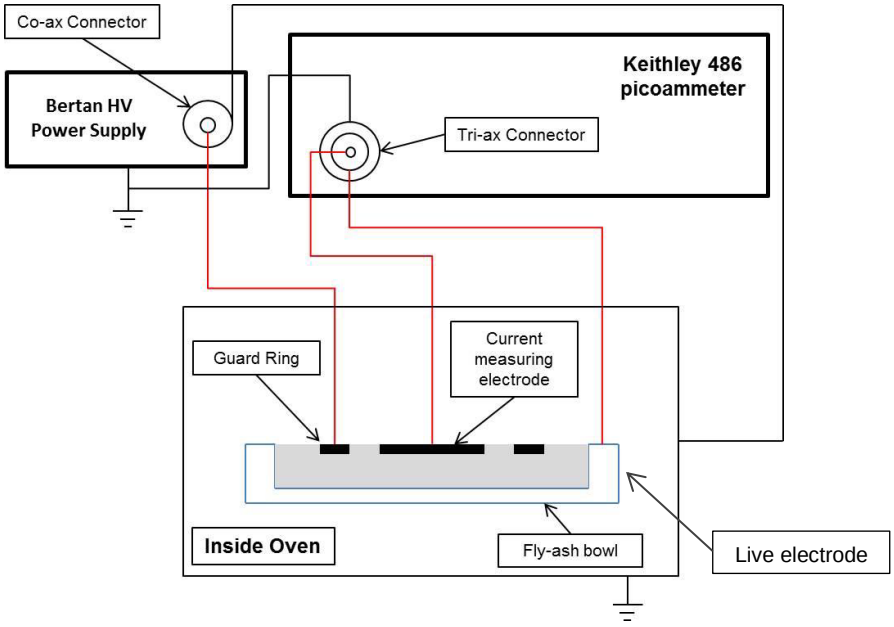

Figure 4-2: Wiring diagram for fly ash resistivity measurements [47]

Figure 4-3 shows the positioning of the live, current measuring and guard ring electrodes on the ash bowls.

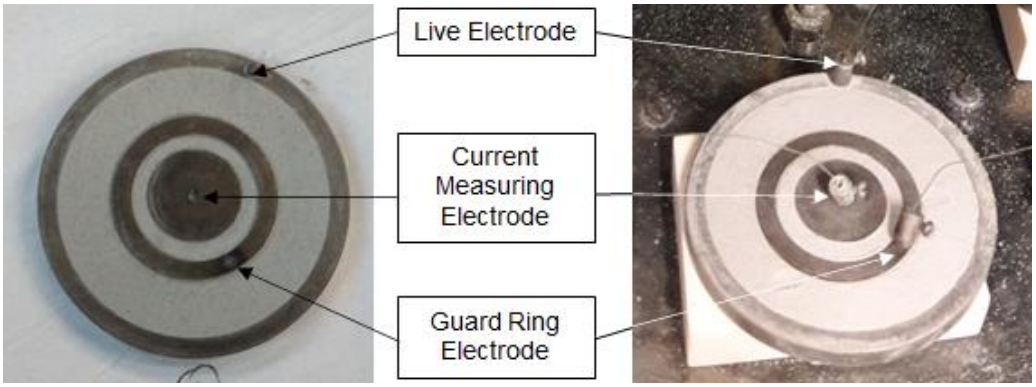

Figure 4-3: An ash sample in the bowl with the electrode connection as per the wiring diagram

It was found that the oven thermostat setting of 95 °C resulted in an ash temperature of 90 °C.

For the test runs requiring moisture injection, the setup is equipped such that dry air is used to transport moisture from heated ultrapure water contained in Erlenmeyer flasks connected in series, as depicted in Figure 4-1. The water is heated indirectly in an oil bath (the water

temperature is controlled by controlling the temperature of the oil). The actual moisture percentage in the final gas stream entering the oven is a function of the gas flow rate and the water temperature. The gas flow rate was measured using a bubble flow meter. The moisture content of the gas was measured by recording the mass increase of a gel-filled moisture trap over a certain time. The flow rate of the gas and the temperature of the water are used to adjust the moisture concentration until the desired concentration is achieved.

4.2 Experimental Procedure

To verify the fly ash resistivity measurements and the consistency / error ratio (higher value divided by the lower value) [64] of the fly ash resistivity results for the three sample bowls, the unconditioned ash sample from PS-1 was loaded into the three bowls, and the ascending (increasing temperature) and descending (decreasing temperature) fly ash resistivity measurements recorded. These results were compared against each other as well as with the results from other researchers who had conducted earlier fly ash resistivity testing using the similar PS-1 ash samples.

The outcome of the calculations documented in Section 3-2 and 3-3 was used to conclude on the test conditions adopted. The ash samples and the climatic conditions that the samples were exposed to is captured in Table 4-1.

Table 4-1: Test conditions adopted for fly ash resistivity measurements

Wt. % conditioned sample	**PS-1 without moisture**	**PS-1 without moisture repeated**	**PS-1 with 7 vol. % moisture**	**PS-2 without moisture**	**PS-2 without moisture repeated**	**PS-2 with 7 vol. % moisture**
0	x			x		
5	x	x	x			
8	x	x	x			
10	x	x	x			
20	x	x	x	x	x	x
30	x	x	x	x	x	x
35	x	x	x	x	x	x

4.2.1 Loading ash samples into the bowls

The loading of the ash samples was conducted in compliance with the IEEE Standard 548 of 1984 [59]. Excess ash sample was placed in a pestle and mortar for the removal of any lumps before being transferred into each bowl and the bowl plus content lightly tapped on the laboratory bench to remove any air pockets. The ash was compressed into the bowl using a flat, straight-edge tool and the excess scraped off to obtain an ash layer that was level with the edge of the bowl. The electrodes were placed into position on the ash surface, pressed into position with the flat tool, and the displaced ash removed from the surface using the straight-edge tool.

The electrodes were labelled (1, 3 and 4) to identify the ash bowl (see Figure 4-4). Bowl 2 contained the PS-1 raw fly ash sample for the ash temperature measurement as explained in section 4.1. The ash bowl selection was performed from the control panel and the fly ash resistivity readings taken. Figure 4-4 shows the filled ash bowls as per the procedure described. The electrodes were carefully placed into the indentations on the ring electrodes with careful attention to not disturb the levelled ash samples. The glass dome was placed over the samples to ensure a tight seal on the bottom plate.

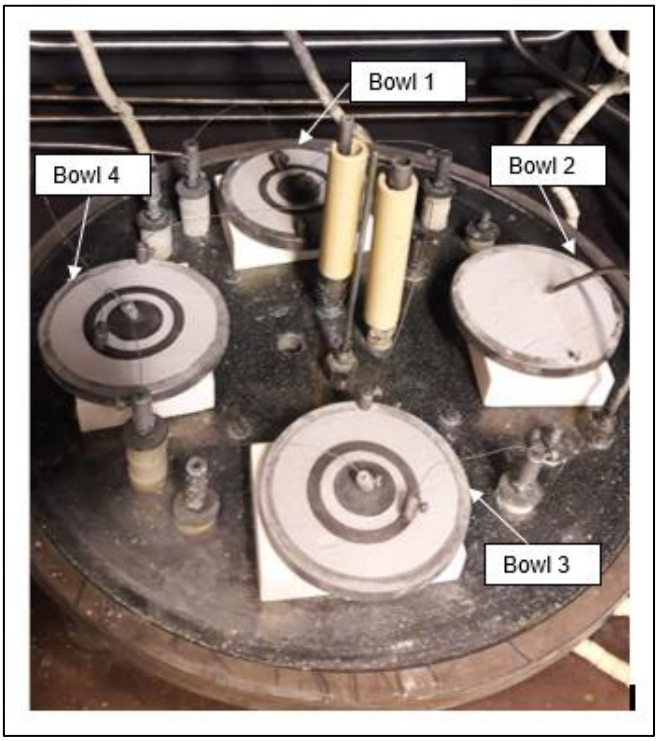

Figure 4-4: Ash bowls in position with electrodes connected in the resistivity oven

4.2.2 Ascending and descending resistivity measurements without moisture

The fly ash resistivity measurements were recorded in accordance with the IEEE standard 548 of 1984 [59]. The ascending temperature measurements were evaluated at 30 °C increments, starting at 90 °C, up to a maximum of 330 °C. The oven was switched on to a temperature setting of 95 °C (which results in an ash temperature of 90 °C) and maintained at this temperature for a minimum of 16 hours prior to testing. This was to ensure that any moisture in the oven and the ash samples was removed and the environmental conditions within the glass dome were stable.

The fly ash resistivity was calculated following collection of a series of data that was recorded from the picoammeter. The picoammeter was switched on and a ‘zero check’ performed as a means of calibrating the instrument. This check was performed at the beginning of each run, i.e., prior to commencing the ascending measurements and prior to the descending measurement recordings. The first set of readings taken at the desired ash temperature was for the induced current (background) readings. The ash bowl to be measured was selected from the control panel. A buffer size of 12 readings was selected and recorded in the log sheet, and the average of 10 values used in the calculation.

The stopwatch was started as soon as the voltage power supply was switched on to ensure that 60 seconds of voltage was applied to the ash bowl being tested. During these 60 seconds, the range of the readings for the sample was confirmed to be within the range of the recorder. Once the 60 seconds lapsed, the picoammeter was triggered to record the 12 data points. On completion of the last reading, the voltage power supply was switched off and the data points logged on the log sheet.

The leakage current was first measured with no voltage applied to the bowl and the 12 readings recorded. Thereafter the induced current was measured. The difference between the leakage current readings and the induced current readings (absolute values) was noted as the current flow (A) for that bowl at the set temperature.

The next bowl was then selected from the control panel and the process repeated to determine the induced current and the applied voltage readings. Once all the readings were obtained for all three bowls, the oven temperature was increased by 30 °C. It took about 20 mins for the oven temperature to reach to next set increment value. When the ash temperature reached the temperature of 120 °C and was stable at that temperature for about 15 min, the induced current and applied voltage readings were recorded as explained above for the three bowls.

This process was repeated until the induced current and applied voltage readings were recorded for the three ash sample bowls at the final maximum ascending temperature of 330 °C. The oven was left on at the maximum temperature overnight. The induced current and applied voltage readings were recorded the following morning, commencing at 330 °C, and then descending to 90 °C in 30 °C intervals. The fly ash resistivity values were plotted on a logarithmic plot for the ascending and descending measurements. An example of the data obtained is provided in Appendix B.

4.2.3 Moisture addition

Control of the temperature of the oil bath is a critical parameter for obtaining the required humidity being transferred to the oven. Two flasks, placed in series, were filled with distilled water and indirectly heated by the oil. The water level in the flasks was monitored during the experiments and topped up with distilled water when required. The temperature of the oil and the water in the flasks was displayed on the control panel. The temperature of the oil was adjusted to obtain the required water temperature. It was determined that a water temperature of 38–39 °C provided 7 vol.% moisture transfer into the oven (see Section 3.3).

Dried air was used as the carrier gas for the moisture into the oven (Figure 4-1). The air flow rate was measured by directing the air through a bubble flow meter. The air flow was set between 135 to 150 l/hr at STP. After opening the three-way valve to direct the air to the moisture sampler, the stopwatch was activated when 100 % of the air stream was directed to the desiccant tube. After an hour of flow with stable water temperature and air flow conditions, the stopwatch was deactivated upon closing of the air valve, the desiccant tube immediately weighed, and the difference noted. The volume of water was set to be 7 vol.% of the total air stream directed to the oven, i.e., 7 vol.% was the set point, and the oil bath temperature was regulated and optimised to obtain this value. The moist air was directed to the oven and allowed to run for a minimum of 60 minutes before the procedure of recording the measurements commenced.

The humidity was controlled by closely monitoring, and adjusting, the oil bath temperature to ensure the water temperature was maintained at 38–39 °C for the ascending and descending measurements taken throughout the ash temperature test range (90–330 °C).

The percentage moisture was verified at the end of the cycle run again. Verification was also conducted at the beginning and end of each day that the measurements were recorded.

4.3 Oven Commissioning and Calibration

Calibration of the resistivity oven involved filling the three bowls with PS-1 unconditioned ash sample as part of the test without moisture on the unconditioned ash samples noted in Table 4-1. Resistivity measurements were recorded as explained in section 4.2. The results were used to determine the cross-bowl repeatability, i.e., if the three bowls yield results within the acceptable error ratio as stipulated in the IEEE standard 548 of 1984 [59], as well as to verify the readings with results obtained in earlier studies using ash samples from the same power stations.

4.3.1 Cross bowl repeatability

The ascending and descending results were plotted for the three bowls with the unconditioned ash sample without moisture (as per Table 4-1). Figure 4-5 shows the collected resistivity data for the dry ash samples at the ascending temperature range from the three sample bowls.

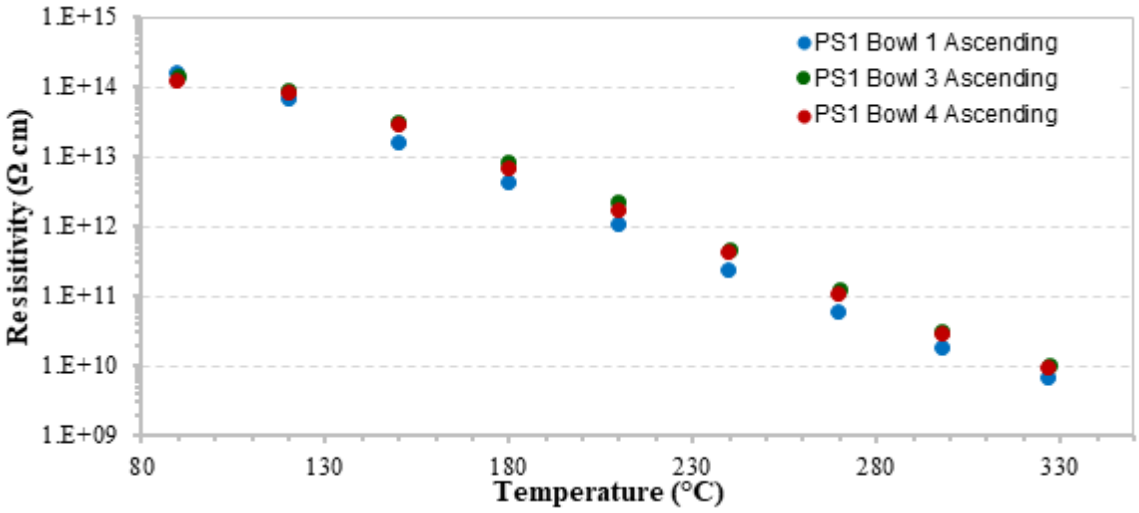

Figure 4-5: Ascending resistivity trends for cross bowl repeatability

The error ratio (higher value divided by the lower value) was determined for all the sample points across the three bowls; results are tabulated in Table 4-2. These error ratios are smaller than the required maximum error ratio of 2.7 that is deemed acceptable in the IEEE standard 548 of 1984 [59].

Table 4-2: Error ratio determined for ascending resistivity measurements

Temp (°C)	Bowl 1 deviation from Bowl 3	Bowl 1 deviation from Bowl 4	Bowl 3 deviation from Bowl 4
90	1.11	1.29	1.16
120	0.77	0.86	1.11
180	0.50	0.56	1.12
210	0.48	0.63	1.32
240	0.50	0.58	1.16
270	0.45	0.55	1.22
300	0.57	0.62	1.08
330	0.65	0.72	1.09

Figure 4-6 shows the collected resistivity data for the dry ash samples at the descending temperature range from the three sample bowls.

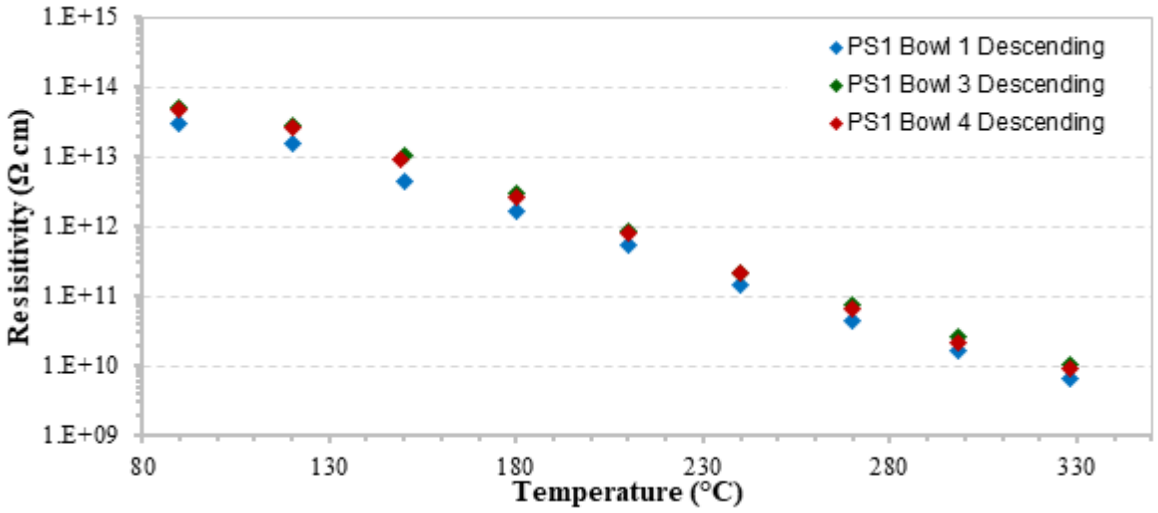

Figure 4-6: Descending resistivity trends for cross bowl repeatability

The error ratio was determined for all the sample points across the three bowls; and the results tabulated in Table 4-3. None of ratios exceed the maximum error ratio of 2.7, therefore the results were deemed acceptable.

Table 4-3: Error ratio determined for descending resistivity measurements

Temp (°C)	Bowl 1 deviation from Bowl 3	Bowl 1 deviation from Bowl 4	Bowl 3 deviation from Bowl 4
90	0.61	0.64	1.05
120	0.57	0.60	1.05
150	0.45	0.51	1.15
180	0.58	0.64	1.12
210	0.65	0.67	1.03
240	0.66	0.67	1.01
270	0.61	0.67	1.09
300	0.62	0.74	1.19
330	0.65	0.72	1.09

The resistivity measurements for both ascending and descending trends where within the acceptable error ratio of each other as stipulated by the IEEE Standard 548 of 1984 [59].

4.3.2 Repeatability Assessment

The results obtained in this study were compared with the measurements obtained, by earlier researchers, on the same ash sample to determine the reliability of the equipment in obtaining repeatable results. Ribberink [15] evaluated the impact of moisture on South African fly ash resistivity and utilised fly ash samples from PS-1 and PS-2 in his research. Ribberink obtained his samples from the same bulk fly ash samples that were obtained by North-West University (Section 3.1.1) that were utilised for the present study. Figure 4-7 shows the resistivity measurements obtained by Ribberink against the measurements obtained by this study for the dry ash samples at the ascending temperature range as per Table 4-1.

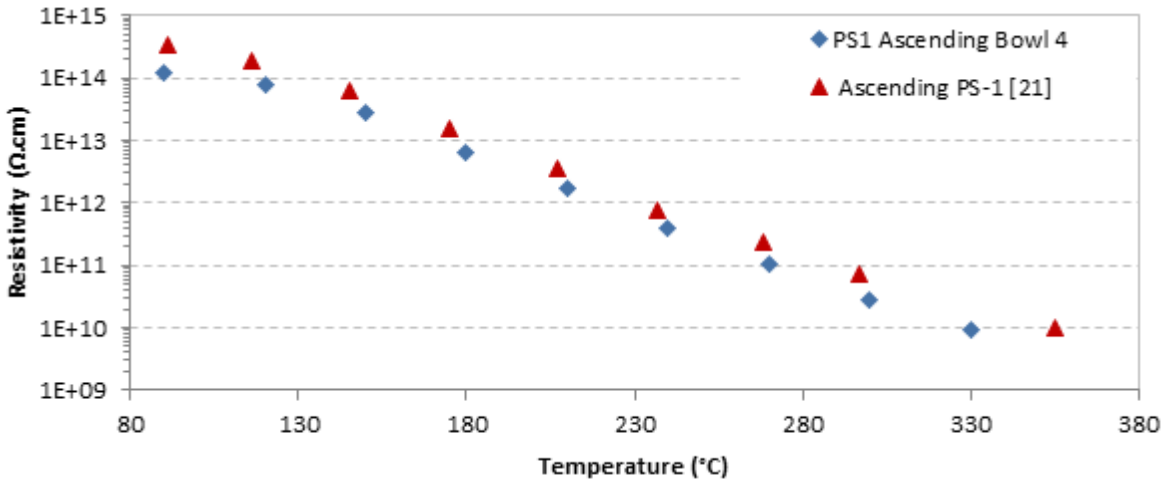

Figure 4-7: Comparison of ascending measurements to assess equipment repeatability

Figure 4-8 shows the resistivity measurements obtained by Ribberink [15] against the measurements obtained by this study for the dry ash samples at the descending temperature range as per Table 4-1.

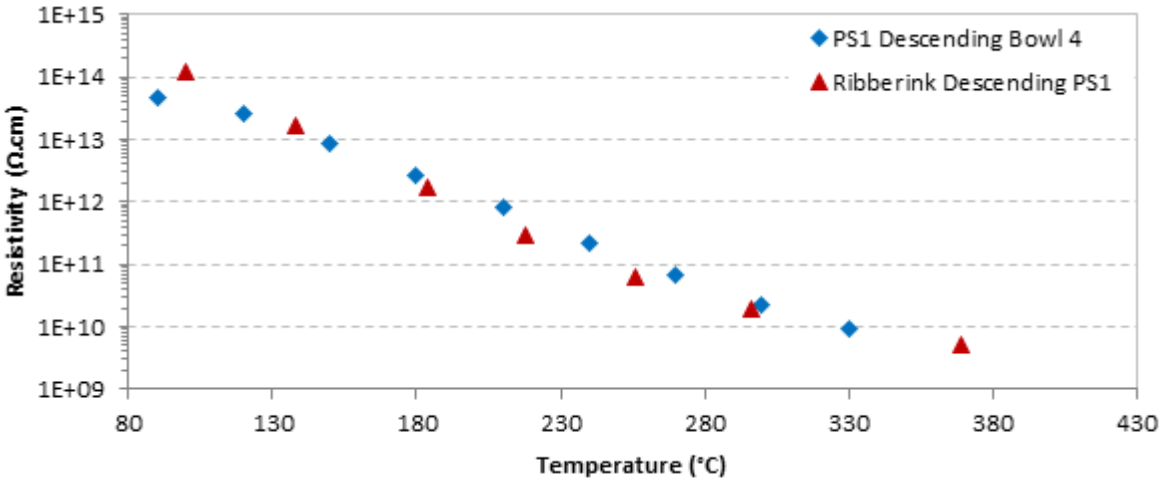

Figure 4-8: Comparison of descending measurements to assess equipment repeatability

The temperatures at which the measurements were taken by Ribberink [15] did not correspond with the temperatures at which the resistivity measurements were recorded, nonetheless the error ratio was determined for values where the temperatures were fairly close. The error ratio was determined for the measurements recorded for the ascending and descending temperature range as captured in Table 4-4—the values are within the IEEE acceptable limit of 2.7 [59].

Table 4-4: Error ratio determined for ascending and descending resistivity measurements to assess equipment repeatability

Temp (°C)	Ascending measurements	Descending measurements
90	2.70	0.18
120	2.42	0.22
150	2.30	1.53
180	2.46	Not determined
210	2.11	2.70
240	1.90	Not determined
270	2.26	Not determined
300		1.16

The trends and error ratios determined confirmed that the values obtained are within the acceptable error ratio for both ascending and descending measurements across the different ash bowls within the oven as well as when compared with previous results obtained.

CHAPTER 5 RESULTS AND DISCUSSION

Chapter 5 presents the fly ash resistivity results obtained for the ash resistivity study performed on both the raw and conditioned, at different saline concentrations, fly ash samples of PS-1 and PS-2. The measurements were recorded at temperatures in the range 90–330 °C (measurements taken at 30 °C intervals) first for the ascending temperature increase, followed by the descending temperatures for 330 °C back to 90 °C. Ash resistivity trends were drawn up and evaluated separately for dry conditions as well as moist conditions, as discussed in Section 5.5. The results obtained were compared with those of other studies conducted, specifically regarding moisture and SO_3 conditioning, on the same ash samples utilised. A correlation was obtained between the ash sample properties captured from the various tests conducted (described in Chapter 3), and the fly ash resistivity trends observed. See Sections 5.2, 5.3, 5.4 and 5.5.

Finally, an assessment of the Bickelhaupt model was performed to determine the ability of the model to predict the resistivity of the ash when conditioned with the varying concentrations of saline solution samples. The original Bickelhaupt model was tested, followed by the sodium-depleted model before regressing and obtaining a revised Bickelhaupt model to fit the data obtained.

5.1 Resistivity Measurement under Dry Air Conditions

In accordance with the IEEE standard 548 of 1984 [59], the first set of fly ash resistivity measurements (the ascending and descending cycles) was performed on all samples from PS-1 and PS-2 as per Table 4-1. The difference between the ascending and descending resistivity measurements provides information on possible physiochemical changes associated with heating as well as the condensation of chemical ions, which influence the resistivity measurements when the temperature is decreased [26].

5.1.1 PS-1 and PS-2 baseline measurements

Fly ash resistivity measurements were determined for the unconditioned ash samples of PS-1 and PS-2 (without the addition of saline solution). The trends were used as the baseline for each power station ash sample, as a means of evaluating the effect of the saline solution on the ash resistivity measurements of the various conditioned samples. The optimum electrostatic precipitator performance is reported to be within a resistivity range 1×10^8 to 1×10^{11} Ω.cm in a temperature range 115–150 °C [12, 20, 26].

Figures 5-1 and 5-2 provide graphical illustrations of the fly ash resistivity data for the ascending and descending temperature ranges, for ash from PS-1 and PS-2.

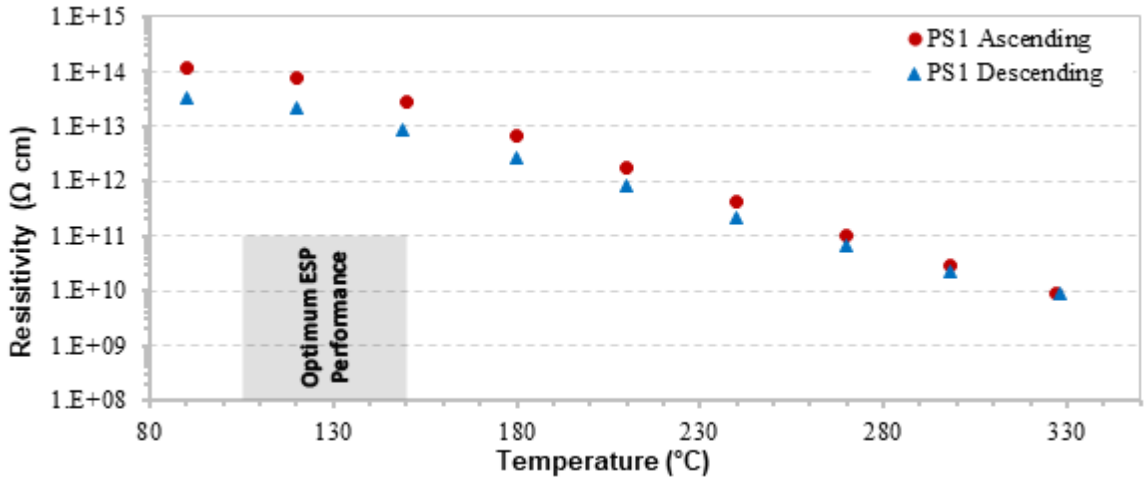

Figure 5-1: Baseline fly ash resistivity trend for PS-1 ash samples (under dry conditions without saline solution addition)

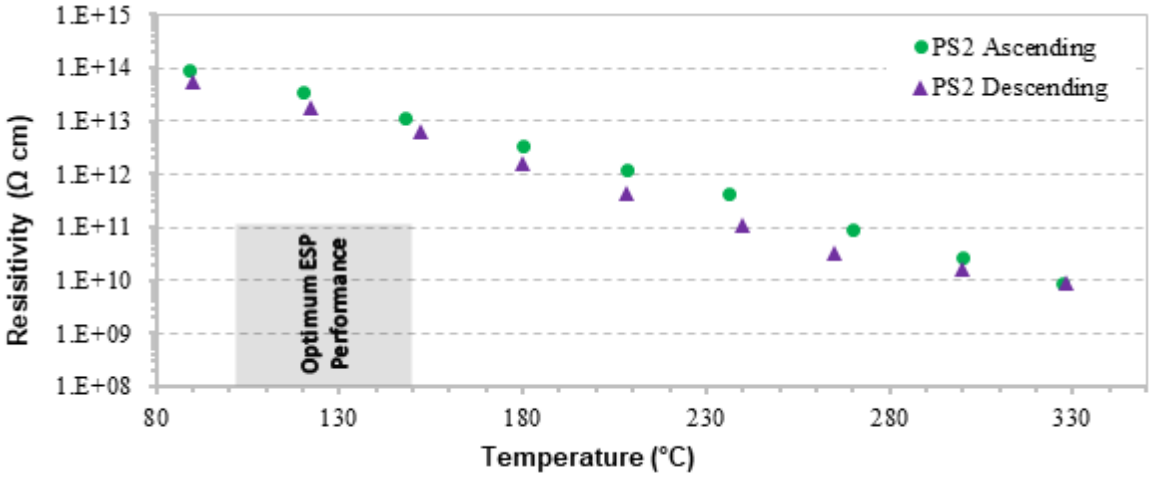

Figure 5-2: Baseline fly ash resistivity trend for PS-2 ash samples (under dry conditions without saline solution addition)

Without any moisture injection, the resistivity measurements for the ascending and descending trends are expected to follow the similar curves [26]. However, a slight deviation between the trends for both power station samples were observed—the deviation in the PS-1 ash sample was greater. The ascending fly ash resistivity measurements were higher than the descending trends, for both power station ash samples. This trend is consistent with the findings of previous studies

conducted on similar samples [12, 47, 53]. The difference between the ascending and descending trends can be attributed to the presence of the unburnt carbon [47], moisture [53] or remnant volatile matter [12] in the ash that is removed during the ascending experiment, resulting in the descending resistivity measurements being lower. This was confirmed by the moisture and volatile matter determined by the proximate analysis conducted on the unconditioned and conditioned ash samples (Table 3-10). The resistivity measurements for temperatures less than 240 °C, which is the range representative of surface resistivity, exceed the optimum operating value of the electrostatic precipitators of 1×10^{11} Ω.cm [8].

South Africa's power plant electrostatic precipitators operate in the temperature range 115–150 °C [20]. Therefore, performance of the electrostatic precipitators with the raw ash samples for both power stations is inadequate, under dry flue gas conditions.

It was also observed that the descending resistivity values for PS-1 ash was slightly lower than for PS-2 ash at temperatures less than 210 °C. This could be attributed to the difference in chemical composition of the fly ashes, as indicated by the X-ray fluorescence results of the raw ash samples (see Table 3-6 and Table 3-7). It is known that certain chemical species in the ash influence the fly ash resistivity differently as reported in Table 5-1 [48].

Table 5-1: Effect of fly ash chemistry on resistivity (adapted from [48])

Chemical constituent	PS-1*	PS-2*	Property	Effect on resistivity
SiO_2	55.27	57.35	Insulator	Increase
Al_2O_3	28.37	29.89	Insulator	Increase
CaO	5.29	4.44	SO_3 absorber	Increase
Fe_2O_3	5.67	3.59	Increases alkali ion solubility and mobility	Decrease
Na_2O	0.14	0.23	Ion contributor	Decrease
P_2O_5	0.37	0.36	Ion contributor	Decrease
K_2O	0.68	0.71	Ion contributor	Decrease
SO_3	0.30	0.20	Ion contributor	Decrease
Li_2O_3	-	-	Ion contributor	Decrease
TiO_2	1.62	1.55	Ion contributor	Decrease
MgO	1.39	0.98	Ion contributor	Decrease

** X-ray fluorescence results normalised on LOI free basis*

With reference to Table 5-1 and Figure 5-1, the PS-2 ash sample had a higher percentage of silica (57.35 wt.% vs 55.27 wt.%) and alumina (29.89 wt.% vs 28.37 wt.%) than the PS-1 ash sample, which according to the published information serve as insulator and will result in an increase in fly ash resistivity measurements. The PS-1 samples had a higher percentage composition of calcium (5.29 wt.% vs 4.44 wt.%) and iron (5.67 wt.% vs 3.59 wt.%), which serve to decrease the fly ash resistivity.

5.2 Conditioned Ash Samples

The ascending and descending resistivity measurements for the samples mixed with the saline solution were performed in sets of three (one sample per bowl). The trend observed for the 8 wt.% conditioned PS-1 ash sample without moisture is shown in Figure 5-3. The similar resistivity measurement trend was observed for all the conditioned samples.

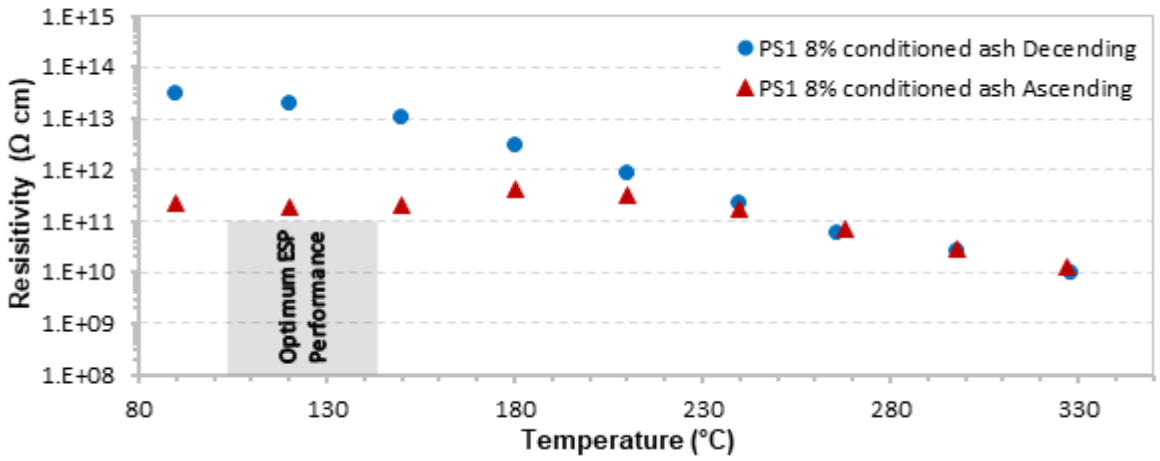

Figure 5-3: Resistivity measurements on PS-1 8 wt.% conditioned ash sample (ascending and descending with 0 vol.% moisture)

The resistivity measurements for the conditioned fly ash samples for PS-2 also followed a similar trend. The trend observed for the 30 wt.% conditioned PS-2 ash sample without moisture is shown in Figure 5-4. The ascending resistivity measurements were found to be lower than the descending at temperatures less than 210 °C. The observed trend could not be attributed to moisture as the samples were dried prior to loading them into the bowls. They were also dried

overnight in an oven at 90 °C prior to carrying out the measurements. This is further supported by the results of proximate analysis, which revealed that the percentage moisture in the samples was relatively low (less than 0.05 % mass loss) (see Section 3.7).

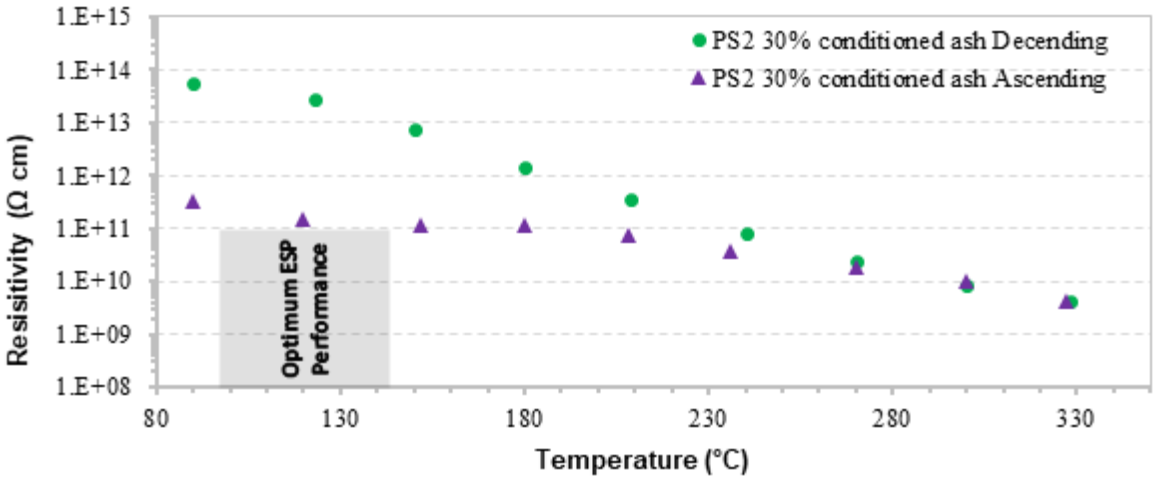

Figure 5-4: Resistivity measurements on PS-2 30 wt.% conditioned ash sample (ascending and descending with 0 vol.% moisture)

The reduced resistivity measurement of the ascending trend is hypothesized to arise from hydrates and soluble chemical species that adsorb onto the ash particles, which are removed when heating the ash samples, such as calcium or magnesium chloride [12, 75, 76]. This suggests a possible influence of the conditioning agent used on the surface resistivity.

The results of the proximate analysis revealed an increase in the percentage of volatile matter mass loss with an increase in saline solution concentration (wt.%) in the ash samples (Table 3-10). Results of thermogravimetric analysis experiments confirmed the loss of mass from all the ash samples (conditioned and unconditioned) occurred at approximately 100 °C. An increase in the derivative weight percentage was observed as the saline solution ratio by mass of the conditioned samples increased (Table 3-8). In all samples, the mass loss stabilises at approximately 150 °C, resulting in the slight increase in fly ash resistivity measurements from this point.

Further studies were not conducted to analyze and quantify volatile species which could have been released at this temperature; however, according to literature, hydrates such as magnesium

chloride ($MgCl_2 \cdot 6H_2O$) vaporise at approximately 117 °C [75] and the dehydration of calcium chloride ($CaCl_2 \cdot 4H_2O$) occurs at approximately 115 °C [76]. Hydrates associated with sodium transition at temperatures 32 - 48 °C [74].

The ascending fly ash resistivity measurements for the conditioned ash samples without moisture addition were observed to be lower than values for the unconditioned ash samples for PS-1, as indicated in Figure 5-5. The results from the proximate analysis suggests that the volatile matter and moisture content of the ash samples influence the initial fly ash resistivity measurements of all the samples up to a temperature of approximately 220 °C. It was also observed that the higher concentration of conditioned ash samples (greater than 20 wt.%) gave a lower fly ash resistivity, compared with the samples of lower concentration (less than 10 wt.%). This is an indication that the fly ash resistivity is influenced by the amount (mass) of saline solution added to the fly ash samples. The higher concentration samples result in more moisture and volatile matter, which was confirmed by the proximate analysis results (Table 3-10). The added ions from the saline solution, in the form of sodium, sulphate, chloride, etc., may also contribute to the increased conductivity / reduced resistivity measurements. There is also an indication that the fly ash resistivity measurements for the high concentration (greater than 20 wt.%) conditioned ash samples fall within the optimum electrostatic precipitator performance range.

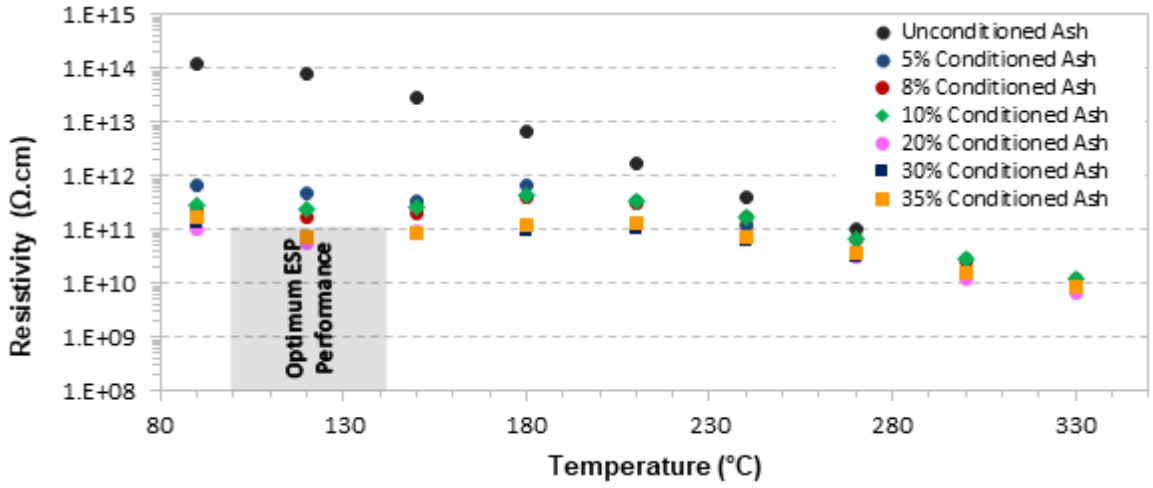

Figure 5-5: Ascending resistivity measurements on PS-1 conditioned ash samples

A similar trend was observed for the PS-2 conditioned ash samples (Figure 5-6). The fly ash resistivity measurements were similar to those of the PS-1 high concentration conditioned ash samples. This suggests that, without moisture added to the oven, the fly ash resistivity measurements obtained for the conditioned ash samples are related to the volatile matter, the effect of the ions and moisture from the saline solution. Upon heating of the ash samples in the oven, the adsorbed moisture and volatile matter were vaporised in the surface resistivity measurement range (less than 240 °C) [26].

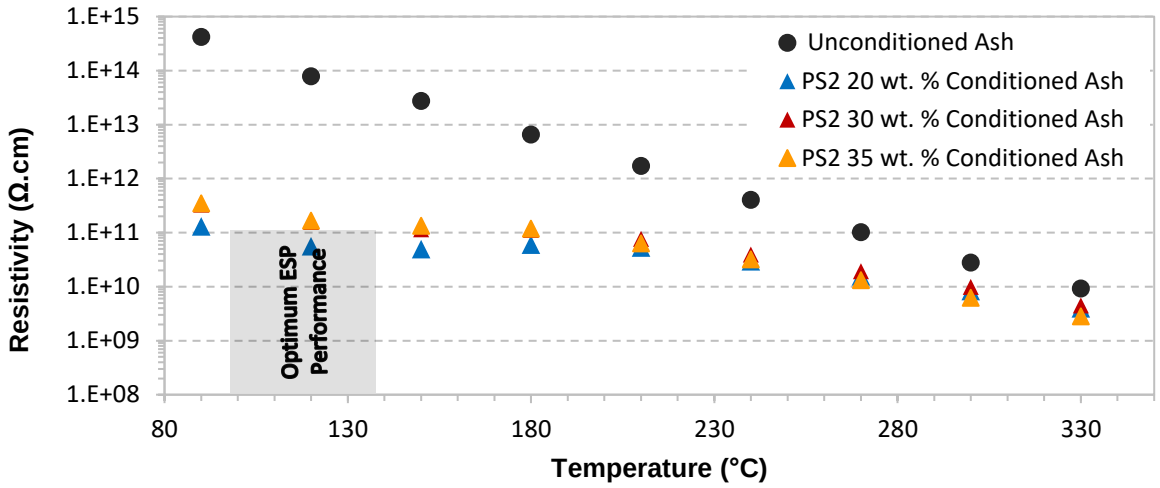

Figure 5-6: Ascending resistivity measurements on PS-2 conditioned ash samples

The resistivity measurements decrease with an increase in the saline conditioning, as can be seen in Figure 5-7 plotted for the 120 °C measurements. The saline solution has a high electrical conductivity of approximately 44 000 µS/cm (as indicated in Table 3-1). When the saline solution is added to the ash sample, the ions from the solution may improve the overall conductivity and therefore the resistivity of the conditioned ash samples. As the concentration of the conditioned samples increases, there is a greater quantity of ionic salts added to the ash, subsequently giving improved resistivity readings.

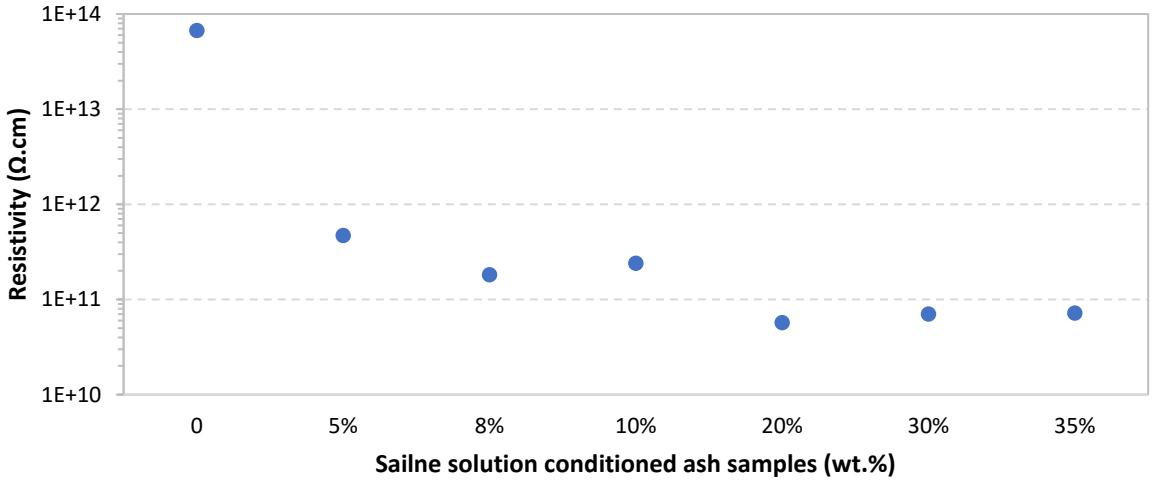

Figure 5-7: Relationship between wt.% saline solution conditioning and resistivity at 120 °C under dry conditions

5.3 Repeat Fly Ash Resistivity Measurement

The resistivity experiments were repeated on the conditioned ash samples to determine whether the peak in the resistivity around 150 °C would be again observed upon repeating the ascending measurements. The samples were dried undisturbed (i.e., they were left in the oven and not handled before subsequent tests) in the oven at 90 °C, then the ascending and descending temperature experiment were repeated. The typical trend observed for all conditioned ash samples is shown in Figure 5-8. The trends for all the ash loadings are given in Appendix B.

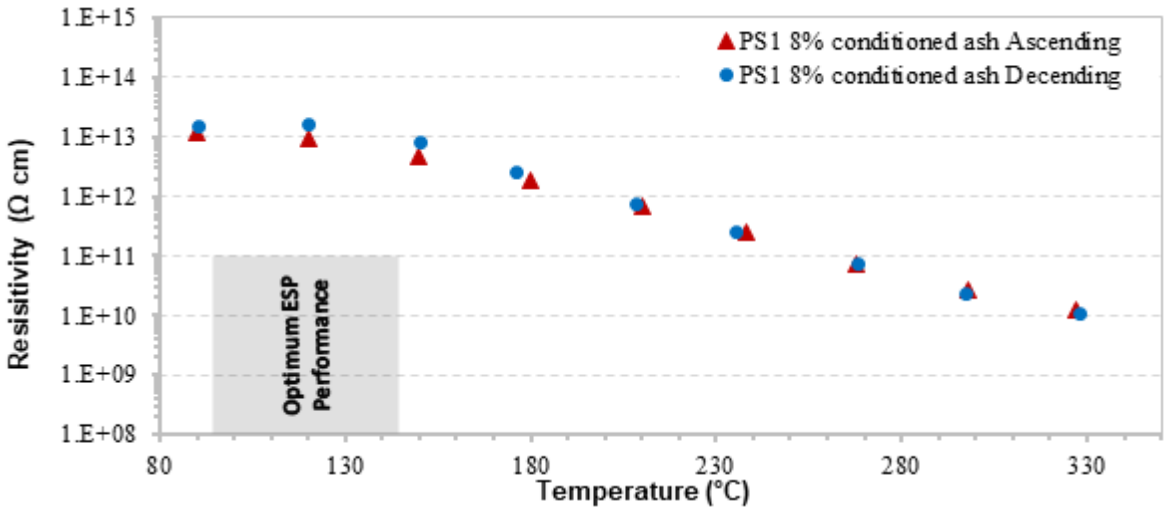

Figure 5-8: Repeat resistivity measurements on PS-1 8 wt.% conditioned ash sample

The ascending resistivity measurements here were higher than in the initial experiment and matched the descending resistivity measurements during the repeat run. This suggested that the volatile matter or hydrates were released during the initial run and the moisture did not return to its original state during the descending experiment, i.e. release of water from the hydrated complex was not reversible [75, 76]. Given that the data matches the descending trend values, the postulation of inherent volatile matter / hydrates could be the cause of the reduced fly ash resistivity measurements during the initial experiment, seeing that the ionic species did not evaporate and they apparently retained their conductivity.

Data for the repeat resistivity measurements were compared to data for the unconditioned ash sample—data for the repeat resistivity experiment were lower for temperatures less than180 °C (see Figure 5-9). This confirms that the ionic species contained within the ash particles affects the reduction in resistivity. The X-ray fluorescence analysis showed an increase in the composition of the sodium as Na_2O between the unconditioned ash sample (0.14 %) and the 8 wt.% conditioned ash sample (0.30 %).

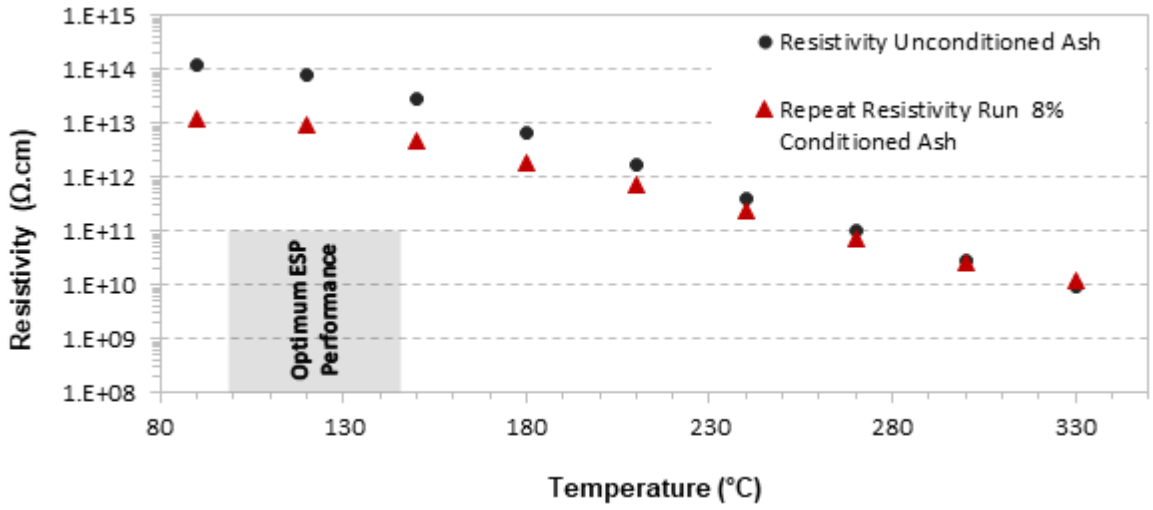

Figure 5-9: Comparison of fly ash resistivity measurement of PS-1 unconditioned ash sample with dry 8 wt.% conditioned sample (repeat resistivity measurements)

The resistivity measurements for the higher concentration conditioned samples (greater than 20 wt.%) did not display a significant improvement when compared with the lower concentration samples without moisture injection, as reflected by the trends in in Figure 5-10. The trend for the

8 wt. % sample is plotted together with the 20 wt.% data and compared against the raw ash sample.

This confirms that the moisture affects the surface resistivity by adsorbing onto the fly ash particles, forming a thin conductive layer through which the transfer of electrons take place along the surface of the fly ash particles [15, 46]. Without the moisture, there is no medium to conduct the electrons irrespective of the ionic loading.

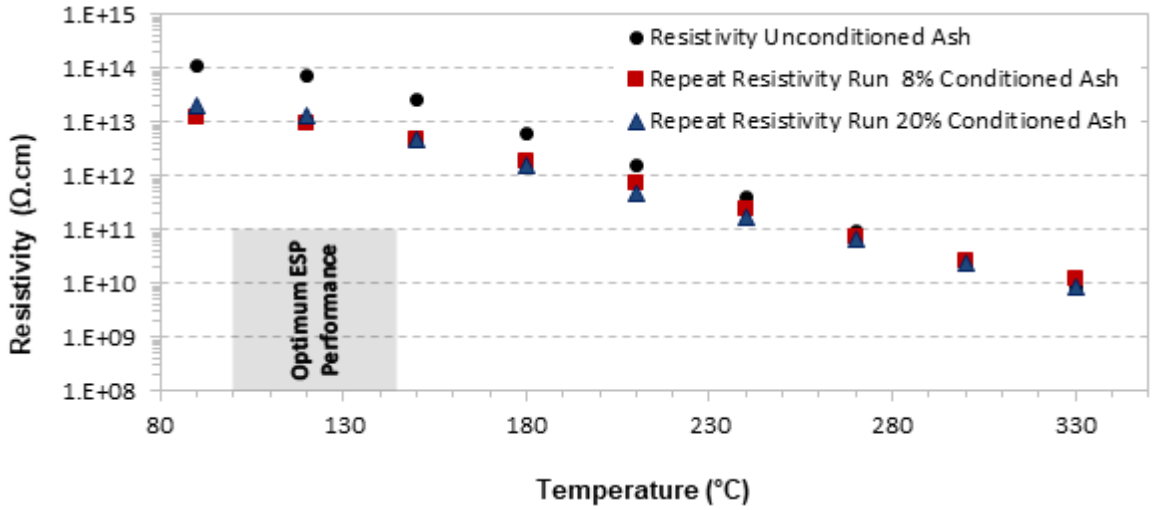

Figure 5-10: Comparison of fly ash resistivity measurement of PS-1 unconditioned ash sample with dry 8 wt.% and 20 wt.% conditioned sample (repeat resistivity measurements)

The PS-2 conditioned ash samples reflected a similar trend for the repeat resistivity measurements when compared with the unconditioned ash samples, as can be seen in Figure 5-11. In the absence of moisture to serve as the charge carrier, the conditioning agent is ineffective in influencing the resistivity measurements irrespective of the amount added.

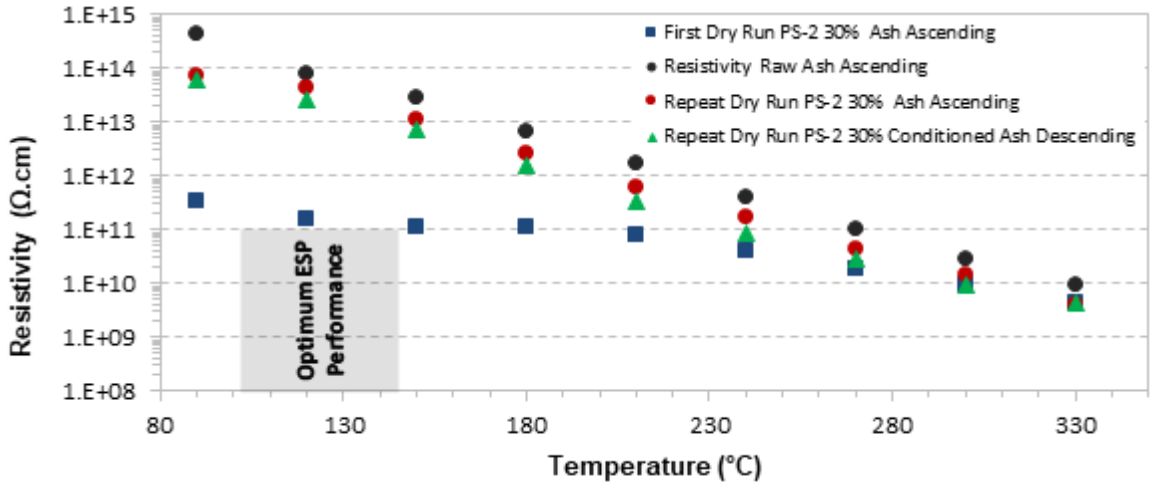

Figure 5-11: Comparison of fly ash resistivity measurement of PS-2 30 wt.% conditioned ash sample

It is hypothesised that the effect of the volatiles / hydrates in the saline solution improved the initial experimental fly ash resistivity results, however, not within the optimum electrostatic precipitator performance range. The repeat experiment on the undisturbed ash sample for PS-1 and PS-2, confirmed that the removal of the volatiles and hydrates was not reversible, because the repeat ascending and descending fly ash resistivity measurements followed a similar curve.

The trends confirmed that the influence of the alkali species alone on the fly ash is insufficient to improve the resistivity to that required for efficient electrostatic precipitator performance [20] without the addition of moisture to serve as the charge carrier [13].

5.4 Fly ash resistivity measurement with moisture injection

Once the repeat resistivity measurements were completed, the ash samples used for the previous test were then exposed to 7 vol.% moisture (refer to Section 3.3) and the ascending and descending fly ash resistivity experiments were conducted. The typical trend observed for all six samples is displayed in Figure 5-12.

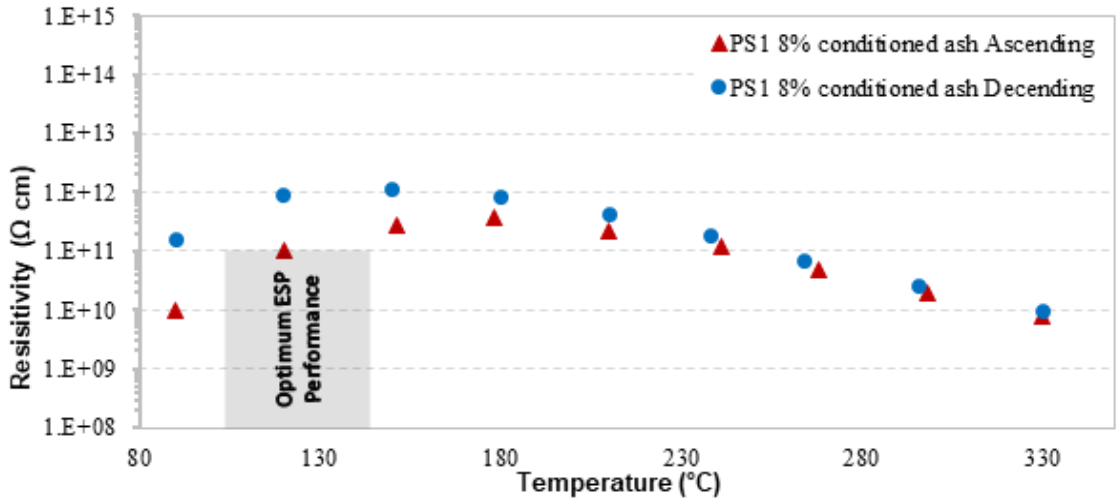

Figure 5-12: Resistivity measurements for PS-1 8 wt.% conditioned ash sample (with 7 vol.% moisture)

The effect of moisture is evident in the surface resistivity range [15]. For temperatures less than 200 °C, ascending resistivity measurements were observed to be lower than the descending. Moisture reduces the surface resistivity by adsorbing onto the ash particles, thereby serving as a charge carrier for the chemical species added with the saline solution [13]. The ash samples conditioned with a higher ratio of saline solution (greater than 20 wt.%) showed a further reduction in fly ash resistivity measurements with the 7 vol.% moisture injection, as seen in Figure 5-13. This is an indication that the increased ionic loading (by mass) in the ash together with the moisture as the charge carrier influences the surface resistivity.

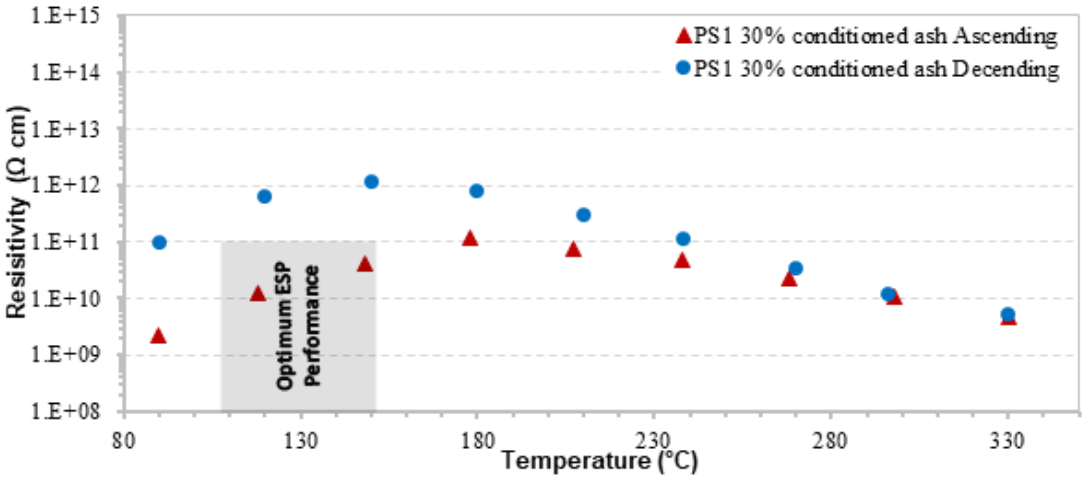

Figure 5-13: Resistivity measurements for PS-1 30 wt.% conditioned ash sample (with 7 vol.% moisture)

Similar trends were observed for the PS-2 conditioned ash samples with the 7 vol.% moisture, as seen in Figure 5-14, with the resistivity measurement at 120 °C marginally within the optimum electrostatic precipitator performance range.

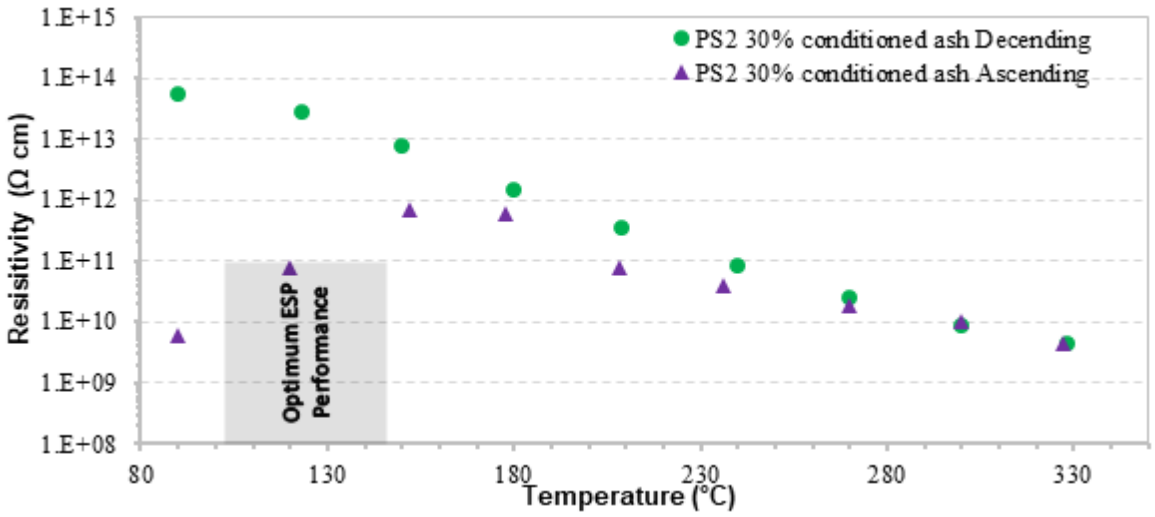

Figure 5-14: Resistivity measurements for PS-2 30 wt.% conditioned ash sample (ascending and descending with 7 vol.% moisture)

The X-ray fluorescence analysis results indicated that the PS-2 unconditioned ash samples contained a much higher percentage of silica (57.4 wt.%) and alumina (29.9 wt.%) compared with PS-1 unconditioned samples (55.3 wt.% and 28.4 wt.%, respectively). The presence of silica and alumina in fly ash is reported to make the surface of the ash particles glassy and less absorbent to the conditioning chemicals [46].

5.5 Comparison of fly ash resistivity results with previous studies

The resistivity of an unconditioned ash sample was compared with that of conditioned samples with 7 vol.% moisture. Results of the experiments indicated a reduction in the resistivity for the higher concentration ash samples. The trends are shown in Figure 5-15.

Experiments were conducted on fly ash samples from PS-1 to determine the influence of varying concentrations of moisture only on the resistivity [15]. A previous study conducted by Ribberink [15] considered moisture addition of 6 vol.% and 9 vol.%. The 6 vol.% moisture was selected for the experiments here as it was the value that best suited the three power stations ashes that were researched at various times of the year. PS-1 was one of the power stations in common between

the experiments. The 9 vol.% moisture was selected as a point exceeding the average 6 vol.% [15]. The results obtained from the previous study [15] for the 6 vol.% and 9 vol.% moisture on PS-1 samples were plotted against the results achieved with the saline solution conditioned ash samples from PS-1 as part of this study with the 7 vol.% moisture (see Figure 5-15).

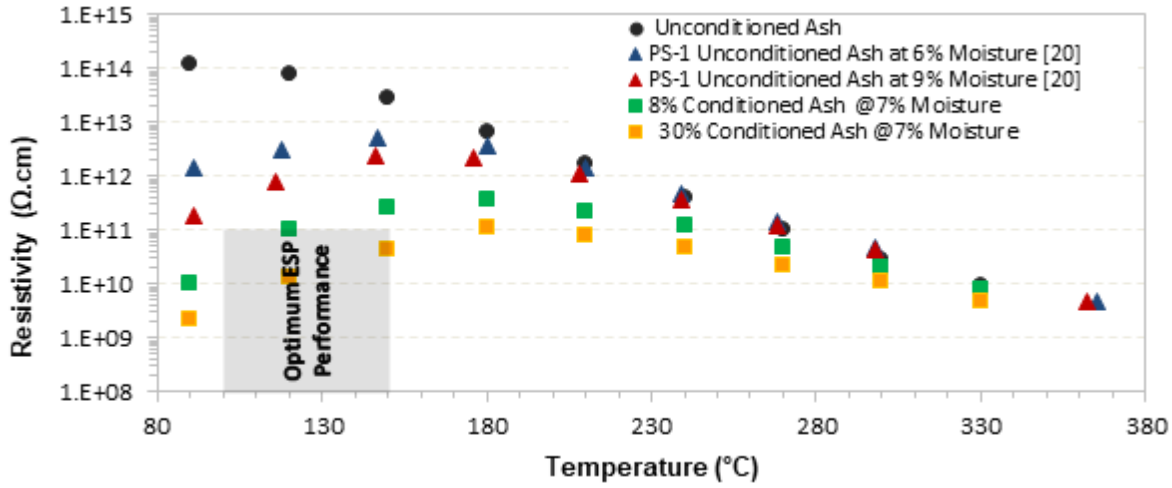

Figure 5-15: Comparison of ascending resistivity measurements for PS-1 ash samples

The results plotted in Figure 5-15 indicate that the moisture of 9 vol.% added to the unconditioned ash sample improves the fly ash surface resistivity [15, 46]. However, it is evident that the ash samples conditioned with saline solution exhibit an even further reduction in the resistivity measurement—the ash sample conditioned with the higher concentration of saline solution exhibited the most improved resistivity measurements. This is similar to the effect of various chemical conditioning agents on reducing fly ash resistivity measurements [14, 46].These results indicated that the ions contained in the saline solution were able to interact with the fly ash particles in a similar manner to a conditioning agent, together with the moisture added as a charge carrier, leading to a reduction in the fly ash resistivity measurement. The higher concentration saline solution conditioned sample (greater than 20 wt.%) together with the 7 vol.% moisture was able to give fly ash resistivity measurements within the optimum operating range of the electrostatic precipitator. The lower concentration saline solution conditioned samples (less than 10 wt.%) did not contain sufficient quantity of the required salts to reduce the resistivity to within the optimum electrostatic precipitator performance range.

5.6 Bickelhaupt Modelling

5.6.1 Original model (developed in 1979)

The previous research studies conducted locally on fly ash resistivity measurements of South African ashes, investigated the use of the Bickelhaupt model in an attempt to predict the resistivity of the different sources of ash [12] or using different conditioning mechanisms (moisture [15], SO_3 [47] or synthetic saline solutions [53]). Outcomes of these studies indicated that the original Bickelhaupt predictive model [22] was unsuitable for use on South African ashes in the surface resistivity range because of the mineralogy of the South African ashes, which differ significantly from the North American ash on which the model was based [12, 15]. The sodium and lithium content of the South African ashes are too low, which has a significant influence on the modelled value of fly ash resistivity [15, 47]. By utilising the saline solution as a conditioning agent, the sodium content of the conditioned ash samples was altered (Table 3-6 and Table 3-7). The elemental composition determined from X-ray fluorescence was utilised to determine the ability of the Bickelhaupt model to predict the fly ash resistivity of the condition ash samples.

The trends for the predicted resistivity values (resultant value of the original Bickelhaupt formulae) were plotted against the measured descending resistivity experiments for the ash samples conditioned with the varying concentrations (by mass) of saline solution. A comparative plot between experimentally determined resistivity results and the Bickelhaupt relationship (equations 2-4, 2-5, 2-6 and 2-7) is provided in Figure 5-16 (a–f).

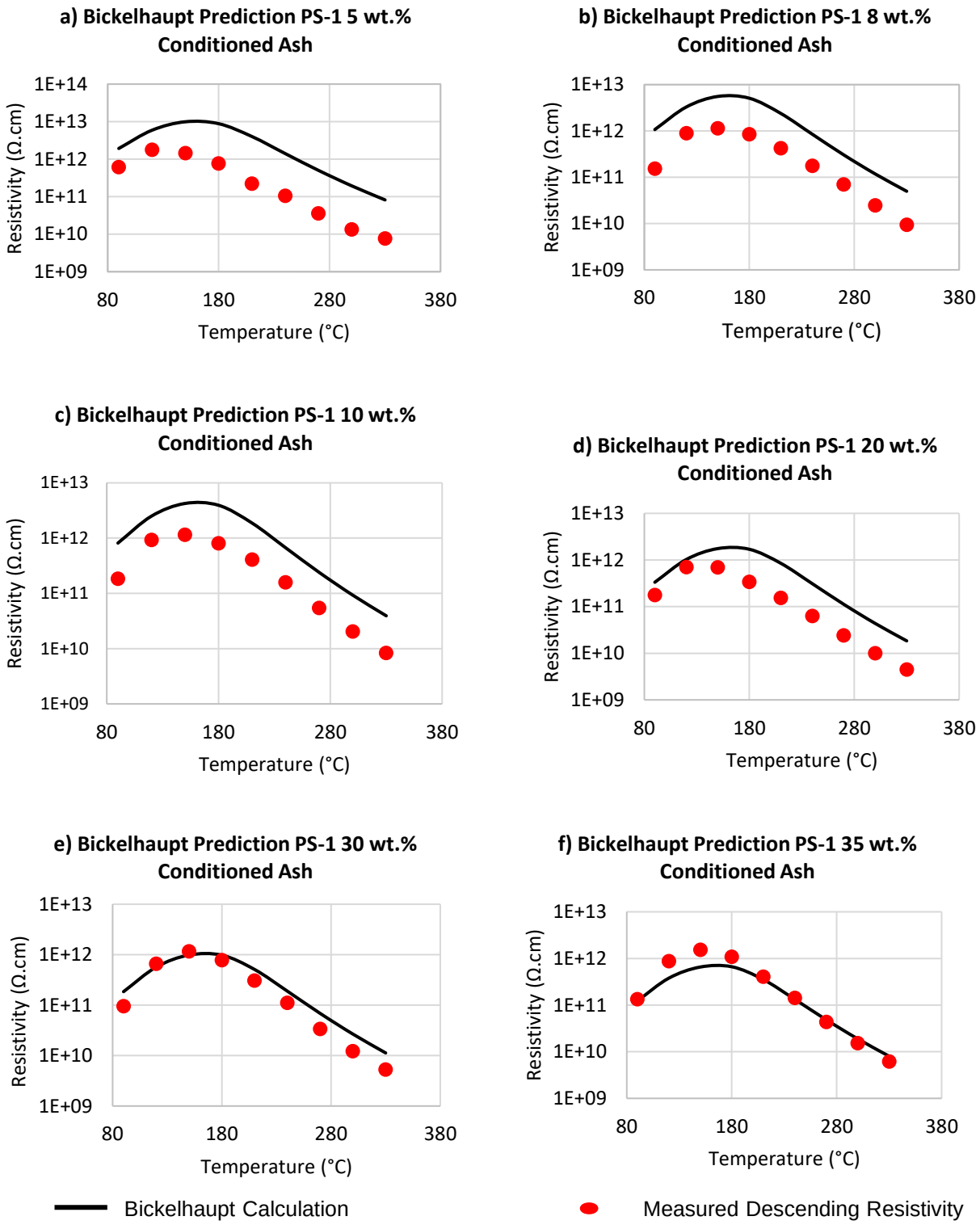

Figure 5-16: Bickelhaupt model predictions for PS-1 at a) 5 wt.%, b) 8 wt.%, c) 10 wt.%, d) 20 wt.%, e) 30 wt.% and f) 35 wt.% conditioned ash

The trends confirm the observations made by the previous studies [12, 15, 47] with the low concentration conditioned ash samples (5 wt.%, 8 wt.% and 10 wt.%) in that the deviation is in the region of one order of magnitude lower between the predicted and measured fly ash resistivity measurements. This is observed to be for both surface and volume resistivity readings. The formula for the surface resistivity determination makes use of the sodium and moisture concentrations [60], while the volume resistivity formula is influenced by the sodium, iron, calcium and magnesium concentrations [60]. The atomic concentrations of these chemical parameters for the different saline solution conditioned ash samples were compared with the average composition of the North American ashes (see later, in Figure 5-18). Figure 5-17 (a-c) shows the trends for PS-2 conditioned ash samples modelled using the original Bickelhaupt model.

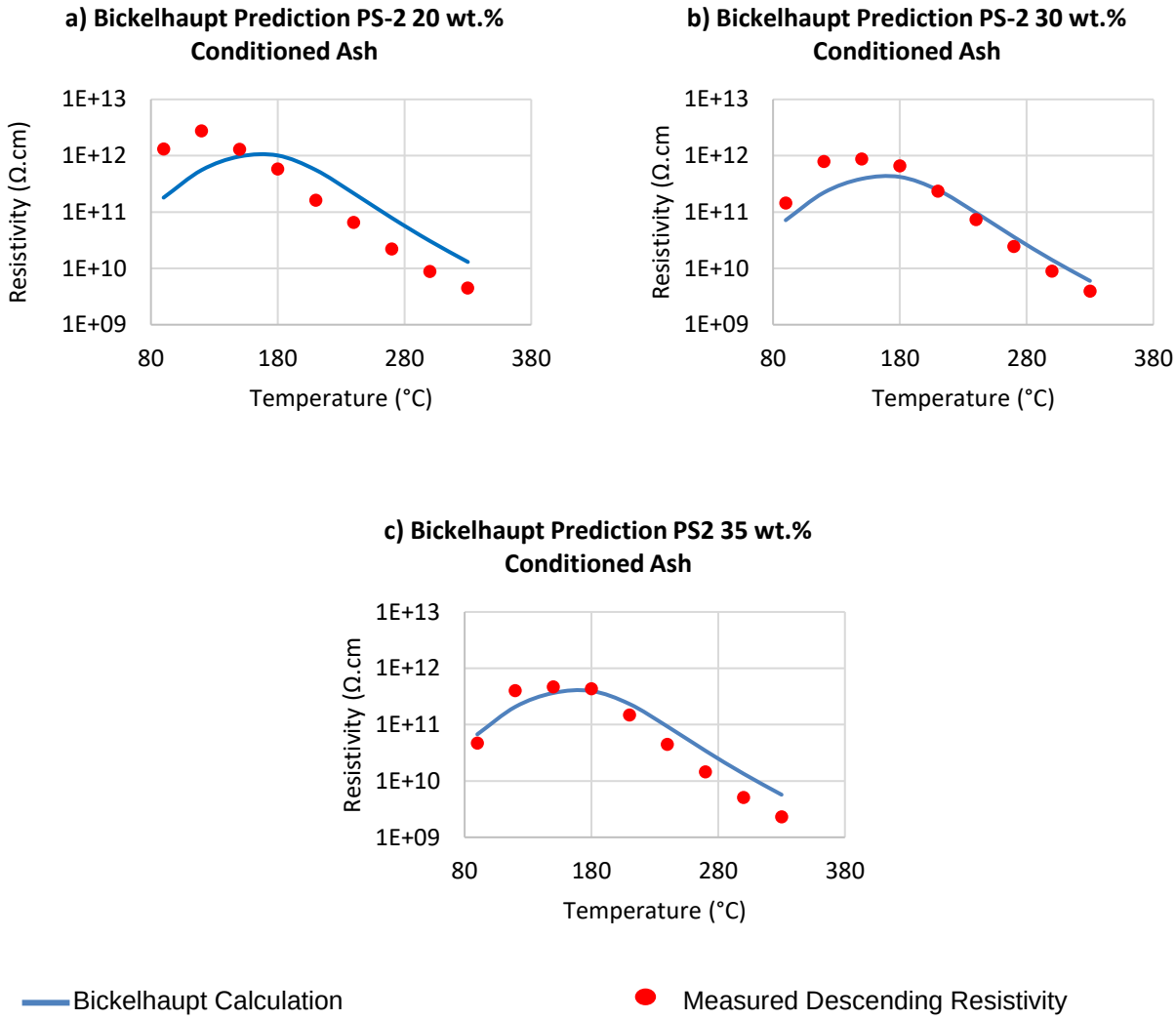

Figure 5-17: Bickelhaupt model predictions for PS-2 at a) 20 wt.%, b) 30 wt.%, and c) 35 wt.% conditioned ash

The atomic concentration of the sodium ions increased with the increasing mass of saline solution added to the ash samples, while the iron, magnesium and calcium remained fairly constant (3 % and 1 % deviation, respectively, between the 35 wt.% saline solution conditioned PS-1 sample and the raw PS-1 ash sample). This confirms that the sodium concentration of the ash samples is the main contributor in the improvement of the correlation between the measured fly ash resistivity and the Bickelhaupt model. It also indicates that, for sodium concentrations less than 0.93 %, the Bickelhaupt formula is inadequate as a prediction tool for the PS-1 ash sample.

When the original Bickelhaupt model was applied to the conditioned ash samples for PS-2, it was found to provide a closer prediction with the volume resistivity prediction but a lower prediction for the surface resistivity when compared with the measured values (Figure 5-17 a-c). However, the sodium concentration in the PS-2 ash samples is almost double that in the PS-1 conditioned ash samples (Figure 5-18). This is despite the PS-2 samples having a higher atomic mass of sodium compared with the PS-1 conditioned ash samples. This confirms that the manner in which the sodium ions are bound to the ash influences the fly ash resistivity measurements. The high alumina and silica (revealed by X-ray fluorescence analysis) makes the surface of the ash particles glassy and less absorbent [46]. The Bickelhaupt formula does not account for this, resulting in a higher surface resistivity for PS-2 ash by only utilising the high sodium concentrations.

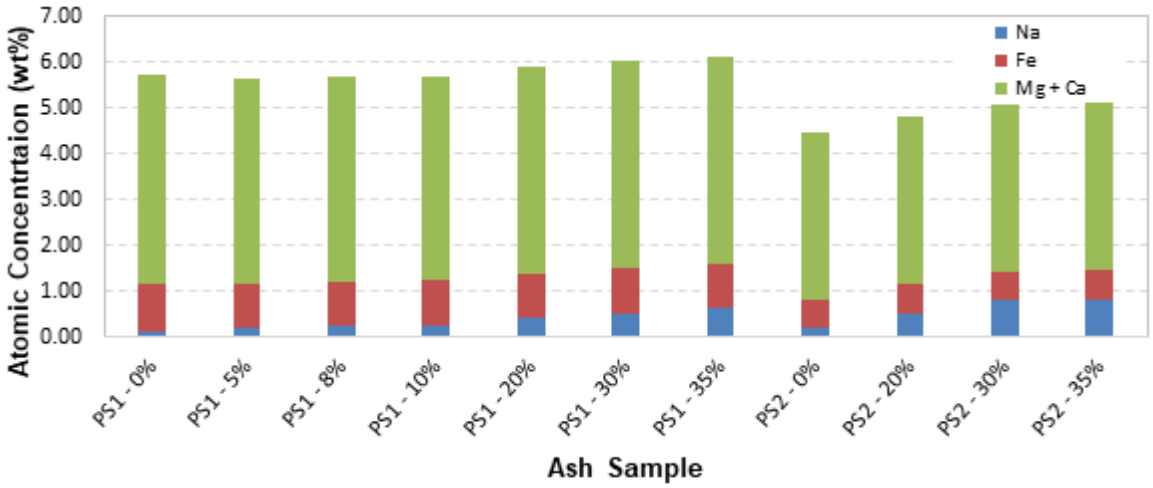

Figure 5-18: Comparison of ash parameters used in Bickelhaupt model (LOI free basis)

The quality of the PS-1 and PS-2 conditioned ash samples was compared with the average composition of the North American ashes, specifically the parameters utilised in the Bickelhaupt model (sodium, iron, calcium and magnesium content). Data are given in Figure 5-19. The composition of the North American ash, upon which the development of the Bickelhaupt model was based, reveals much higher concentrations of sodium (approximately 60 %), iron (approximately 95 %) and calcium (approximately 74 %). The improved prediction observed for the volume resistivity against the measured values suggests that the model may be applicable for varying iron, calcium and magnesium concentrations. However, the deviation observed for the surface resistivity indicates that the model does not sufficiently account for the influence of the sodium ions in the South African ash.

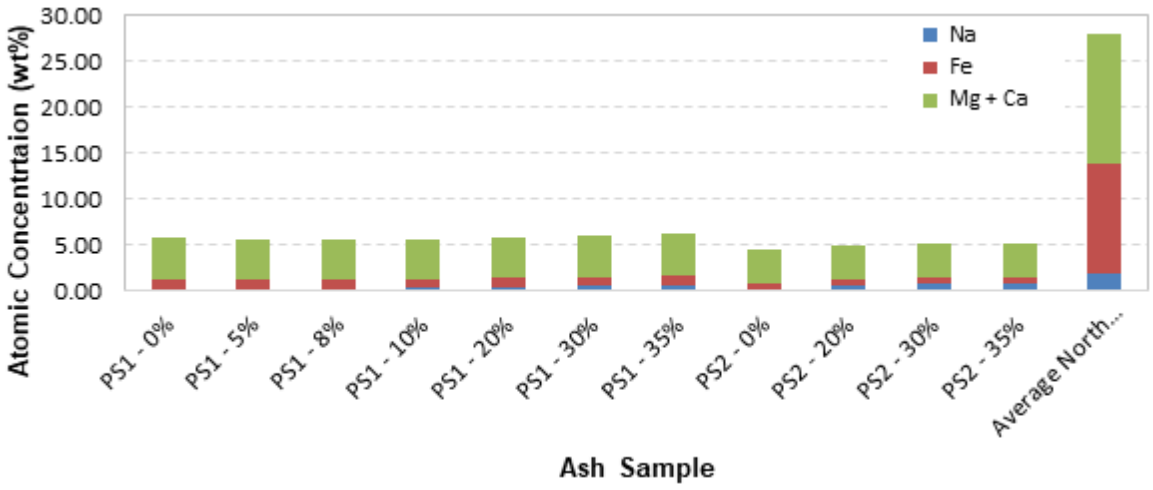

Figure 5-19: Comparison of ash parameters used in Bickelhaupt model with North American ash (LOI free basis)

5.6.2 Refined Bickelhaupt model for sodium-depleted ashes

The Bickelhaupt prediction model was updated between 1980 and 1984 for predicting the resistivity of sodium-depleted fly ashes [61]. X-ray fluorescence analysis data were used to plot the curves for the sodium-depleted Bickelhaupt model. The curves in Figure 5-20 (a–f) show the improvement in the sodium-depleted model correlating with the South African conditioned ashes when compared with the original Bickelhaupt model using equations 2-4, 2-5, 2-6, 2-8 and 2-9.

The modified equation for the sodium-depleted ashes adjust the volume resistivity, because the model was developed on the basis that the sodium ions responsible to be the charge carriers for volume conduction become depleted over time. This modification proved successful in predicting the volume resistivity for the PS-1 conditioned ash samples for the higher saline conditioned samples (greater than 20 wt.%).

The sodium-depleted model was applied to PS-2 ash samples, as shown in Figure 5-21 (a–c). A similar improvement was noted for the volume resistivity, as was observed for PS-1 ash samples. However, the modified formula did not address the surface resistivity calculations for ashes with high alumina and silica composition.

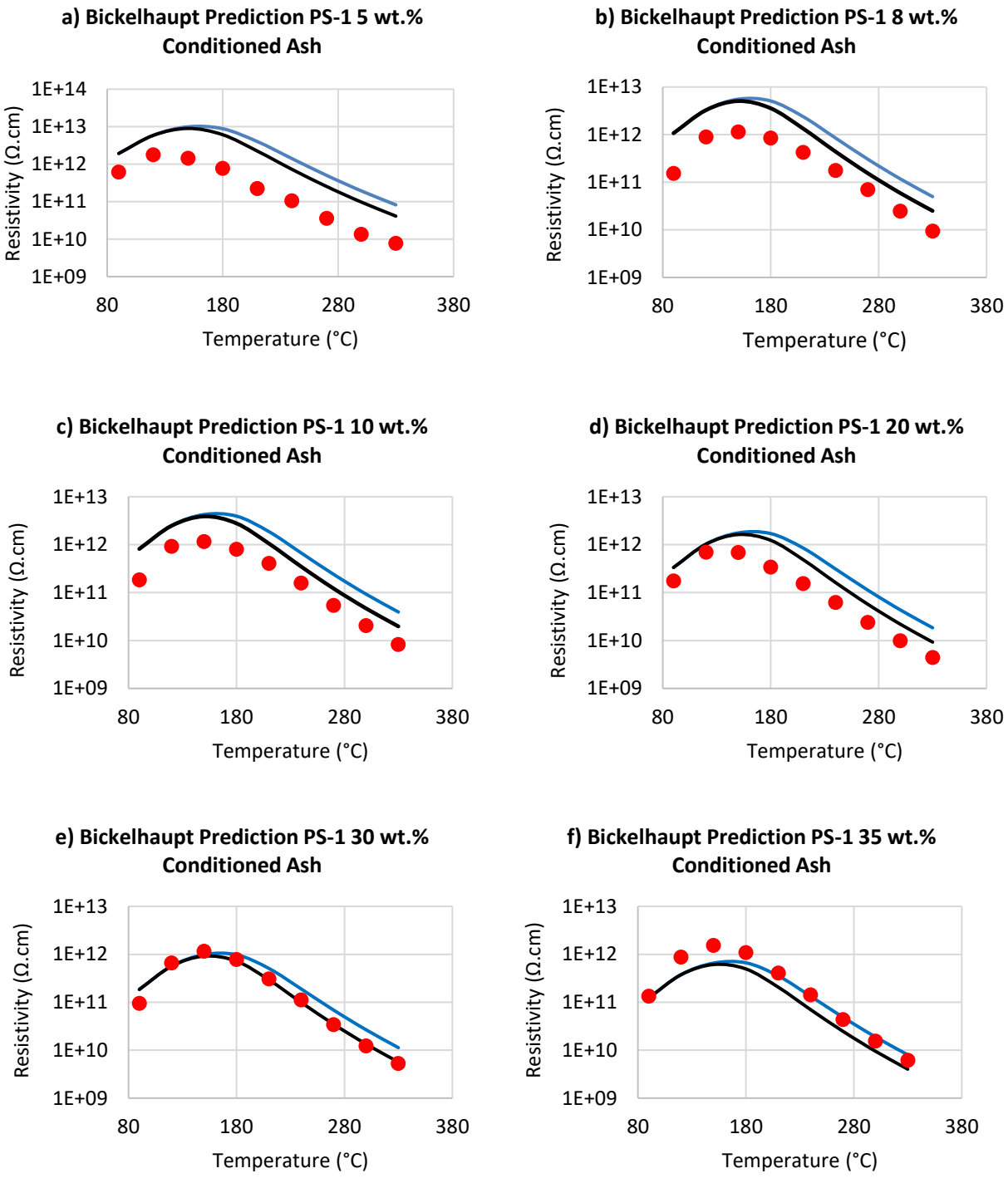

Figure 5-20: Sodium-depleted Bickelhaupt model predictions for PS-1 at a) 5 wt.%, b) 8 wt.%, c) 10 wt.%, d) 20 wt.%, e) 30 wt.% and f) 35 wt.% conditioned ash

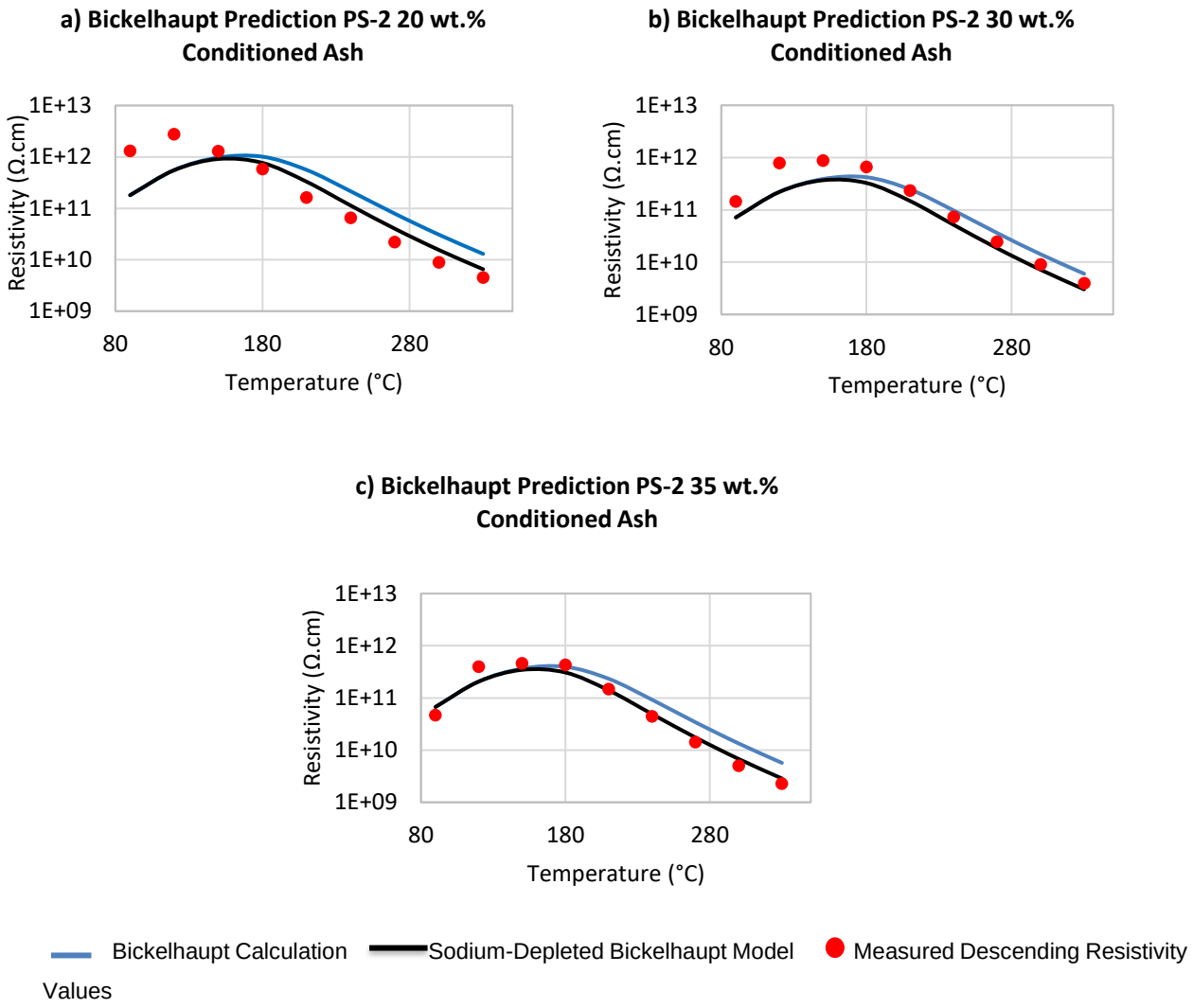

Figure 5-21: Sodium-depleted Bickelhaupt model predictions for PS-2 at a) 20 wt.%, b) 30 wt.%, and c) 35 wt.% conditioned ash

5.6.3 Modified Bickelhaupt model for South African ash

A modification to the Bickelhaupt model was conducted. The detailed methodology utilised is explained in Appendix E. Non-linear regression was performed by changing the fitting parameters to such an extent that the error sum of squares between the predicted model data and the actual experimental data is minimised. The constants in the surface resistivity Bickelhaupt formula were set to be the variables and the ion composition was fixed. The solution was obtained when the outcome of the formula was able to match the measured fly ash resistivity for the selected temperature. This step was repeated for all temperatures and the formula with the least square difference between the values among all the saline solution conditioned ash samples (i.e., the

varying concentrations) was accepted as the modified formula for the ashes used in this research. The trends showing the measured resistivity values, the values obtained from the original Bickelhaupt model and the modified formula (equations E-2 and E-4) are shown in Figure 5-22 (a-f).

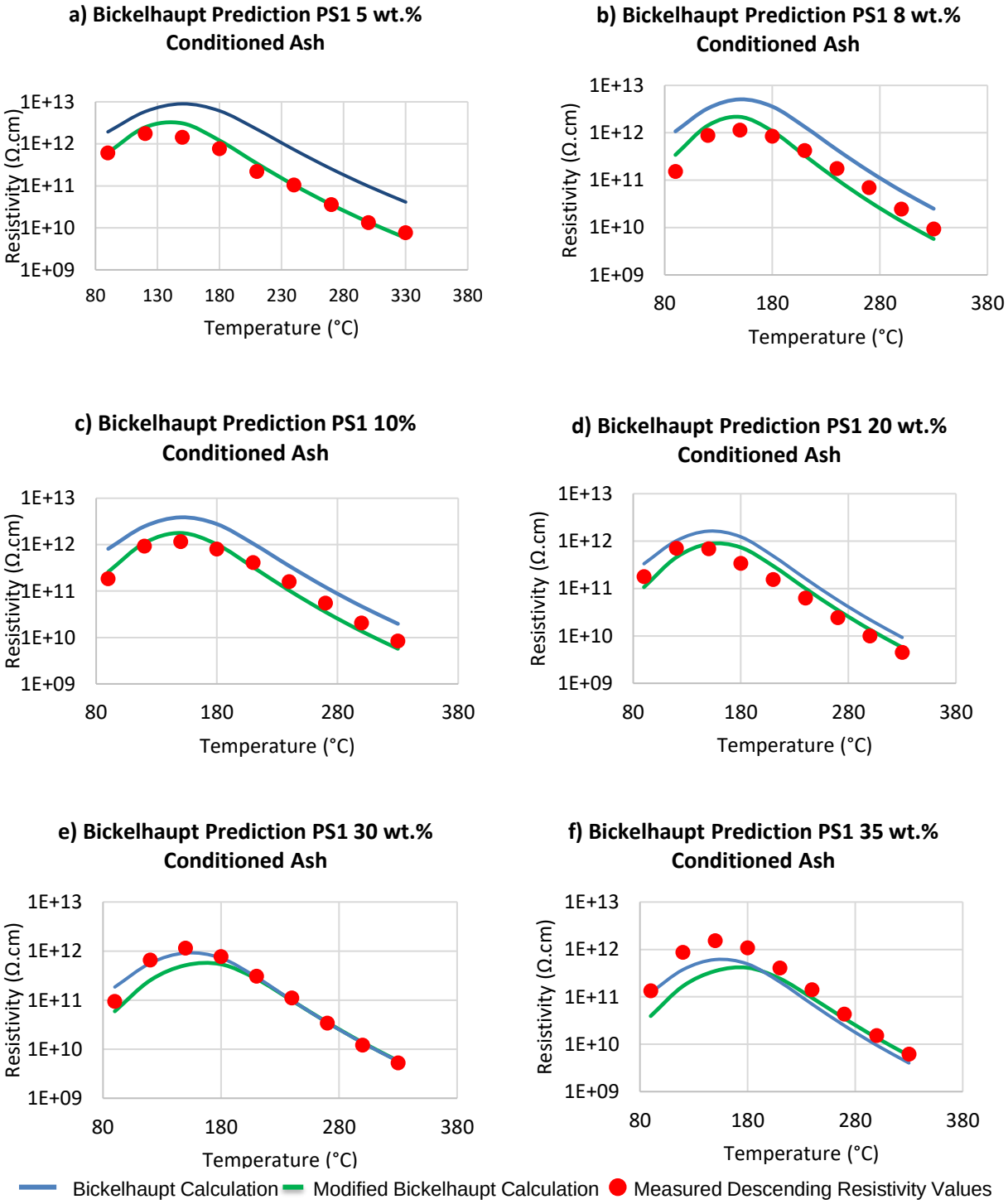

Figure 5-22: Modified Bickelhaupt model predictions for PS-1 at a) 5 wt.%, b) 8 wt.%, c) 10 wt.%, d) 20 wt.%, e) 30 wt.% and f) 35 wt.% conditioned ash

The modified Bickelhaupt formula that was developed for the PS-1 ash samples was applied to PS-2 ash samples to evaluate if the optimised parameters for PS-1 could be applied to other South African ashes, and the trends shown in Figure 5-23 (a–c).

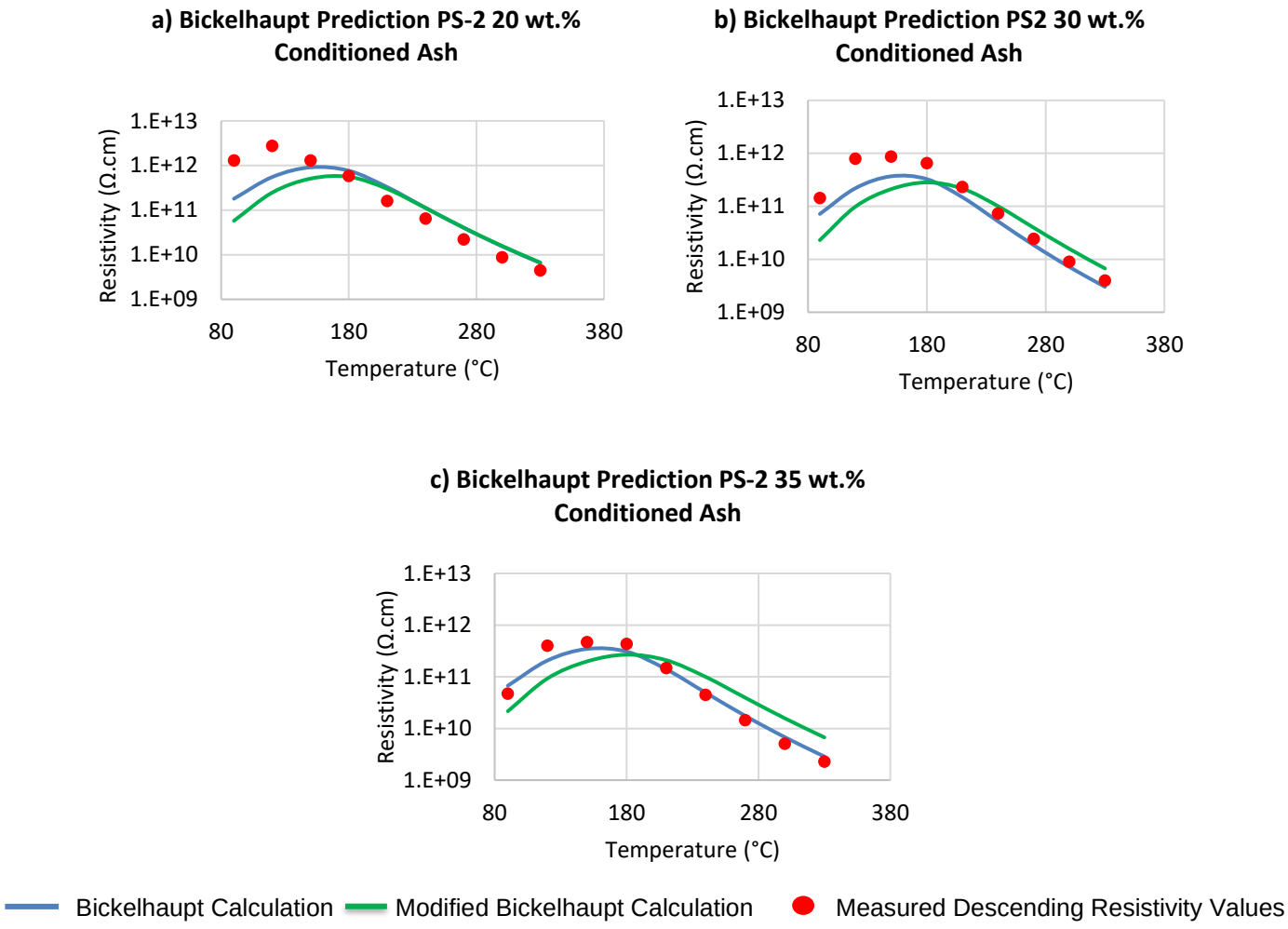

Figure 5-23: Modified Bickelhaupt model predictions for PS-2 at a) 20 wt.%, b) 30 wt.% and c) 35 wt.% conditioned ash

However, the modified model that was developed for the PS-1 ash samples does not offer an improved correlation for the PS-2 ash samples. This is an indication that adjusting the atomic composition alone is insufficient to making the model suitable across all South African ashes.

5.6.4 Applying Ribberink's [15] modified Bickelhaupt model

An attempt was made to apply the Bickelhaupt model where the parameters were optimised for an improved fit to data obtained in earlier studies using the same ash sample, to the results

obtained in the present study. Ribberink's model [15] was selected because the baseline comparison for equipment repeatability (Section 4.3.2) proved a positive comparison against the results obtained [15]. The research conducted by Ribberink was on the effect of moisture on the fly ash resistivity of selected South African ashes [15], with ash samples selected from the same power stations that were included in the present study. Trends obtained upon comparison of the applied modified model to the measure data for the 5 wt.%, 10 wt.%, 20 wt.% and 35 wt.% PS-1 conditioned ash samples, as well as the 20 wt.% and 35 wt.% PS-2 conditioned ash samples, are presented.

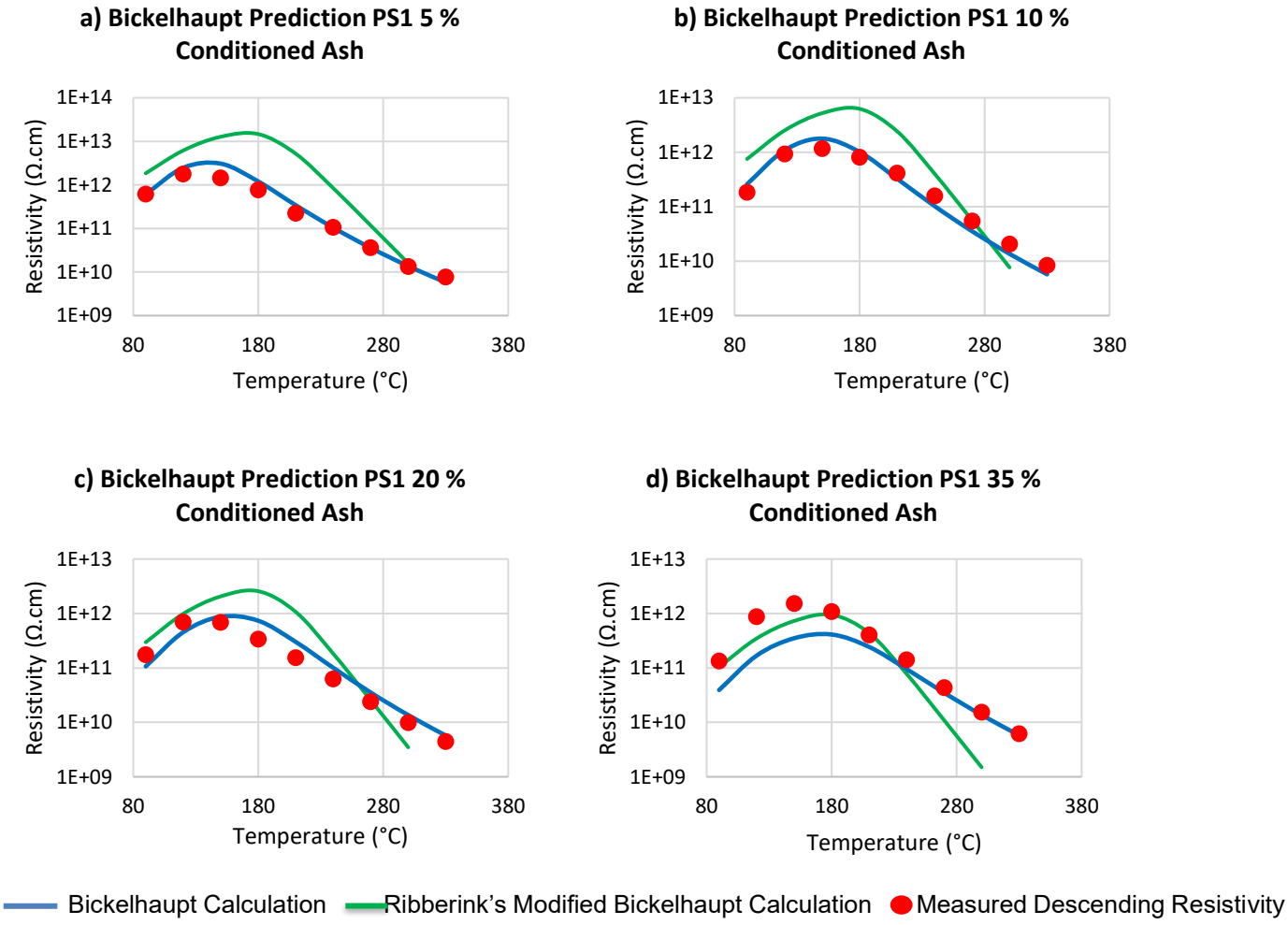

Figure 5-24: Comparison of modified Bickelhaupt model predictions for PS-1 at a) 5 wt.%, b) 10 wt.%, c) 20 wt.% and d) 35 wt.% conditioned ash

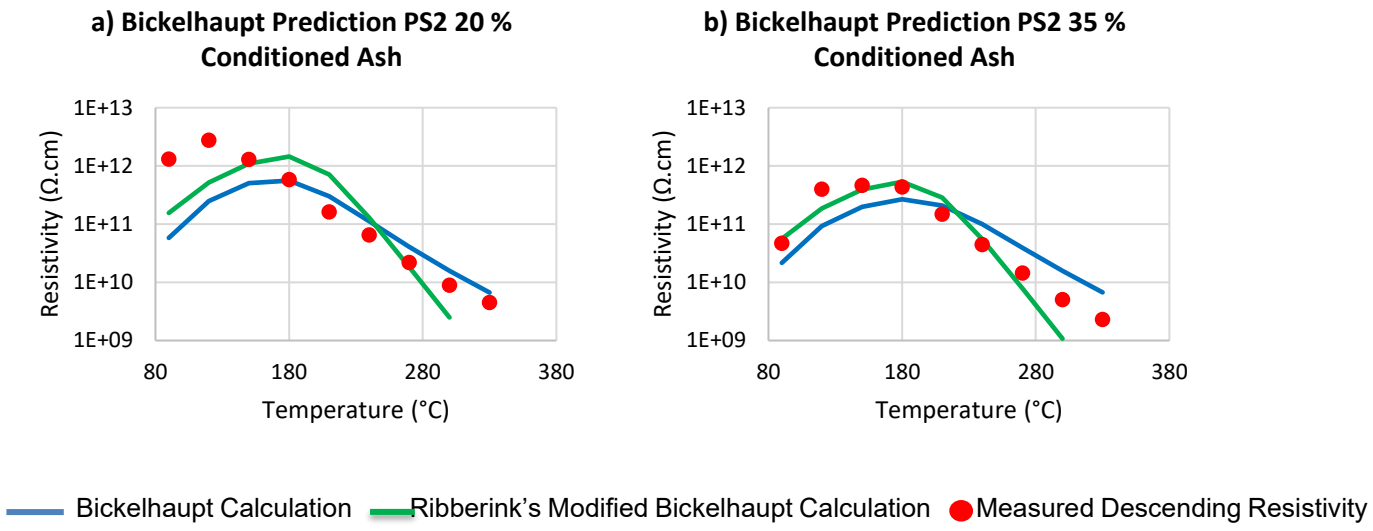

Figure 5-25: Comparison of modified Bickelhaupt model predictions for PS-2 at a) 20 wt.% and b) 35 wt.% conditioned ash samples

The trends plotted in Figure 5-24 (a-d) and Figure 5-25 (a-b) demonstrate that the modification conducted on the original Bickelhaupt model to align with the measured values for moisture alone on ash samples of the two selected South African power station [15] does not suitably account for the ionic loading from the saline solution conditioning on the ash samples. The Pearson correlation coefficients were determined to quantitatively demonstrate the quality of fit for each experimental set.

5.7 Pearson correlation coefficients

The Pearson correlation method is a method that is used for numerical variables, whereby a value between − 1 and 1 is determined to indicate the degree of correlation between two sets of data. A value of 0 indicates no correlation, 1 is total positive correlation, and −1 indicates total negative correlation [80]. The Pearson coefficient was determined for the results after applying the Bickelhaupt model directly as well as the results from the modified model. The results are presented in Table 5-2. The cells where the coefficient is greater than 0.9 are highlighted in grey. This indicates a close correlation to the measured fly ash resistivity values and indicates the suitability of applying the model in that scenario.

Table 5-2: Pearson coefficient for the correlation models

Correlation	PS-1 5 wt.%	PS-1 8 wt.%	PS-1 10 wt.%	PS-1 20 wt.%	PS-1 30 wt.%	PS-1 35 wt.%	PS-2 20 wt.%	PS-2 30 wt.%	PS-2 35 wt.%
Original Bickelhaupt Model	0.79	0.97	0.96	0.81	0.96	0.96	0.62	0.98	0.98
Sodium-Depleted Model	0.89	0.99	0.99	0.91	0.99	0.99	0.53	0.95	0.97
Modified Bickelhaupt Model	0.96	0.97	0.98	0.84	0.94	0.89	0.33	0.69	0.76
Ribberink Modified Bickelhaupt Model	0.64	0.89	0.87	0.95	0.86	0.91	0.24	0.77	0.86

The results obtained from the Pearson coefficient indicate that the sodium-depleted Bickelhaupt model provides the best correlation to the measured fly ash resistivity measurements for PS-1 conditioned ash samples as well as the higher wt.% conditioned samples from PS-2. The modified Bickelhaupt model is suitable for PS-1 ash samples, however the model does not offer a suitable prediction to the conditioned ash samples from PS-2. This indicates that the modified equation may not be applied directly to the ash samples of other power stations.

The modified Bickelhaupt model developed by Ribberink [15] offers a reasonable prediction to the PS-1 conditioned ash samples, although not as high as the sodium-depleted model of the modified Bickelhaupt model conducted on the conditioned ash samples. The model does not offer an adequate prediction to the PS-2 conditioned ash samples and may not be applied directly.

These results indicated that the constants applied in the models are influenced by the mineralogy of the ash samples and any adjustments made for a specific salt loading may not be applied directly to all ash samples. A summary of the original and derived constants for the Bickelhaupt parameters is provided in table using equations 2-4 and 2-5.

Table 5-3: Summary of the original and derived constants applied in the Bickelhaupt model

Equation for volume resistivity: $\rho_v = \exp[A_1\, lnX - B_1\, lnY + C_1\, lnZ + D_1) - (F_1)E + \frac{G_1}{T}]$			
Constants	**Original model**	**Modified model**	**% Change**
A_1	-1.8916	0	-100
B_1	0.9696	0.9705	0.09
C_1	1.237	1.313	6.14
D_1	3.62876	4.06442	12.00
F_1	0.069078	0.068763	-0.45
G_1	9980.58	9980.58	0
Equation for surface resistivity: $\rho_s = \exp[A_2 - B_2\, lnX - C_2(H_2O) - D_2E - F_2(H_2O)(\exp\left(\frac{G_2}{T}\right)]$			
Constants	**Original model**	**Modified model**	**% Change**
A_2	27.59774	27.21581	-1.38
B_2	2.233348	2.229107	-0.19
C_2	0.00176	0.00176	0
D_2	0.069078	0.069078	0
F_2	0.00073895	0.000743	0.55
G_2	2303.3	2384.0	3.50

The most significant changes were applied to constants A_1, C_1 and D_1 of the volume resistivity equation. The model evaluation showed that volume resistivity is independent of sodium concentration suggesting that the addition of sodium in the saline solution is adsorbed on the ash particles and not absorbed [24].

CHAPTER 6 CONCLUSION AND RECOMMENDATIONS

The fly ash resistivity measurements of raw ash samples from two South African power stations (PS-1 and PS-2) exceeded 1×10^{11} Ω.cm which is the required resistivity for optimum electrostatic precipitator dust collection. One of the methods most commonly employed for fly ash resistivity adjustment is the use of conditioning agents. Flue gas conditioning allows the chemical parameters of the fly ash to be modified in order to improve the fly ash resistivity. Sodium conditioning is a suitable agent that may be applied to South African fly ashes because of its high fly ash resistivity, specifically surface resistivity.

6.1 Conclusion

The first objective of the study to evaluate the effect of the Eskom saline solution concentration and fly ash chemical composition with the fly ash resistivity and evaluate if the fly ash resistivity for optimum electrostatic precipitator performance can be achieved, was met.

Sodium conditioning has proved effective in numerous applications and research globally for the reduction of fly ash resistivity. The high sodium concentration in the saline solution produced at one of the South African power stations was able to alter the composition of the fly ash samples, based on the varying degree of conditioning (by mass percentage) to the ash, and showed a positive influence in reducing the fly ash resistivity measurements for both power station ashes.

Initial fly ash resistivity experiments with the conditioned ash samples without moisture revealed the presence of hydrates / water of crystallisation when using the saline solution for conditioning. It was observed that the release of the hydrates plays a role in reducing the fly ash resistivity measurements.

The reduction in the surface resistivity measurements improved as the concentration of the saline solution increased (which resulted in an increase in the sodium ion concentration). The results obtained for PS-1 ash samples revealed that conditioning the fly ash samples from PS-1 with saline solution in excess of 20 wt.%, is sufficient to obtain fly ash resistivity measurements to within the values regarded for optimum electrostatic precipitator efficiency.

It was evident that the sodium contained in the saline solution was responsible for the reduced resistivity due to adsorption thereof onto the surface of the particles (influencing the surface

resistivity). In fly ash samples with higher calcium mineralogy, the latter seem to serve as the seed for the sodium salt precipitation from the saline solution.

The second objective to evaluate the suitability of the Bickelhaupt model for predicting fly ash resistivity with the saline solution conditioning revealed that the original Bickelhaupt model (1979) offered a good prediction for samples with the higher conditioning agent concentrations by mass when compared with the lower concentration conditioned samples.

A modification to the Bickelhaupt model provided a suitable prediction for the lower and higher concentration ash samples for PS-1 however the same formula was not as suitable for PS-2 ash samples although it did offer a better prediction than the original Bickelhaupt formula. The Bickelhaupt model for sodium-depleted ashes was modelled for both power station ash samples and showed an improvement for the volume resistivity of both power station conditioned ash samples.

6.2 Recommendations

It is recommended that future research be conducted on the hydrates / water of crystallisation effect so that this mechanism can also be evaluated for reducing the fly ash resistivity measurements. The source of the hydrates and temperatures at which it decomposed must be studied for application. It is also recommended that coal ash at similar conditions at which the boilers of PS-1 and PS-2 operate be sourced and evaluate resistivity measures again.

Further work is required using synthetic solutions of sodium sulphate to confirm the optimum conditioning ratio of sodium and fly ash. The study that was conducted focused on the mass volume of the saline solution and not on the individual ions.

Research on the mineralogy of the ash material and the ability to adsorb the sodium ions is required. The observation with PS-2 ash having the higher sodium but not observing the same or further reduction in fly ash resistivity measurements when compared with PS-1 ash samples needs to be researched.

It is further recommended that the testing of the research in an operating unit be carried out to confirm the practical field application of the laboratory results. The research and its outcomes were presented at the Pittsburgh Coal Conference (September 2022) with positive feedback received as well as interest from industry.

BIBLIOGRAPHY

[1] *Air Quality Guidelines* - Update 2021. Copenhagen, Denmark: WHO Regional Office for Europe, 2021.

[2] V. A. Southerland, *Global urban temporal trends in fine particulate matter ($PM_{2.5}$) and attributable health burdens: estimates from global datasets*, The Lancet Planetary Health, vol. 6, pp. E139–E146, 2022

[3] S. Armstrong, *Air Quality - Department of Environmental Affairs,* Air Quality - Chapter, vol. 10., Readkong.com. [Online]. Available: https://www.readkong.com/page/air-quality-department-of-environmental-affairs-6485135?p=3. [Accessed: 16-June-2021].

[4] *How Does Your Air Measure Up Against the WHO Air Quality Guidelines?* A State of Global Air Special Analysis. Boston MA, 2022

[5] *Strategy to Address Air Pollution in Dense Low-Income Settlements*, South African Government Gazette No, vol. 42464, 2018.

[6] S. Moletsane, *Intra-urban variability of $PM_{2.5}$ in a dense, low-income settlement on the South African Highveld*, Clean Air Journal 31(1) 1—9, 2021.

[7] E. E. McDuffie et al., *Source sector and fuel contributions to ambient PM2.5 and attributable mortality across multiple spatial scales*, Nature Communications, vol. 12, no. 1, p. 3594, 2021.

[8] B. Hattingh, *Factors Impacting on the use of coal*, Eskom Power Series Book, 2022.

[9] E. Patel, *Practical Considerations in the Implementation of Emissions Reduction Solutions at Eskom's Coal Fired Power Plant*, Kempton Park, RSA, 2012.

[10] C. Cassim, *Eskom Integrated Report*, 2021

[11] E. M. Patel, *474-12454 Air Quality Control, Generation Engineering Strategic Report*, pp. 474–12454, 2021.

[12] L. Van Wyk, M.Sc. Thesis, *The Correlation Between Mineralogy and Resistivity in Typical South African Coal Ashes,* North-West University; Potchefstroom, 2015.

[13] S. Shanthakumar, D. N. Singh, and R. C. Phadke, *Flue gas conditioning for reducing suspended particulate matter from thermal power stations*, Prog. Energy Combust. Sci., vol. 34, no. 6, pp. 685–695, 2008.

[14] R. E. Bickelhaupt, *Sodium Conditioning to Reduce Fly Ash Resistivity*, Southern Research Institute, 1974.

[15] J. A. Ribberink, M.Sc. Thesis, *Influence of moisture on the resistivity of selected South African fly ashes*, North-West University; Potchefstroom, 2019.

[16] L. Qi and Y. Yuan, *Mechanism of the effect of alkali metal on the electrostatic precipitability of fly ash*, Fuel (Lond.), vol. 107, pp. 848–851, 2013.

[17] A. Lowe, *Effect of Sodium Dosing on ESP Performance*, Delta Energy, 2005.

[18] M. D. Durham, *Flue Gas Conditioning for Improved Particle Collection in Electrostatic Precipitators,* 1993.

[19] R.F. Altman, *Guidelines for Upgrading Electrostatic Precipitator Performance Volume 2: Electrostatic Precipitator Upgrade Options*, vol. 2. Electric Power Research Institute: EPRI, 1999.

[20] G. V. Chauke, M.Sc. Thesis, *Ash resistivity profiling and effect of a high frequency power supply on electrostatic precipitator efficiency*, North-West University; Potchefstroom, 2015.

[21] G. S. Castle, *Mechanisms Involved in Fly Ash Precipitation in the Presence of Conditioning Agents A Review*, IEEE Transactions on Industry Applications, no. 2, pp. 1A – 16, 1980.

[22] *A Study of Resistivity and Conditioning of Fly Ash*, Southern Research Institute, 1972.

[23] L. J. Roberts, *Investigating the impact of an Al-Si additive on the resistivity of biomass ashes*, 2018.

[24] Caplinq.com. [Online]. Available: https://www.caplinq.com/blog/wp-content/uploads/2013/05/bulk-resistivity-vs-surface-resistivity.jpg. [Accessed: 27-August-2021].

[25] S.-C. Yung, R. G. Patterson, B. L. Hancock, and S. Calvert, *Flue Gas Conditioning*, 1985.

[26] H. J. White, *Electrical resistivity of fly ash*, Air Repair, vol. 3, no. 2, pp. 79–86, 1953.

[27] E. Karakatsanis, *Plant Operation Manual*, in ESKOM Holdings Ltd SRO Plant Upgrade, 2006.

[28] G. Lok, RR/06/28091 *SRO Brine Disposal - Tutuka Power Station*, in Eskom Resources And Strategy Technology Strategy And Planning Research Report, 2007.

[29] L. Burger, *Impact Of Proposed Brine Evaporation At Tutuka Power Station (Mpumalanga) On Particulate Air Emissions,* 2011.

[30] B. Nyembe, *240-55864856 Integrated Water and Waste Water Management Plan Guideline*, Eskom Holdings, 2021.

[31] O. O. Fatoba, L. F. Petrik, R. O. Akinyeye, W. M. Gitari, and E. I. Iwuoha, *Long-term brine impacted fly ash, Part II: Mobility of major species in the ash residues*, Int. J. Environ. Sci. Technol. (Tehran), vol. 11, no. 6, pp. 1641–1652, 2014.

[32] H. Van Gool, *Water Resources and Environment Technical Note F.3 Wastewater Reuse, The International Bank for Reconstruction and Development*/THE WORLD BANK, 2003 .

[33] Epa.gov. [Online]. Available: https://www.epa.gov/coalash/coal-ash-basics, [Accessed: 07-June-2021].

[34] J. Yu, *International Conference on Future Electrical Power and Energy Systems,* 2012.

[35] T. Adams et al., *List of contributors, in Coal Combustion Products (CCP's),* Elsevier, pp. xi–xii, 2017

[36] A. Bhatt, S. Priyadarshini, A. Acharath Mohanakrishnan, A. Abri, M. Sattler, and S. Techapaphawit, *Physical, chemical, and geotechnical properties of coal fly ash: A global review*, Case Stud. Constr. Mater., vol. 11, no. e00263, p. e00263, 2019.

[37] Department of Environmental Affairs, *National Environmental Management: Air Quality (Act No. 39 of 2004),* 2013.

[38] United States Environmental Protection Agency, *Particulate Matter Emissions*, 2018.

[39] *Health effects of particulate matter, Policy implications for countries in eastern Europe, Caucasus and central Asia*, WHO, 2013.

[40] *Electrostatic Precipitator (ESP)*, Savree.com, 01-Jan-1970. [Online]. Available: https://savree.com/en/encyclopedia/electrostatic-precipitator-esp. [Accessed: 02-June-2021].

[41] J. Keir, *Emission Control Strategies and Equipment*, Eskom Power Series, 2022.

[42] J. Turner, *United States Environmental Protection Agency*, 1999.

[43] G. Chauke and R. Gouws, *Fly ash resistivity profiling for south African coal fired power stations*, J. Energy Power Eng., vol. 7, no. 12, 2013.

[44] *Basics of electrostatic precipitator (ESP) operation*, Babcock & Wilcox. [Online]. Available: https://www.babcock.com/home/about/resources/learning-center/basic-esp-operation. [Accessed: 02-June-2021].

[45] R. Mastopietro, *Fly Ash Resistivity with Injected Reagents and Predicted Impacts on Electrostatic Precipitators*, 2016.

[46] J. S. Narayan, *Studies on factors influencing fly ash resistivity from electrostatic precipitator - with reference to India*, Journal of Scientific and Industrial Research, 2011.

[47] J. Burger, M.Sc. Thesis, *The Influence of SO_3 conditioning on the resistivity of selected South African fly-ashes*, North-West University; Potchefstroom, 2020.

[48] A. Chandra, *Some investigations on fly ash resistivity generated in Indian power plants, in Electrostatic Precipitation*, Berlin, Heidelberg, pp. 399–405, 2009

[49] J. Xu, Z. Gu, and J. Zhang, *Experimental study on fly ash resistivity at temperatures above 673 K*, Fuel (Lond.), vol. 116, pp. 650–654, 2014.

[50] H. Brauer, *Design and Operation of Electrostatic Precipitators, Air Pollution Control Equipment*, 1981.

[51] H. Zhao, Y. He, and J. Shen, *Effects of temperature on electrostatic precipitators of fine particles and SO_3*, Aerosol Air Qual. Res., vol. 18, no. 11, pp. 2906–2911, 2018.

[52] Tai & Chyun, *ESP retrofit with high frequency transformer rectifier upgrade in petrochemical plant,* , 26-Nov-2020. [Online]. Available: https://www.taichyun.com.tw/case-studies/esp-retrofit-with-high-frequency-transformer-rectifier-upgrade-in-petrochemical-plant/. [Accessed: 28-May-2022].

[53] J. Schroeder, *The effect of brine on South African fly ash resistivity*, North-West University; Potchefstroom, 2018.

[54] *A Study of Resistivity and Conditioning of Fly Ash*, Environmental Protection Agency CPA 70-149, 1972.

[55] R. E. Bickelhaupt, *Sodium Conditioning to Reduce Fly Ash Resistivity*, 1974.

[56] *Advanced Flue Gas Conditioning as a Retrofit Upgrade to Enhance PM Collection from Coal-Fired Electric Utility Boiler*, U.S DOE Report, 2003.

[57] 2.12: Hydrates, Chemistry LibreTexts, 07-Jul-2019. [Online]. Available: https://chem.libretexts.org/Courses/University_of_Arkansas_Little_Rock/Chem_1402%3A_General_Chemistry_1_(Kattoum)/Text/2%3A_Atoms%2C_Molecules%2C_and_Ions/2.12%3A_Hydrates. [Accessed: 20-April-2022].

[58] O. O. Fatoba, *Long-Term Brine Impacted Fly Ash. Part 1: Chemical and Mineralogical Composition of the Ash Residues*, International Journal of Environmental Science and Technology, 2013.

[59] *Criteria and Guidelines for the Laboratory Measurement and Reporting of Fly Ash Resistivity*, IEEE, Standard, vol. 984; New York: Institute of Electrical and Electronics Engineers, 1984.

[60] R. E. Bickelhaupt, *A Technique for Predicting Fly Ash Resistivity, Southern Research Institute*, 1979.

[61] R.F. Altman, *Fly Ash Property Study*, Electric Power Research Institute, 2000.

[62] R. E. Bickelhaupt, *A Method for Predicting the Effective Volume Resistivity of a Sodium Depleted Fly Ash Layer*, Journal of the Air Pollution Control Association, 1984.

[63] N. Mukherjee, *Acid dew point temperature of flue gas vs excess air*, Linkedin, 2021. [Online]. Available: https://www.linkedin.com/pulse/acid-dew-point-temperature-flue-gases-vs-excess-air-mukherjee/. [Accessed: 02-Jan-2021].

[64] B. Ramasamy, *Short review of salt recovery from reverse osmosis rejects*, in Salt in the Earth, IntechOpen, 2020.

[65] P. Xu, T. Y. Cath, A. P. Robertson, M. Reinhard, J. O. Leckie, and J. E. Drewes, *Critical review of desalination concentrate management, treatment and beneficial use*, Environ. Eng. Sci., vol. 30, no. 8, pp. 502–514, 2013.

[66] R. F. Altman, *A Manual on the Use of Flue Gas Conditioning for ESP Performance Enhancement,* Electric Power Research Institute, 1985

[67] M. A. Ahmad, *Fly Ash Slurry Transportation: Indian Scenario*, vol. 2, no. 1, pp. 1–7, 2014.

[68] J. Chisholm, *Fundamentals of Gas Laws*, Texas A&M University, 2003.

[69] C. Zheng et al., *Measurement and prediction of fly ash resistivity over a wide range of temperature*, Fuel (Lond.), vol. 216, pp. 673–680, 2018.

[70] O. Aliku, *Desalination: A Means of Increasing Irrigation Water Sources for Sustainable Crop Production*, 2017," Intech, 2017.

[71] H. L. Li, G. L. Liu, and Y. Cao, *Content and distribution of trace elements and polycyclic aromatic hydrocarbons in fly ash from a coal-fired CHP plant*, Aerosol Air Qual. Res., vol. 14, no. 4, pp. 1179–1188, 2014.

[72] H. M. Ng, N. M. Saidi, F. S. Omar, K. Ramesh, S. Ramesh, and S. Bashir, *Thermogravimetric analysis of polymers*, Encyclopaedia of Polymer Science and Technology. John Wiley & Sons, Inc., Hoboken, NJ, USA, pp. 1–29, 2018.

[73] A. Sciubidlo, *Novel Sorbents for Flue Gas Purification*, Journal of Power Technologies, 2012.

[74] R. L. Magin, *Transition Temperatures of the Hydrates of Na_2SO4, Na_2HPO_4, and KF as Fixed Points in Biomedical Thermometry*, Journal of Research of the National Bureau of Standards, vol. 86, 1980.

[75] J. Xu, T. Li, T. Yan, J. Chao, and R. Wang, *Dehydration kinetics and thermodynamics of magnesium chloride hexahydrate for thermal energy storage*, Sol. Energy Mater. Sol. Cells, vol. 219, no. 110819, p. 110819, 2021.

[76] S. Karunadasa, *Dehydration of Calcium Chloride as Examined by High-temperature X-ray Powder Diffraction*, International Multidisciplinary Research Journal, 2019.

[77] S. V. Pisupati, *Utilisation of coal in IGCC systems*, 2017.

[78] C. van Alphen, *Tutuka Colling Tower Sludge*, Eskom Technical Memorandum, 2015

[79] *Water conductivity - Lenntech,* Lenntech.com. [Online]. Available: https://www.lenntech.com/applications/ultrapure/conductivity/water-conductivity.htm,. [Accessed: 28-May-2021].

[80] D. Nettleton, *Analysis and Modelling for Predictive Analytics Projects*, 2014.

[81] L. Jestin and S.J Piketh, *Environmental protection and emissions control technologies, In: Overview of the Power Plant Industry MEC4115Z*, Department of Mechanical Engineering, University of Cape Town, Cape Town, pp. 9 - 93, 2020

APPENDIX A: SAMPLE CALCULATION FOR MOISTURE

The ideal gas law (A-1) was used to calculate the volume of moisture introduced with the saline solution at the different unit load factors.

$$V_{(water)} = \left(n_{(Water)}\ R\ T\right) / P_{(system)} \qquad \text{A–1}$$

The number of moles of water injected for the two flow rates was calculated using the fact that the mass of one mole of water is 18.01 g.

$$\text{Therefore, } 5\ \frac{m^3}{hr} = 1400\ \frac{g}{s} = 1400\ \frac{g}{s} / 18.01\ \frac{g}{mole} = 77.73\ moles\ per\ second \qquad \text{A–2}$$

$$\text{Similarly, } 25\ \frac{\boldsymbol{m^3}}{\boldsymbol{hr}} = 6944\ \frac{g}{s} = 6944\ \frac{g}{s}\ / 18.01\ \frac{g}{mole} = 385.59\ moles\ per\ second \qquad \text{A–3}$$

Using the final flue gas temperatures determined in Table 3-4, the number of moles of water calculated in equations 3-5 and 3-6 as well as the boiler design flue gas pressure, the volume of water (moisture) added was calculated. For final flue gas temperature of 169 °C (442 K) at 100 maximum continuous rating for a saline solution flow rate of 5 m^3/hr we apply the following:

$$V_{(water)} = \frac{(77.73\ x\ 8.314\ x\ 441.12\ )}{82800} = 3.42\ m^3/s \qquad \text{A–4}$$

The resultant volumes of moisture added are given as follows: in Table 3-5 for the saline solution injection rate of 5 m^3/hr and in for the injection rate of 25 m^3/hr.

APPENDIX B: FLY ASH RESISTIVITY RESULTS

The resistivity data for PS-1 initial ascending measurements are the following.

Table B-1: PS-1 Initial Ascending fly ash resistivity Measurements

PS-1 Initial Ascending Measurements							
Temp (°C)	**Resistivity Unconditioned Ash**	**5% Conditioned Ash**	**8% Conditioned Ash**	**10% Conditioned Ash**	**20% Conditioned Ash**	**30% Conditioned Ash**	**35% Conditioned Ash**
90	1.20E+14	6.72E+11	2.27E+11	2.88E+11	1.10E+11	1.38E+11	1.65E+11
120	7.84E+13	4.70E+11	1.82E+11	2.41E+11	5.71E+10	7.03E+10	7.20E+10
150	2.74E+13	3.41E+11	2.06E+11	2.61E+11	9.93E+10	9.00E+10	8.82E+10
180	6.51E+12	6.83E+11	4.09E+11	4.43E+11	1.24E+11	9.85E+10	1.18E+11
210	1.71E+12	3.46E+11	3.32E+11	3.30E+11	1.36E+11	1.10E+11	1.27E+11
240	4.05E+11	1.25E+11	1.73E+11	1.67E+11	7.07E+10	6.50E+10	7.11E+10
270	1.02E+11	4.12E+10	6.98E+10	6.74E+10	3.26E+10	3.19E+10	3.69E+10
300	2.79E+10	1.65E+10	2.81E+10	2.92E+10	1.26E+10	1.45E+10	1.64E+10
330	9.21E+09	8.02E+09	1.25E+10	1.19E+10	7.09E+09	8.04E+09	8.86E+09

The graph with the data plotted is shown in Figure B-1.

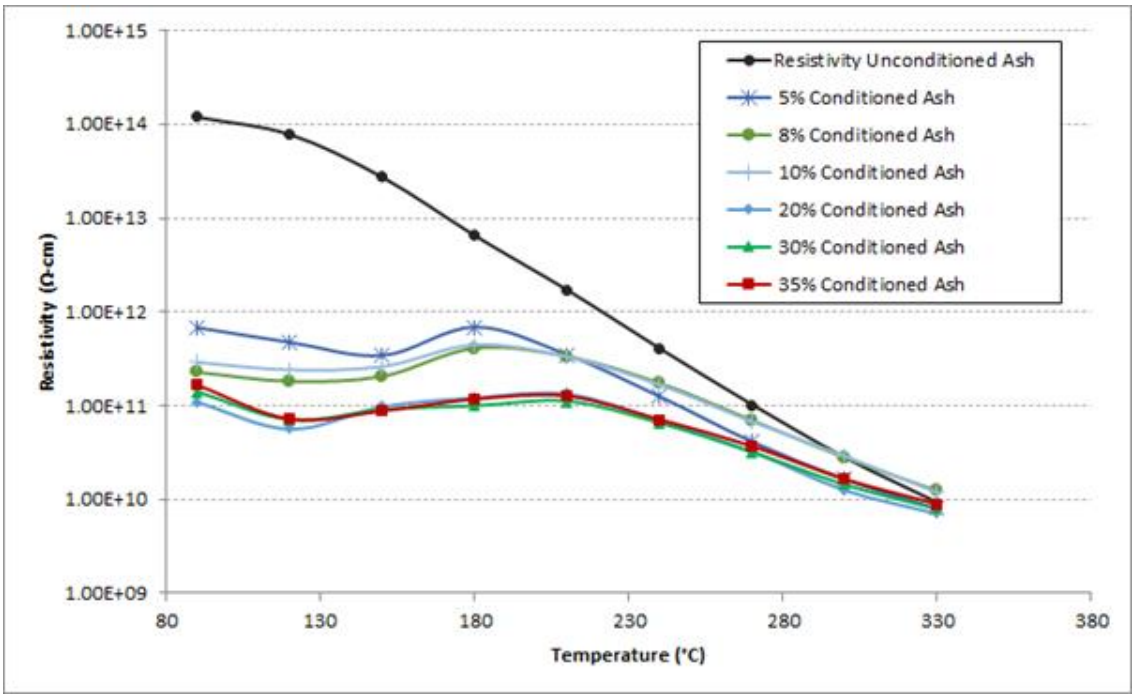

Figure B-1: Graph showing the trends of fly ash resistivity measurements for PS-1 ash samples

The repeat dry run resistivity measurements for PS-1 ash samples, conditioned ≥ 20 wt.% are the following.

Table B-2: Fly ash resistivity measurements for PS-1 repeat ascending experiment

Repeat Resistivity Runs Ascending				
Temp (°C)	**Resistivity Unconditioned Ash**	**Repeat Resistivity 20% Conditioned Ash**	**Repeat Resistivity 30% Conditioned Ash**	**Repeat Resistivity 35% Conditioned Ash**
90	1.20E+14	2.06E+13	3.45E+13	4.61E+13
120	7.84E+13	1.27E+13	2.52E+13	2.96E+13
150	2.74E+13	4.84E+12	1.16E+13	1.24E+13
180	6.51E+12	1.53E+12	3.52E+12	4.43E+12
210	1.71E+12	4.68E+11	1.06E+12	1.35E+12
240	4.05E+11	1.77E+11	3.23E+11	3.63E+11
270	1.02E+11	6.53E+10	1.00E+11	1.19E+11
300	2.79E+10	2.45E+10	3.39E+10	3.87E+10
330	9.21E+09	8.61E+09	1.15E+10	1.25E+10

The fly ash resistivity measurements were plotted together with the data from the initial fly ash resistivity experiment and is shown in Figure B-2.

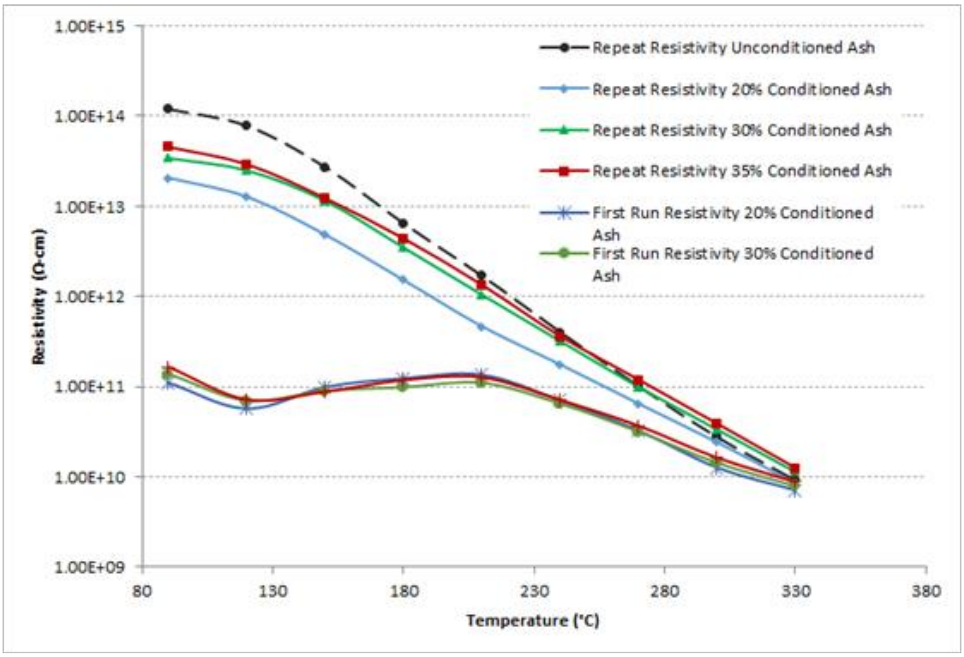

Figure B-2: Graph showing the data for PS-1 initial and repeat resistivity experiments for less than 20 % conditioned ash samples

APPENDIX C: ORIGINAL BICKELHAUPT CALCULATIONS

The atomic concentrations of the elements contained in the ash serve as input to the Bickelhaupt model. The data obtained from X-ray fluorescence analysis (LOI free basis) was utilised as the basis for the calculations. The steps to determine the atomic concentration (wt.%) is explained below.

Table C-1: Table showing the conversion of the atomic wt.% from X-ray fluorescence to atomic concentrations (wt.%)

Ash Component	Determined from X-ray fluorescence	Normalised	Molecular Weight	Molar Amount	Molecular %	Cation Molar Amount	Cation Mass Amount	Atomic Conc. (wt.%)
Al_2O_3	28.43	28.47	102	0.279	19.82	0.4	7.93	28.43
CaO	5.31	5.32	56.1	0.095	6.73	0.5	3.36	5.31
Cr_2O_3	0.04	0.04	152	0.000	0.02	0.4	0.01	0.04
Fe_2O_3	5.68	5.69	159.7	0.036	2.53	0.4	1.01	5.68
K_2O	0.69	0.69	94.2	0.007	0.52	0.7	0.36	0.69
MgO	1.39	1.39	40.3	0.035	2.45	0.5	1.23	1.39
MnO	0.04	0.04	70.9	0.001	0.04	0.5	0.02	0.04
Na_2O	0.16	0.16	62	0.003	0.18	0.7	0.13	0.16
P_2O_5	0.38	0.38	141.9	0.003	0.19	0.3	0.06	0.38
SiO_2	55.47	55.55	60.1	0.924	65.62	0.3	19.69	55.47
TiO_2	1.62	1.62	79.9	0.020	1.44	0.3	0.43	1.62
V_2O_5	0.02	0.02	181.9	0.000	0.01	0.3	0.00	0.02
ZrO_2	0.07	0.07	123.2	0.001	0.04	0.3	0.01	0.07
BaO	0.13	0.13	153.3	0.001	0.06	0.5	0.03	0.13
SrO	0.12	0.12	103.6	0.001	0.08	0.5	0.04	0.12
SO_3	0.3	0.30	80.1	0.004	0.27	0.3	0.08	0.3

a) Normalised data – the formula used to determine the normalised data was the following:

$$Xn = \frac{X_d}{\Sigma X_D}\, x\, 100 \qquad \text{C–1}$$

where X_n is the normalised value for the specific ash component n, X_d is the determined % of the specific ash component and $\sum X_D$ is the sum of all the determined values.

b) Molecular weight – as determined from the periodic table

c) Molar amount – normalised weight % / molecular weight

d) Molecular percentage:

$$Xmpn = \frac{X_{man}}{\Sigma X_{MA}}\ 100 \qquad \text{C–2}$$

where X_{mpn} is the molecular percentage for the specific ash component n, X_{man} is the determined molecular amount for the specific ash component as determined in (c) and $\sum X_{MA}$ is the sum of the molecular amount for all the components.

e) Cation molar amount – determined using information from the periodic table
f) Cation mass amount – determined using the cation molar amount and the molar amount for each parameter
g) Atomic concentration – determined using the formula:

$$Xacn = \frac{X_{cmn}}{\Sigma X_{CM}}\ x\ 100 \qquad \text{C–3}$$

where X_{acn} is the atomic concentration for the specific ash component n, X_{cmn} is the determined cation mass amount for the specific ash component as determined in (f) and $\sum X_{CM}$ is the sum of the cation mass amount for all the components.

Once the atomic concentrations are determined, the values required for the Bickelhaupt calculation are noted, as follows:

Table C-2: Table showing the calculated concentration for PS-1 conditioned ash samples used in the Bickelhaupt calculation

Atomic Species	PS-1 0%	PS-1 5%	PS-1 8%	PS-1 10%	PS-1 20%	PS-1 30%	PS-1 35%
Na (X)	0.128	0.184	0.239	0.270	0.403	0.524	0.630
Fe (Y)	1.011	0.970	0.969	0.969	0.984	0.977	0.975
Mg + Ca (Z)	4.591	4.472	4.466	4.451	4.509	4.510	4.523

Table C-6-3: Table showing the calculated concentration for PS-2 conditioned ash samples used in the Bickelhaupt calculation

Atomic Species	PS-2 0%	PS-2 20%	PS-2 30%	PS-2 35%
Na (X)	0.18	0.53	0.80	0.82
Fe (Y)	0.64	0.63	0.63	0.63
Mg + Ca (Z)	3.66	3.67	3.66	3.67

The following original Bickelhaupt equation was used to determine the surface resistivity of each ash sample:

$$\rho_s \ = \exp[\mathrm{A}_2 - \mathrm{B}_2\ lnX - \mathrm{C}_2(H_2O) - \mathrm{D}_2E - \mathrm{F}_2(H_2O)(\exp\left(\frac{\mathrm{G}_2}{T}\right)] \qquad C-4$$

where A_2 = 27.59774, B_2 = 2.233348, C_2 = 0.00176, D_2 = 0.069078, F_2 = 0.00073895, G_2 = 2303.3 are the constants applied and the variables X is the atomic molar fraction of sodium in the ash sample, H_2O is the volume percent of moisture added, E is the electrical field strength applied to the ash sample and T is the temperature in °Kelvin. The surface resistivity is calculated for the various temperature points along the range 90–330 °C, at 30 °C intervals.

The volume resistivity is determined using the following equation:

$$\rho_v \ = = \exp[-1.8916\ lnX - 0.9696lnY + 1.237lnZ + 3.62876) - (0.069078)E + \frac{9980.58}{T}] \quad \text{C–5}$$

where X is the atomic mole fraction of sodium in the ash sample, Y is the atomic concentration of iron and Z is the atomic mole fraction of the sum of magnesium and calcium ions. T and E are as per the formula for surface resistivity (C-4).

The total resistivity is determined using the formula below:

$$\rho_{overall} \ = \frac{\rho_{surface}\,\rho_{volume}}{\rho_{surface} + \rho_{volume}} \qquad \text{C–6}$$

The overall resistivity values are plotted against the corresponding temperature to trend the predicted fly ash resistivity behaviour of a specific ash sample.

APPENDIX D: SODIUM-DEPLETED BICKELHAUPT CALCULATIONS

The methodology to determine the predicted resistivity measurements for the sodium-depleted Bickelhaupt model is the same as described in Appendix C, except that the formula for the volume resistivity calculation is different. The surface resistivity was calculated as explained in Appendix C.

For the volume resistivity, the following formula was utilised:

$$\log \rho_{vi} = 1.2159 - 1.8916\, logX - 0.9696\, logY + 1.2370\, logZ + \frac{4334.5}{T} \qquad \text{D–1}$$

where X is the atomic mole fraction of sodium in the ash sample, Y is the atomic concentration of iron and Z is the atomic mole fraction the sum of magnesium and calcium ions.

The overall resistivity is then determined as per Appendix C and plotted for the various temperature values.

APPENDIX E: MODIFIED BICKELHAUPT MODEL

The process adopted to modify the original Bickelhaupt model was not to formulate a new fundamental model but revising or reviewing the parameters of the existing Bickelhaupt model. The intent was to change the constants in the existing equation to fit the experimental data obtained. The objective function was to reduce the error between the predicted values and the experimental determined values.

The constant values in the equation were optimized or revised based on the experimental results for the resistivity measurements at each temperature point per saline loading with the moisture additions. The model constants were revised in such a way that the modified model provides the best fit to all data obtained.

The resistivity curve theoretically is composed of a contribution of the surface resistivity and the volume resistivity. The Bickelhaupt equation includes parameters with their own constants as expressed in equation 2-4 and 2-5. The approach when optimizing the model is that the revised model resistivity is determined by using the concentrations of the species identified at the various concentrations as well as resistivity measurements obtained at the different temperatures. This resulted in a modelled value that was compared to the experimental value obtained for that point. The approach is based on assuming values for the constants $A_{1,2}$, $B_{1,2}$, $C_{1,2}$, $D_{1,2}$, $E_{1,2}$, $F_{1,2}$ and $G_{1,2}$ as per equation 2-4 and 2-5 respectively.

For example, for the volume resistivity equation

$$\rho_v = \exp[\mathrm{A}_1\, lnX - \mathrm{B}_1\, lnY + \mathrm{C}_1\, lnZ + \mathrm{D}_1) - (\mathrm{F}_1)E + \frac{\mathrm{G}_1}{T}] \qquad \text{E-1}$$

where A_1, B_1, C_1, D_1, F_1 and G_1 are the constants applied and the variables X is the atomic molar fraction of sodium in the ash sample, Y is the atomic concentration of iron, Z is the atomic molar fraction of the sum of magnesium and calcium ions, E is the electrical field strength applied to the ash sample and T is the temperature in °Kelvin, the modelled value ($\boldsymbol{\rho_{v,M}}$)was determined for each temperature point and compared with the experimental value ($\rho_{v,E}$)to determine the error sum of squares.

$$\text{Error sum of squares 1: } \sum_{T=T_1}^{n} (\rho_{v,M} - \rho_{v,E})^2 \qquad \text{E-2}$$

where n is the number of temperature points evaluated for the same saline solution conditioned concentration sample and T refers to the various temperature points at which the resistivity measurements were applied.

The objective function for the concentration of saline solution sample = error sum of squares 1 tends to 0

The error sum of squares was applied to each of the saline solution conditioned concentration samples as per the following equation.

$$\text{Error sum of squares 2: } \sum_{x=x_1}^{m} \sum_{T=T_1}^{n} (\rho_{v,M} - \rho_{v,E})^2 \qquad \text{E-3}$$

where m is the number of different concentrations of the saline solution conditioned ash samples including the unconditioned sample and x is the concentration of the conditioned sample evaluated.

The objective function for the final optimized model = error sum of squares 2 tends to 0 E-4

The same methodology was conducted for the surface resistivity equation. No constraints were applied to the constants in that it could be either positive or negative values, however the best fit results obtained were of the same sign as the value of the constants in the original model (Table 5-3).

The Microsoft Excel Solver tool was utilised to modify the constants in the Bickelhaupt formula in order to obtain a best fit curve to the measured resistivity values. The objective was set for the program to obtain the measure resistivity value for a specific temperature point, by changing the seven constants in the Bickelhaupt formula. The program would obtain a new set of constants for that point.

The formula with the new set of constants was then tested on the other temperature points by evaluating the calculated value against the measured resistivity value. The iteration was repeated until the least squares of the deviation for all sets of results was as close to 1 as possible. The final modified prediction that was determined is as follows. The figures highlighted in yellow is an indication of the constant values that have been amended.

Bickelhaupt Formula for Surface Resistivity:

$$\rho_{surface} = \exp[27.59774 - 2.233348lnX - (0.00176)H_2O - (0.069078)E - 0.00073895\ x\ H_2O\ x \exp\left(\frac{2303.3}{T}\right)]$$

E–1

Modified Bickelhaupt Formula for Surface Resistivity. The highlighted values indicate the new constants obtained.

$$\rho_{surface} = \exp[27.21581 - 2.229107lnX - (0.00176)H_2O - (0.069078)E - 0.000743\ x\ H_2O\ x \exp\left(\frac{2384.023}{T}\right)]$$

E–2

Bickelhaupt Formula for Volume Resistivity

$$\rho_{volume} = \exp\left[(-1.8916lnX - 0.9696lnY + 1.237lnZ + 3.62876) - (0.069078)E + \left(\frac{9980.58}{T}\right)\right]$$

E–3

Modified Bickelhaupt Formula for Volume Resistivity. The highlighted values indicate the new constants obtained.

$$\rho_{volume} = \exp\left[(0lnX - 0.970547lnY + 1.312641lnZ + 4.063322) - (0.068763)E + \left(\frac{9980.58}{T}\right)\right]$$

E–4